University of Southern Queensland

Investigating potential of metal mesh to contain wildfires

A thesis submitted by

Javad Hashempour

BSc, Kiev Polytechnic Institute, Ukraine, 2007

MSc, University of Manchester, United Kingdom, 2010

For the award of

Doctor of Philosophy

2016

Abstract

This work concerns an exploration of the ability of various metal screens to contain both fire radiant heat flux and firebrand attacks in a wildfire. Wildfires are a growing concern in many parts of the world today. Fighting wildfires is a highly complex and dangerous venture due to their unpredictable nature and fast propagation velocity caused by firebrand attack and radiant heat flux. The unchanged trends of losses indicate the inefficiency of current firefighting techniques and motivate the development of new techniques that are capable of effectively containing wildfires and therefore avoiding losses.

Metal meshes are currently being used as flame arrestors and their practice in fire engineering sector has precedent. Metal screens are used with limited applications to protect structures in wildfire-prone areas. The Australian Standard for construction in bushfire-prone areas mandates covering all house openings by metal meshes to minimise the penetration of firebrands into the structures and contain the effect of fire radiation. Likewise, American standards such as the California residential code mandate screens to cover house ventilation openings in order to contain firebrands and flame impingements. Similar recommendations are evident in standards published by the International Code Council (ICC) and the National Fire Protection Association (NFPA) for structures in wildfire-prone areas. All indications imply that metal screens have a potential to contain wildfires' propagation mechanisms. Therefore, it is expected that metal screens can be effective as barriers in containing the wildfires. This study aims to investigate the potential of metal screen to be used as wildfire barriers.

In this study, the performance of various metal screens to contain both fire radiant heat flux and firebrand attacks was explored in two steps. In the first step, an experimental setup using a light source and UV-visible spectrometer was designed and manufactured to determine the direct radiant flux through square woven wire screens with porosities ranging from 41% to 66%. The tunnel-vision effect of screens was measured and an empirical correlation between screen porosity and the angle of tunnel vision was developed. The results indicate that screens are able to block radiation more than the value suggested by their porosity, and more importantly, screens are more effective for larger radiant sources. Three empirical formulas were

presented to calculate the direct radiant heat flux of different size fires through screens.

In the second stage, an Ember Shower Simulator (ESS) was developed to study the performance of various metal screens against firebrand attacks. The ESS is capable of generating firebrands from various types of vegetation and performing experiments with low porosity screens at relatively high wind speeds. In a series of experiments, the effects of screen opening size, opening shape, wire diameter, screen manufacturing type and orientation of screens with respect to the firebrand flow on their performance against a Eucalyptus leaf firebrand shower were investigated. Further in this study, the combined effect of screen with different opening sizes and a buffer zone behind the screen was examined.

Two important mechanisms of firebrands passing through the screens were identified. Some firebrands shatter into smaller firebrands called secondary firebrands and then pass the screen opening. Some others that are less vulnerable keep burning behind the screen to reduce their size and pass through the screen opening. The screen opening size and wire diameter were found to have a great effect on the shattering intensity and the size of firebrands leaving the screen. Flat screens had a lower shattering intensity with respect to woven screens. An inclined screen increased the retention of firebrands behind screens in comparison with a vertical screen. This study could confirm that buffer zones are effective in improving the protection of objects shielded by a screen against firebrands. The experiments showed a relation between screen opening size and the size of the buffer zone as more firebrands quenched within the buffer zone for smaller opening size screens. It was found that the combination of buffer zone and screen remarkably reduced the number and size of firebrands on the fuel bed. As a result, the number of firebrand-induced ignitions significantly decreases in comparison with the condition that the screen is absent.

A discussion on the effectiveness of screens to contain the two propagation mechanisms is provided. Based on the discussion, it was found that metal screens are effective in containing the fire radiant heat flux and to considerably reduce the safety distance from a fire. The screens are efficient in substantially mitigating firebrand showers when a relatively short buffer zone is established. The results imply that

screens may be capable of eliminating the risks of both firebrand attacks and radiant heat flux if an appropriate buffer zone is established.

Certification of Thesis

I certify that the ideas, experimental work, results, analyses, software and conclusions reported in this dissertation are entirely my own effort, except where otherwise acknowledged. I also certify that the work is original and has not been previously submitted for any other award, except where otherwise acknowledged.

_Javad Hashempour_____

Signature of Candidate

_____

Date

ENDORSEMENT

_____

Signature of Supervisor/s

_____

Acknowledgments

I would like to appreciate all the people who contributed in some way to the work described in this thesis. Foremost, I express my sincere gratitude to my principal supervisor, Dr Ahmad Sharifian, who always supported me with patience and enthusiasm since the day I started my PhD research. His flexibility, motivation and sense of humour made for a good working relationship. I thank him for his priceless efforts in developing the initial ideas for this research, providing me excellence guidance on the analysis of data and experimental setup and insightful comments on writing my thesis.

I am also thankful to my associate supervisor, Professor John Billingsley, for his brilliant help, especially for the parts of this work on screens' tunnel vision and radiant heat flux. He has always been a motivating and enlightening man who carries you through to develop a solution. I appreciate him for sharing his expertise and valuable suggestions that were the impetus for me to fulfil this PhD research.

My special appreciation goes to Mrs Weide Wandel for her exceptional work on proofreading this dissertation. I am thankful to Mr Chris Galligan and Mr Brian Aston at USQ workshop for their hard work and genuine care in fabricating parts and equipment. They will always be remembered as smiling faces and friendly hearts that assisted me to complete the research on time. I would like to take this opportunity and express my gratitude to Dr Paul Baker and Ms Kath O'Donnell, who without their precious support it would not be possible to fulfil the risk and safety assessment of my research equipment. My gratitude is also extended to Mr Mohan Trada and Mr Adrian Blokland who have been tremendously helpful in providing on-time access to the laboratories and their generous support of tools and accessories for my research work.

Last, but certainly not least, I must acknowledge with heartfelt and deep thanks to my family, especially my mum and dad who always supported and encouraged me during the research. They have been key to my completion of this study as they have given me confidence and motivated me in so many ways. There are no words that can express my gratitude and appreciation for all they have done and been for me.

Publications

Journal Papers

- Hashempour, J., Sharifian, A., & Billingsley, J. (2016). Experimental measurement of direct thermal radiation through single-layer square-cell plain woven screens. ASME Journal of Heat Transfer, 138(1), 012701.

- Hashempour, J., & Sharifian, A. Effective factors on the performance of woven wire screens against leaf firebrand attacks. International Journal of Fire Sciences, Under Review since July 2016.

- Sharifian, A., & Hashempour, J. (2016). A novel ember shower simulator for assessing performance of low porosity screens at high wind speeds against firebrand attacks. Journal of Fire Sciences, 34(4), pp. 335-355.

- Sharifian, A., & Hashempour, J., The combined effects of woven wire screens and buffer zone in mitigating risks associated with firebrand showers. Fire Safety Journal, Under Review since January 2016.

- Hashempour, J., & Sharifian, A. (2013, September). Optimizing the coupling of a firebrand generator to a horizontal wind tunnel. In Advanced Materials Research (Vol. 726, pp. 971-976).

Conference Papers

- Hashempour, J., & Sharifian, A. (2012, September). Potentials of metal mesh to contain bushfires. In *Proceedings of the 2012 Qld Southern Regional Engineering Conference (SREC 2012)*. Engineers Australia.

- Hashempour, J., Sharifian, A., & Billingsley, J. (2015, March). Bushfire traps: the application of mesh screens to contain bushfires. In *Fire Protection Australia Conference (FPA2015).*

Contents

List of Figures

List of Tables

Nomenclature

Symbol	Unit	Description
q	W/m^2	Emissive
s	W/m^{2}K^4	Stefan-Boltzman constant
T	K	Absolute temperature
f	-	View factor
e		Emissivity
$VF_{obj \rightarrow fire}$	-	View factor of an object to the fire through single square woven wire screen
R	-	Porosity
β_c	degree	Cut-off angle
d	mm	Diameter
L	mm	Cell size
$\vec{F}_D$	N	Drag force
$\vec{F}_g$	N	Gravitational force
m_p	g	Mass of firebrand
C_d	-	Drag coefficient
A	m^2	Maximum projected area of ember
V_R	m/s	Relative velocity of the firebrand to the wind speed
V_{WIND}	m/s	Wind velocity
$V_{FIREBRAND}$	m/s	Firebrand velocity
ρ_{Air}	Kg/m^3	Air density
t	S	Time
V_p	m/s	Particle velocity
PR	%	Penetration ratio
Δt	S	Time interval
FB_a	Number	Number of firebrands approaching the mesh screen
FB_l	Number	Number of firebrands leaving the mesh screen
λ	nm	Wavelength
h	J.S	Planck constant
k	J/K	Boltzman constant
c	m/s	Speed of light
B_λ	W/nm	Spectral radiant per unit wavelength
a	mm	Opening size
PR(%)	%	Passing ratio
I_{screen}	counts	Light intensity in the presence of screen

$I_{no-screen}$	counts	Light intensity in the absence of the screen
I_{dark}	counts	Light intensity in the absence of light and screen
α_{TU}	degree	Angle of tunnel vision
VF_{TU}	-	View factor of tunnel vision area
h	mm	Distance between two parallel circles
r_1	mm	Radius of the object
r_2	mm	Radius of the tunnel vision area
VF_s	-	View factor of a light source with respect to a sensor
$I_{A>L_{v-noscreen}}$	counts	Light intensity of the source greater than tunnel vision area
$PR_{S>L_V}$	%	Passing ratio of source greater than tunnel vision area
PR_{TU}	%	Passing ratio of source same size as tunnel vision area
PR_{inf}	%	Passing ratio of source with infinite size
VF_{screen}	-	View factor of the screen with respect to the object
q_{IRHF}	W/m^2	Indirect radiant heat flux emitted toward the object
ΔP	Pa	Pressure difference
$T(\%)$	%	Turbulence intensity
u_{rms}	m/s	Root mean square of turbulent velocity fluctuation
u_{ave}	m/s	Average velocity
u_i	m/s	Instantaneous velocity
FR	m/s	Fragmentation ratio
w	m	Width of object and fire

Chapter 1

Introduction

1.1. Opening

This study aims to assess the potential of metal screens as an additional technique to combat wildfires. The research focuses on two most important mechanisms of wildfire propagations: firebrand attacks and fire radiation, with an investigation of the capability of metal screens to act as fire barriers against these. Following in this chapter, the details about the background, motivation and aims and objectives of the study are presented.

1.2. Wildfire impacts and complexity

Wildfires are devastating in terms of the scale of human and financial losses. The concern over wildfires is growing since their occurrences have become more frequent in many parts of the world. For example, in Australia, outburst of wildfires took the lives of 696 people between 1850 and 2001 (CSIRO 2007). In 2009, the worst wildfire in the history of the country occurred in the state of Victoria and killed 173 people in only two days (Cruz et al. 2012). The total losses in that event exceeded four billion Australian dollars (Australian Institute of Criminology 2009). In Europe, more than 85% of wildfires happen mainly in Mediterranean regions

(San-Miguel-Ayanz et al. 2012). In Portugal, in the period from 2003 to 2005, wildfires caused the deaths of 39 people across the country (San-Miguel-Ayanz et al. 2013). Wildfires also killed 186 and 20 people in Spain and France respectively in the period 1982–2007 (Viegas 2009). In the United States, wildfires took the lives of 10 people between 1975 and 1994 (Mileti 1999). The insured losses within that period were also reported to be around $US3.1 billion.

The frequent occurrence of fires in the global scale shows that the number of fires is increasing. Wildfires can be tragic when they move toward Wildland-Urban Interface (WUI) areas. The fires intensely attack these areas and can burn dwellings and kill humans. The concern over fires in WUI areas is growing due to increasing population in these areas (Hammer et al. 2009). The growing population causes the development of more houses and infrastructure in WUI areas and leads to greater human and financial losses at the time of fire. Also, it is well known that climate change has a great effect on increasing frequency and intensity of wildfires due to rise in global average temperature (Fried et al. 2004). As the problem posed by climate change is expected to grow, wildfires are expected to become more frequent and have a greater impact on WUI communities. This will jeopardise lives and assets in many areas, especially in parts of Europe, North America and Australia which have already shown records of significant losses.

The complexities associated with wildfires arise from their enormous size and rapid propagation. There are reports that firefighters lost their lives as they were trapped by a rapid fire spread that even didn't allow them to climb a few metres to reach their truck (Xanthopoulos 2007). Haynes et al. (2010) also provided a review of fatalities in Australian bushfires which shows that many people were trapped on the roads by the rapid propagation of fire after they evacuated from their houses late. The rapid propagation of fires also were reported by many post-fire investigations (Maranghides and Mell 2011; Butler et al. 1998). Cohen (2010) explains the problem of Wildland-Urban Interfaces areas are due to fire rapidly attacking these areas and burning a number of houses simultaneously through extensive ember attacks and heat exposure of long and intense flames. The massive number of house fires overwhelms firefighters' efforts and causes them to lose control of wildfires, leading to a disaster. Leonard et al (2004) classified ember attacks and radiant heat flux as key fire propagation mechanisms (Leonard et al. 2004). These factors have also been

identified as fire spread mechanisms and the direct cause of house ignitions in other research and reports (Tolhurst and Howlett 2003; Ramsay, Rudolph, and Rudolph 2003; Building, Commission, and Victoria 2010).

1.3. Current status of controlling wildfires

In the previous section, the significant losses of wildfire incidents and their growing trends were reviewed, and firebrand attack and fire Radiant Heat Flux (RHF) were introduced as key fire propagation mechanisms. Fire "embers" or "brands" are airborne debris which are sourced from burning vegetation that may fly kilometres ahead of fire front by means of the air stream (Chandler et al. 1983; Wells 1968). Wind speed has a great impact on severity of firebrand attacks. Chen (2004) noted a wind speed of 18 m/s for the Canberra fire in 2003 and Butler et al. (1998) noted wind speeds ranging between 13-20 m/s for the South Canyon Fire in Colorado in 1994. These burning brands fall on the ground and start spot fires. The process which is called firebrand or ember "spotting" induces a number of spot fires and spreads fire in a vast area surrounding the fire front. Firebrand spotting is the main cause of house destruction during wildfires (Chen 2004; Wang 2006 ; Stephen L. Quarles et al. 2010) and induces ignition by landing on houses or entering the structure via house openings or broken windows (Barrow 1944; Long and Randall 2004; Poon and England 2002) from excessive fire radiant heat exposure (Ramsay et al. 2003). The fire intensity can reach 100 MW/m (Wahlquist 2006) and has a large role in drying the surrounding areas and creating suitable conditions for possible ignition by firebrands or flame impingement. The radiant heat flux can itself be a source of ignition in cases of long exposure. Butler and Cohen (1998) reported a radiation intensity of 80 kW/m^2 for a 20-metre-wide fire. Cohen (2004) investigated the fire radiation and showed that the intensity varies from 80 kW/m^2 at a distance of 10 metres to 20 kW/m^2 at a distance of 40 m from the fire front. This is extremely high since human skin experiences pain at an intensity level greater than 2 kW/m^2 and skin burns instantly at an intensity of 12 kW/m^2 (Valendik and Kosov 2008). Moreover, timber can be ignited after a long exposure to a radiant intensity of 12.6 kW/m^2 and above, and mechanical failure of steel structures is expected to take place at an intensity of nearly 25 kW/m^2 (Zárate et al. 2008).

Existing suppression techniques are unable to protect people and houses when wildfires fiercely attack WUI areas and burn a number of houses simultaneously (Cohen 2010). The ground firefighting operation is not quite effective in this type of fire due to severe ember attacks, fire radiation and rapid changes of fire behaviour which jeopardise the lives of exhausted firefighters. Also, there is doubt over the effectiveness of aerial firefighting as the efficiency is estimated to be only 5%-15% (Pekic 2007). One of the major problems of aerial firefighting is that water is dropped in an uncontrolled manner and a high proportion of water is evaporated before reaching the fire core. Moreover, water bombardment by aerial firefighting in WUI areas is limited due to vulnerability of houses and people. An example is the death of a fire crew due to water drops by a helicopter in Greece (Xanthopoulos 2007). The application of chemical retardants instead of water as quenching agent is associated with difficulties because of health and safety concerns for humans and the environment (Kalabokidis 2000). Besides this hurdle, special transport equipment is required to deliver large quantities of chemical retardants to remote areas (Pekic 2007), which draws questions over their cost justification.

In terms of management, many codes and guidelines provide strategies to secure the safety of people and houses in WUI areas, such as the International Urban-Wildfire Interface code (International Code Council (ICC) 2012), California Residential code (California Residential Code 2014) and the Australian Standard for construction in bushfire prone areas (AS3959-2009)(Standards Australia 2009). However, these standards and codes have been determined using minimal scientific investigations and data, and therefore their effectiveness is poorly known (Stephens et al. 2009). Also, the unchanged trend of house destructions (Chen 2004;Stephens et al. 2009) raises alerts that the codes' implementation has not been efficient as initially expected. In addition, some argue the cost of modification of current houses in fire-prone areas is an obstacle to correct implementation of standards (Ian Weir 2015; Mitchell 2006; Mitchell and Patashnik 2006). Other guidelines such as prescribed fuel management or reducing availability of fuels in ignitions zones around houses are suggested. While they might be effective in avoiding fire propagation through radiation and flame impingement, they cannot avoid ignitions of houses by firebrand attack (Cohen 2000). Firebrands can easily fly over the ignition zones and land on houses, thereby starting fires.

All evidence implies that an efficient protective technique which saves houses and residents is missing. In recent years, attempts to develop new misting systems that meet the drastic wildfire environment have been made. A new sprinkler system "WEEDS" has been designed and tested to quench wind-driven firebrands and to prevent house ignition (Mitchell 2006). The system was mounted on a house during Cedar fire in California and the house survived during and after the passage of the fire front. However, the author could not verify that the house survival was the outcome of WEEDS or other factors; there were no observations during the passage of the fire front. The water spray systems in general are not accepted by fire agencies as a protection method because of many issues associated with their efficiency and other factors such as their dependency on municipal water and electricity supply (Mitchell and Patashnik 2006).

1.4. Metal screens as a potential solution

For many years, screens have been used as filters and sieves. Perforated metals (porous metals) are being used as filters in electronic and optics to block waves. Application of metal mesh in fire engineering is not unprecedented and flame arrestors on Bunsen burners or in combustion engines are examples. Metal meshes are also currently being utilised in wildfire-prone areas as mandated by codes and regulations to cover vents (California Residential Code 2014), doors, windows and gutters (Standards Australia 2009). The intention is to avoid or at least limit firebrand intrusion and radiant heat flux, or in some cases the flame impingement into the houses. It is noteworthy that metal screens are likely to be effective in minimising all mechanisms of fire propagation, which is reason to assume there is a real possibility of success in applying them as fire barriers.

1.5. Background on the potential of metal screens

The potential of mesh screens in saving houses from wildfires was initially stated in a post-fire investigation of the Beaumaris fire in Australia in 1944 (Barrow 1944). The author stated in his report that the house openings covered with wire screens and fly wires nets had provided significant resistance against the burning debris penetration. The idea of metal mesh application in wildfire protection was well

supported some decades later when Grantham (1984) suggested that the possible application of metal mesh for bushfire protection since they were already used as flame arrestors. The idea was supported by reports from a bushfire incident stated that screen fences ceased fire propagation toward a military base in Surrey, UK. The author also addressed reports on a similar incident in Australia where a house surrounded by a wire mesh fence survived from the fires, while nearby houses completely destroyed.

Currently, using metal mesh is mandated by many codes and regulations for construction at wildfire-prone areas as mentioned previously. The Australian standard for construction in wildfire-prone areas mandates covering house openings such as windows and eave ventilations by screens with a maximum aperture size of 2 mm (Standards Australia 2009). Also, based on the residential code of California, any vents in houses shall be covered by screens with an aperture size in the range of 1.6–3.2 mm (California Residential Code 2014). The National Fire Protection Association (NFPA) provided a compulsory standard for reducing structure ignition hazard from wildland fire by covering external ventilation openings with screens with an opening size of 6.3 mm (National Fire Protection Association 2008). Similarly, the international Urban-Wildland Interface code also mandated construction of buildings in these areas to cover vents using screens with a maximum aperture size of 6.4 mm (International Code Council (ICC) 2012).

In addition to reports and standards, some recent research has focussed on wire screen resistance capability against wildfire propagation factors. A computational work by Sharifian and Buttsworth (2008) addressed the capabilities of metal meshes in containing the direct radiant heat flux of fires. The authors stated that shielding an object with screen against a radiant flux of approaching fire divides radiant heat flux into two distinct types. The first is the radiation that passes through the screen cell openings and reaches the object: Direct Radiant Heat Flux (DRHF). A portion of radiation which is blocked by metal screen causes a temperature rise in the screens and makes the screens a radiation source. This type of radiation is called Indirect Radiant Heat Flux (IRHF). Sharifian and Buttsworth numerically modelled single woven wire screens with various porosities between a fire and an object, and calculated the view factor. They found the blockage of DRHF is more than what the porosity values suggest. Also, double layers of woven wire screens with identical

porosities were modelled and the results showed that double layer screens with lower porosities can significantly block DRHF, while the drag force penalty can be negative for the second screen (Sharifian and Buttsworth 2010). The authors also declared in another computational work that if the object is too close to the metal screen, the total RHF would be equal to or greater than the RHF without using screens owing to the increased effect of IRHF (Sharifian and Buttsworth 2005). This resulted in a recommendation of a minimum standoff distance based on screen cell size that mitigates the effect of IRHF.

The effect of screens on blocking firebrand attacks has been studied by a few researchers. Manzello et al. (2007) used a firebrand generator (NIST dragon) to study the effect of three screens with aperture sizes of 6 mm, 3 mm and 1.5 mm in blocking firebrand penetration into the vents. They found that the firebrands did not quench in the presence of screens and burnt until they could fit through the screens. The penetrated firebrands could ignite materials placed behind the screens. In subsequent work, Manzello and his colleagues conducted the same study in more detail using screens with cells sized 1.04–5.72 mm (Manzello et al. 2010; Manzello et al. 2011) and found similar results. They also discovered that screen cell size has a significant effect on the number and sizes of passing firebrands. Despite the penetration of firebrands through the screens, authors concluded that the metal screens are effective to mitigate the risk of firebrand attacks.

1.6. Potential benefits of metal screen application

The review on current application of metal screens strongly suggests their possible potentials as fire barriers. Due to possible high costs and negative visual impacts, temporary fencing is likely to be the more viable option. The temporary application of screens as a fire barrier has several potential advantages in comparison to the conventional techniques of cutting trees and spraying water. The first advantage is that screens have the potential to stop wildfires regardless of their intensity. Wahlquist indicated that the maximum intensity fire that could be extinguished using current techniques is about 2.5 MW/m of fire front but big wildfires can be up to 100 MW/m of fire front (Wahlquist 2006). The proposed technique is not particularly sensitive to fire intensity if an appropriate material is selected for the screen. The

second advantage is related to transportation. In comparison to water, metal screens do not need a container – transportation of solids is much easier than transportation of liquids. Metal screens can be stored in wildfire prone areas without risk of degradation. It should be possible to re-use screens or to redeploy them to other sites during a wildfire event. The third potential advantage in the use of metal screens as wildfire barriers is the significant weight advantage at higher fire intensities in comparison to currently available techniques. Robertson et al. (1997) and Alexander (2001) estimate the amount of water required to extinguish a fire in a balsam fir slash forest would be about 5.57 litre/m^2. The weight of 1 m^2 of stainless screen which complies with AS 3959-2009 is about 0.5 kg which is the equivalent of 0.5 litre/m^2 of water. This weight remains unchanged for higher intensity fires. The fourth advantage is that the proposed system provides a safer work environment for fire-fighters, volunteers and property owners. It should be possible to deploy metal screen barriers well ahead of fire arrival, in contrast to fighting fires with water which generally requires personnel in the vicinity of the fire. Deployment well ahead of fire arrival would reduce the possible risks to fire-fighters, volunteers or time miscalculation by property owners. The required mass of metal screen is defined by the length of the fire front and the height that it should cover, while in the case of conventional techniques it is the burning area and the height of vegetation that define the amount of required time to suppress or extinguish the wildfires. For example, as vegetation height increases, the conventional techniques require greater time and effort to suppress the fire, but this does not significantly affect the required screens and mounting time for the proposed technique. This is the fifth advantage of metal screens. The metal screen barriers may also have some advantages for industrial or urban fires. One of the main concerns during such situations is the propagation of fire to nearby buildings. Due to building roofs, aerial firebombing is not practical. In industrial or urban situations, the screen barrier technique could be a much faster method of containment than conventional techniques. The aerial deployment of metal screens using helicopters (fitted with the appropriate equipment) has the potential to contain fire more quickly.

1.7. Research gap

Previous work is not sufficient to confirm the potential of metal screens to be employed as wildfire barriers. Some information became available from the

observations that do not provide firm and conclusive evidence. The research study on square woven wire screens against fire direct radiant heat flux indicated the significant capabilities of woven wire screens in containing DRHF due to their tunnel vision effects (Sharifian and Buttsworth 2008). However, the computational results have never been experimentally verified.

The experiments on woven wire screens to cover vents against firebrands were completed without quantifying the effect of opening sizes. Previous studies argue the effectiveness of screens without a clear definition of effectiveness. Unlike screens placed on house vents, a standalone screen barrier can be erected in various arrangements. Available screens in the market have different opening sizes, wire diameters and porosities. Screens are also manufactured with different opening shapes such as rectangular, circular and square or fabricated as woven wires or as a flat sheet with holes. Moreover, the barriers can be arranged in any orientation with respect to an approaching fire and they can be erected with a buffer zone from an object. It is possible to arrange the screen in a multi-layer arrangement rather than a single-layer screen. The screens might have various performances in any of above arrangements that could change the conclusion on their potential in containing fire radiant heat flux and firebrands. Some configurations might hinder, while others promote, burning caused by firebrand and fire RHF. Therefore, further studies are needed to investigate and quantify the potential of metal screens under consideration for use as wildfire barriers and provide clear answers to the following questions:

- Do screens have the potential to effectively protect objects by containing fire radiant heat flux?
- Do screens have the potential to contain firebrand attacks and prevent objects' ignition?

1.8. Aims and Objectives

The above mentioned potential of metal screens led to consider their broader use as fire barrier. The fire barrier with the support of scaffold poles and securing cables/wires can be temporarily erected on the approaching fire side or all sides of the property. They can also be temporarily or permanently mounted along the side of roads to prevent or limit fire propagation. The delivery of the screens to the intended site can be aerial or ground-based. There will be a need for cranes or specially

designed machineries to facilitate the prompt and professional installation. In the case of temporary installation, after the passage of fire front, the barriers will be dismantled and returned to stowage. There are many aspects to be considered before proceeding with the plan and putting it into practice. Those aspects such as cost-effectiveness, drag force, design of special machineries, mounting mechanism, material properties at high temperature are beyond the scope of this study. The most important question to be conclusively answered prior to addressing the above issues is the extent of the effectiveness of the proposed fire barrier.

The purpose of this study is to evaluate the potential of screens as a fire barrier and to provide useful information for their possible design. To be more specific, this study assesses the potential of screens in containing firebrand attacks and fire radiant heat flux. The objectives of the study are listed as follows:

1. Develop an experimental formula to determine the correlation between screen porosities and RHF and compare the experimental formula with available computational formula
2. Develop an apparatus that facilitates experimental studies of low-porosity screens against firebrand attacks at high wind speeds
3. Find the relation between the opening size of single-layer screens and their capability to contain firebrand attacks
4. Discover the impact of screen porosity on their potential to contain firebrands
5. Determine the potential of screens with different opening shapes to contain firebrands
6. Evaluate the effect of screens' manufacturing type on minimising firebrand attack
7. Assess the impact of angle between a single layer screen and firebrand flow on the containment of firebrands
8. Assess the possible effect of buffer zone between screen and object on the protection against firebrand attacks

1.9. Thesis Outline

The thesis contains six chapters. Chapter 2 includes a thorough literature review of previous studies in two separate sections. In the first section, an introduction to RHF characteristics leads into studies related to metal screen and transmission of RHF

through screens. In the second section, a review of theoretical and experimental studies on firebrands and spotting mechanism are described followed by a review of the application of metal screens in containing firebrands.

Chapter 3 reports the results of experiments on the ability of square woven wire screens to contain radiant heat flux. It includes the methodology and experimental setup at the beginning of the chapter. The chapter continues with an explanation of the tunnel-vision effect of screens, and then details the transmission of light intensity through the screen. At the end of the chapter, the experimental correlations are developed for the infinite light source and then the results are compared to those of computational correlations.

The development and characterization of the Ember Shower Simulator (ESS) are explained in Chapter 4. The ESS is a combined wind tunnel and firebrand generator that was designed to facilitate experiments on metal screens' performance against firebrand attacks. In the chapter, the design and development processes are described including a thorough discussion on the necessity of the design. The chapter also reports the characteristics and the performance of the ESS.

Chapter 5 includes the results of experiments on metal screen performance against firebrand attacks using the ESS. The chapter begins with reports on the results of the experiments carried out on the performance of various screens to contain leaf firebrands. It continues with explaining the experimental investigation on a combined effect of buffer zone and screen in containing firebrands.

The discussion of experimental results is provided in Chapter 6. The chapter describes and gives a thorough review on the potential applications of metal screens as fire barriers. The discussion describes the advantages of metal screens as fire barriers from different perspectives.

Chapter 7 summarises the dissertation and lists the main conclusions of this research study. At the end of the chapter, recommendations for the future work are provided.

1.10. Summary

The significant previous financial and human losses due to wildfires were explained at the beginning of this chapter. It was stated that the difficulties associated with the

wildfires are the severity and rapid propagation of fires owing to firebrand spotting and radiant heat flux. The inefficiency of present suppression techniques to control wildfires and current wildfire management practices were discussed. It was stated that an effective containment technique is needed and use of metal screen was proposed as a potential solution. The advantages and benefits of using metal screens were presented and a review of metal screen application mandated by current codes and standards in wildfire-prone areas were explained. Moreover, the results of previous investigations on the performance of screens against firebrand attacks and fire radiant heat flux were summarised. It was found that previous investigations are unable to confirm the potential of commercial screens as fire barriers, and further study to assess their potential against both propagation mechanisms is required. The aim of this study was explained and a list of objectives was presented. At the end, an overview of the thesis was provided.

Chapter 2

Literature review

2.1. Introduction

In this chapter, a review of previous studies is presented in two separate sections. In section 2.2, previous studies on fire radiant heat flux passing through the screens are explained. It begins with describing the characteristics of fire radiant heat flux and continues with explaining screen potentials in containing fire RHF. A summary of the section is provided at the end.

In section 2.3, previous studies on the firebrand attacks are considered. It presents the firebrand attack phenomena by explaining the firebrand characteristics at different stages of spotting process. Following that, studies on the capabilities of screens to stop firebrand attacks are provided and finally highlights of the section are presented. The last part of the chapter identifies the research gaps.

2.2. Metal screens and Fire RHF

2.2.1. Fire RHF characteristics

A vegetation fire transfers heat via the three mechanisms of conduction, convection and radiation. However, the radiative heat transfer is known as the main mode of heat transfer in vegetation fire propagation and was even cited as the sole mechanism of heat transfer in an no-wind condition in one study (Weber 1989). The radiation of a blackbody can be calculated based on the Stefan-Boltzmann equation as follows (Lienhard 2011),

$$q = \sigma T^4 \qquad (2.1)$$

where σ is the Stefan-Boltzmann constant ($5.67 \times 10^{-8}\ \mathrm{Wm^{-2}K^{-4}}$), T represents the absolute temperature of the radiant surface (K) and q is the emissive power per unit area (W m^{-2}). The blackbody surfaces absorb and emit radiation at all wavelengths and directions, and the radiation intensity varies as direction changes with the cosine of angle from the normal to the blackbody surface (Lambertian surfaces). However, blackbody surfaces do not represent the real surfaces. The emissive power of real surfaces is always less than the emissive power of a black body. The emissivity of a real surface is the proportion of radiation emitted by the surface to the radiation emitted by a blackbody at the same temperature. Also, the radiation emitted from a surface to a receiving surface is related to a geometrical parameter named view or configuration factor. The factor is the proportion of the hemispherical field of view of a radiating body that is occupied by elements of a receiving surface. If the elements fill all the hemispherical field, then the factor is equal to unity. Including these terms in equation (2.1), the Stefan-Boltzmann equation for the real surfaces (Drysdale 1999) becomes as follows,

$$E = \varphi \varepsilon \sigma T^4 \qquad (2.2)$$

where φ is the view factor and ε stands for the emissivity of the radiating surface.

This formula is used by many models to estimate the radiation power of fire fronts. Sullivan et al. (2003) stated that it is hard to assign an emissivity to fires due to their transient behaviour. The view factors of fires are also difficult to calculate due to varying height, angle and shape. Butler and Cohen (1998) calculated a safe distance

for firefighters as a function of the flame height and distance from the flame. A flame and a firefighter were modelled as flat sheets with given heights and widths. The temperature and emissivity of the flame were assumed to be 900°C and one (blackbody) respectively while the emissivity of 0.8 and temperature of 45°C were assumed for the surface representing the firefighter. The exchanged radiant heat flux of the flame increases proportionally with the increase of the flame height and the decrease of the distance of the two surfaces due to change in the view factor between two surfaces. However, Knight and Sullivan (2004) showed that the assumption of setting the emissivity based on opaque box models leads to an overestimation of RHF, by comparing the results of the opaque model to those obtained from experiments with an array of propane burner jets. The opaque box is terminology for rectangular boxes of different sizes with constant temperature and emissivity used to represent a fire in computational studies. They argued that the major errors in the models are pre-set assumptions of emissivity. They presented a semi-transparent flame model assuming different emissivity for random size soot particles. The model provided a better approximation of real flame in comparison with solid models. Both computational and experimental work showed that the flame angle with respect to an object, flame depth and flame height affect the RHF received by the object. However, the received RHF reduces with an increase of the distance between the object and the fire. Zárate et al. (2008) modelled the radiant heat flux of a wildfire flame as a rectangular opaque box with various heights and at different distances between an object and the flame. They found the same results as (Butler and Cohen 1998).

Many researchers investigated the wildfire flame's radiation properties in full- and laboratory-scale experiments using spectroscopy techniques. Àgueda et al. (2010) studied the emissivity of branches and leaves of typical Mediterranean forest fuels. It was discovered that the emissivity of a forest fuel flame is reliant on the thickness of the flame and the flame exhibits an emissivity near a blackbody (0.9) when its thickness is greater than 3.2 m. The infrared radiation emitted by burning vine branches and excelsior was considered by Parent et al. (2010). The burning flame was monitored by a combined infrared camera and Fourier-transformed data from an infrared spectrometer. The authors stated that the emissivity of burning vegetation varied with the height and was much less than that of a blackbody. The investigation

estimated an emissivity below 0.3 and a temperature of 1000 K for the flame. For the burning litter, a higher emissivity of 0.8 at the same temperature was obtained. An experimental study by Boulet et al. (2011) reported that the peak intensity occurs at a wavelength of approximately 4.3 μm for a flame of burning wood shavings and kermes oak shrubs (Boulet et al. 2011). The authors used the same instrumentation applied in Parent et al. (2010) to monitor flames of the burning vegetation in a fire tunnel. The vegetation fuels were arranged in various lengths to obtain flames with various thicknesses. Boulet et al (2011) indicated the large effect of optical thickness of flame on its emissivity. In a thin flame, there is a dominant contribution of CO_2 and burning gases around a wavelength of 4.3 μm. However, the growth of flame thickness increases the contribution of glowing soot which enhances the emission intensity and consequently the overall emission of the fire.

Some research studies focused on measuring the radiant heat flux of full-scale fires using heat flux sensors. Silvani and Morandini (2009) measured the radiant heat flux and temperature of four vegetation fires using an arrangement of two heat flux sensors and a thermocouple. The vegetation site included pine needles, oak branches, a combination of oak and arbutus branches and broom in various terrain slopes. The measured average flame temperatures were in the range of 700–900˚C in the vicinity of the thermocouple. The peak heat flux was between 40 kW/m^2 for pine needles to more than 100 kW/m^2 which occurred for broom. The results indicated that the temperature and heat flux gradually increase as the fire front approaches. A report addressed the variation of RHF along the height of a flame (Cruz et al. 2011). The full scale experiments were performed in shrubland in Portugal using several K-type thermocouples and three Narrow Angle Radiometers (NAR) which were mounted at three different heights on a 1.7 m tower of thick ceramic blanket and aluminium foil. The ignition of shrubland started 25 metres from the tower and the fire moved towards the tower by means of local wind. The peak RHF was recorded at the vicinity of tower and ranged between 150 kW/m^2 and 175 kW/m^2 and the temperature of the flame was measured between 1200 K and 1330 K. It was reported that the emission of RHF varies along the height of the flame. Frankman et al. (2013) measured the convective and radiative heat flux from full-scale burning of various vegetation in different terrain slopes. They embedded two heat-flux micro-sensors consisting of a differential thermopile heat flux gauge and a platinum resistance

temperature sensor in the vegetation where the fire took place. The authors investigated three types of fires including crown fire, brush fire and surface fire at various terrain slopes. Peak RHFs varied between 20 kW/m^2 and 300 kW/m^2; the highest and lowest peaks were recorded for crown fire and surface fire, respectively. The authors stated the great role of terrain slope on influencing RHF.

2.2.2. Potentials of metal screens versus fire RHF

There are a limited number of studies that investigated fire RHF when a commercial screen is placed between a fire and an object. As discussed before in chapter one, an object behind a screen receives a portion of RHF directly through the screen aperture which named as direct radiant heat flux (DRHF). However, other portion is blocked by the solid area of the screen and increases the screen temperature. The hot screen emits heat named as indirect radiant heat flux (IRHF) to the object. Therefore, the total amount of transmitted RHF through the screen to the object is the sum of DRHF and IRHF. DRHF depends on the view factor of the object to the fire through the screen and emissivity as well as temperature of the approaching fire, while IRHF relies on the screen emissivity, screen temperature and the view factor of the object to the screen.

For the first time, Sharifian and Buttsworth (2008) investigated fire DRHF transmission through screens to an object and presented a model to estimate the view factor of the object to an infinite fire while an infinite square woven wire screen was between the object and fire. It was revealed the view factor increases with the rise of porosity, but always remains less than the porosity value. They presented the correlation for view factor of an object to the fire ($VF_{obj\rightarrow fire}$) through single square woven wire screens in which screen porosity (p) ranged between 25% and 90% as follows (Sharifian and Buttsworth 2008),

$$VF_{obj\rightarrow fire} = 0.25p^2 + 0.9p - 0.132 \qquad (2.3)$$

As the emissivity and temperature of fire are known, the DRHF varies only with the view factor. It should be noted that the above correlation is valid under certain

conditions. The screen should be large enough that the fire does not come into direct view of the object at the edges of the screen, and the fire should be large enough that nothing other than the fire can be seen through the screen.

The authors also addressed the effect of screen tunnel vision on the view factor and DRHF passing through the screen. The tunnel vision limits the passage of light at a certain angle through the screen which is related to the screen wire diameter and cell size. Beyond this angle the wires seem to overlap as seen by the object, and nothing from the other side of the screen is visible. Möller et al. (2010) explains the tunnel vision effect of woven wire screens as the cut-off angle at which the incident light cannot directly pass through the screen cells. The cut-off angle (β_c) was presented as a function of wire diameter (d) and cell size (L) as follows

$$\beta_c = 90 - \arcsin\left(\frac{d}{L}\right) \qquad (2.4)$$

The ratio of $(\frac{d}{L})$ and porosity are related (Böttcher and Wedemeyer 2006) as follows

$$P = \frac{(L-d)^2}{L^2} = (1 - \frac{d}{L})^2 \qquad (2.5)$$

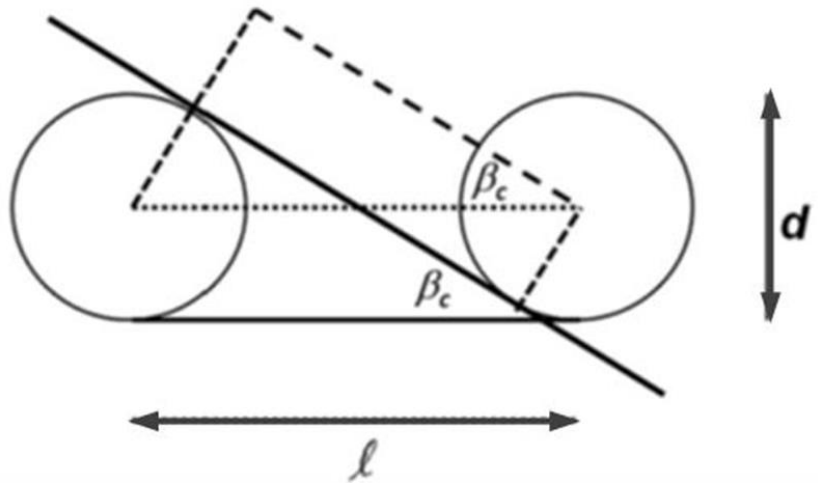

Figure 2.1 Geometry for deriving analytical solution of cut-off angle adopted from (Möller et al. 2010)

Therefore, the formula (2.4) can be re-written as a function of screen porosity as follows

$$\beta_c = 90 - \arcsin\left(1 - \sqrt{P}\right) \qquad (2.6)$$

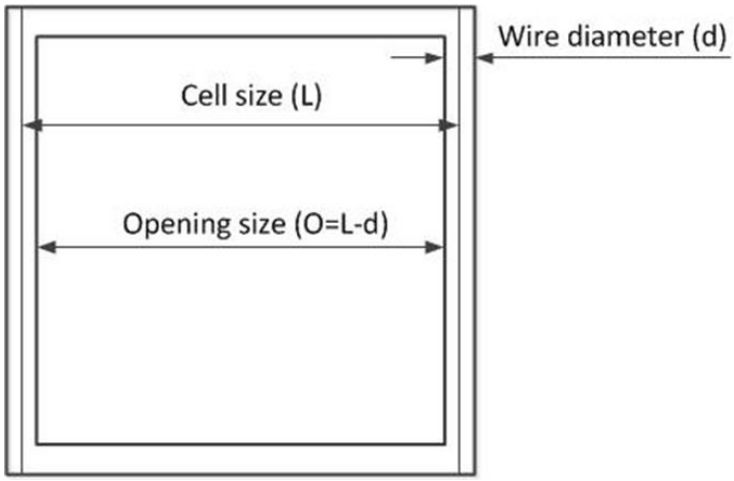

Figure 2.2 The scheme of screen cell size and the geometrical variables.

2.2.3. Summary

Previous investigations addressed the complexity of the estimation of the wildfire RHF. Based on the Stefan–Boltzmann heat-transfer law, the amount of transmitted RHF of a fire to a receiver depends on the view factor of the receiver to the fire, temperature and emissivity of the fire. The previous research indicated that it is hard to determine the view factor of an actual fire's flame since the flame shape and dimensions are transient. The temperature and emissivity of fires show great variance along the height of the flame and for different types of vegetation. The experimental studies addressed the flame temperature, flame thickness and type of vegetation as the effective parameters in determining the emissivity. The measured peak intensity of vegetation fires was in the range of 20 kW/m^2 to 300 kW/m^2.

Available investigations on shielding an object by single square woven wire screens against a fire indicated that the view factor decreases with the reduction of screen porosity. The investigations addressed the relation of the view factor and tunnel vision angle of screens. The tunnel vision was explained and an analytical formula to find the angle was presented.

2.3. Metal screens and firebrand attacks

2.3.1. Firebrands Classification

Firebrands are the airborne particles that detach from different parts of burning vegetation and are lofted by means of the fire plume buoyancy force into the air stream. The sources of firebrands are varied. Leaves, barks, twigs and branches of a tree or grasses and shrubs are well known sources of firebrands (Bradstock et al. 2012). However, all firebrands are not equally dangerous in terms of their heat capacity and maximum spotting distance. Davis and Byram (1959) classified barks, charcoal, dry moss and duff as the most hazardous firebrands for long-distance spotting (Davis and Byram 1959). Also, they found the low risks associated with leaf embers at long-distance spotting. A firebrand can burn in flaming or glowing states (Babrauskas 2003). The flaming combustion is the exothermic combustion of distilled gases obtained from pyrolysis of firebrands which requires sufficient gas concentration and airflow as well as adequate heat to ignite the gas mixture. The glowing combustion of firebrands is the rapid oxidation of the surface of solid-phase char material (Babrauskas 2003). However, flaming firebrands are scarce in spotting process unless for short distances and glowing firebrands are more common (Davis and Byram 1959). Ganteaume et al. (2011) examined the combustion characteristics of various firebrands involved in a spot fire. Pine cones, leaves and barks as well as Eucalyptus leaves and barks were placed on a 500 W disk-shape radiator. The flammability properties such as time to ignition, flaming duration and weight loss as well as gross heat of combustion of these samples were measured. It was discovered that heavy firebrands such as pine cone firebrands sustain flames for longer periods and are risky for longer spotting distances. Also, light firebrands with a high surface-to-volume ratio such as eucalyptus leaf and thin barks are risky only for short spotting distances whereas their flaming duration are too short. Ganteaume et al (2011) addressed a group of light firebrands with low surface-to-volume ratio that is in between these two groups. They are risky for short spotting distances and occasionally long spotting distances.

2.3.2. Theories of firebrand transport

Aerodynamic and combustion properties of fire embers are essential in determining their flying distance. The trajectory of fire embers is mainly affected by the drag and lift forces that are exerted by air flow and gravitational force. The motion of fire embers has been modelled based on classic Newtonian physics (Tarifa et al. 1967; Tse and Fernandez-Pello 1998; Woycheese and P. J. Pagni. 1999; Anthenien et al. 2006; Kortas et al. 2009). The equation of motion is defined as follows (Anthenien et al. 2006),

$$m_p \frac{\overrightarrow{dV_p}}{dt} = \overrightarrow{F_D} + \overrightarrow{F_g} \tag{2.7}$$

where $\overrightarrow{F_D}$ denotes the drag force exerted on firebrands and $\overrightarrow{F_g}$ represents gravitational force. By inserting the formulas for each term, equation (2.7) becomes

$$\overrightarrow{F_g} = m_p \vec{g} \tag{2.8}$$

$$\overrightarrow{F_D} = \frac{1}{2}\rho_{air} C_d A \left|\overrightarrow{V_R}\right|^2 \frac{\overrightarrow{V_R}}{\left|\overrightarrow{V_R}\right|} \tag{2.9}$$

where ρ_{air} is the air density, C_d represents the drag coefficient of a fire ember, A is the maximum projected area of the ember, V_R stands for the relative velocity of the firebrand to the wind speed ($V_R = V_{WIND} - V_{FIREBRAND}$) and m_p is the mass of the firebrand. By substituting equations (2.8) and (2.9) into equation (2.7) the vertical (x-axis, parallel to the wind direction) and horizontal (z-axis) components of equation (2.7) become

$$\frac{dv_{p,x}}{dt} = \frac{1}{2m_p}\rho_{air} C_d A \left|\overrightarrow{V_R}\right| \left(V_{w,x} - V_{p,x}\right) \tag{2.10}$$

and

$$\frac{dv_{p,z}}{dt} = -\frac{1}{2m_p}\rho_{air} C_d A \left|\overrightarrow{V_R}\right| V_{p,z} - g \tag{2.11}$$

where,

$$V_{p,x} = \frac{dx_p}{dt} \tag{2.12}$$

$$V_{p,z} = \frac{dz_p}{dt} \tag{2.13}$$

Several models were presented for estimation of firebrands' spotting distance. Albini (1979) and Albini (1981) developed several predictive models for spotting distance from torching and crown fires derived from the firebrands motion model. Tse and Fernandez-Pello (1998) presented a predictive numerical model for calculating the trajectory and temperature variation of melting spherical copper particles, aluminium particles and burning firebrands with various sizes and wind conditions. They found that the embers with lower density and larger diameter have the potential to fly longer distances because of greater drag force. Woycheese et al. (1999) introduced the wooden spherical firebrand lofting and propagation model using the Baum and McCaffrey plume model (Baum and McCaffrey 1989) and modelled the equations of motion. They also calculated variations of wind speed with height. They stated that firebrands released at a higher height of the fire plume into the air stream burn with lower spotting risks. The initial diameter and the burning rate of firebrands were found to be important parameters in firebrand propagation distance. Anthenien et al. (2006) investigated the trajectory of spherical, cylindrical and disk fire embers lofted from a bent-over fire plume in a cross-wind. The trajectory model included the motion of fire embers, their combustion and convective-radiative heat transfer during their flight time. In the study, the disk-shaped wooden fire embers could travel further distances in comparison with spherical and cylindrical fire embers, and land on the ground while they were still alight. Also, it was shown that the burning embers' propagation distance has an approximately linear relation with wind speed.

2.3.3. Firebrand transports (Experimental results)

2.3.3.1. Existing apparatuses

Wind tunnels have been an effective experimental apparatus for many years and have been used by many researchers to study aerodynamic and combustion properties of various firebrands. Tarifa et al. (1967) designed a horizontal and two vertical wind tunnels to measure aerodynamic drag and terminal velocity of tethered and untethered firebrand samples. The aerodynamic drag of tethered firebrands were

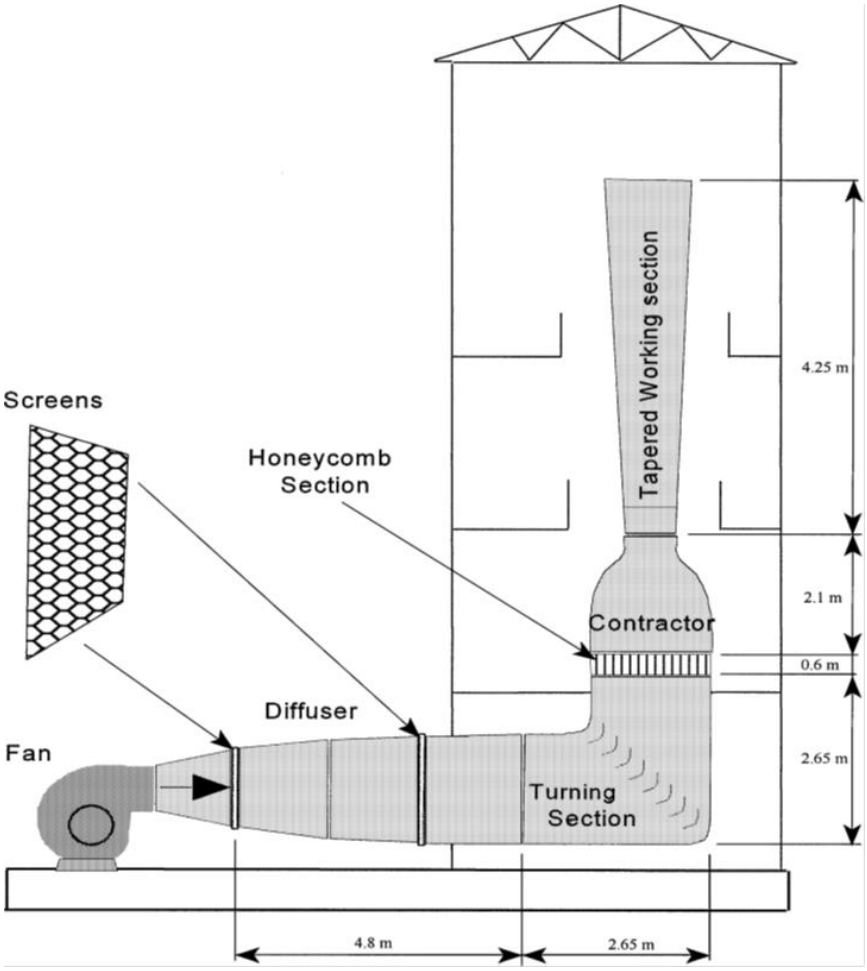

Figure 2.3 Scheme of wind tunnel with tapered work section designed by Knight (Knight 2001).

measured with a two-component ring-type strain gauge balance in a suction horizontal wind tunnel of 5800 mm length where the wind speed could continuously vary. They also used a vertical wind tunnel to measure the terminal velocities of samples by holding firebrand samples with a thin steel wire provided with a counter-balance in the intake of the tunnel. Tarifa et al. (1967) used another suction vertical wind tunnel with 3000 mm height and tapered work section to measure the falling terminal velocity of untethered burning embers.

The application of wind tunnels has been continued in the current century to study the combustion and aerodynamic properties of various firebrands. Similar to the work of Tarifa et al. (1967), Knight (2001) designed a vertical wind tunnel with a tapered work section of 4250 mm height to study untethered samples of burning barks (see figure 2.3). The author improved the non-uniformity of flow induced by an air blower. He removed the tumbling motion of samples inside the work section

using a 4800 mm horizontal intake which was formed as a diffuser and was filled with two screens. The intake section was connected to the vertical tapered work section through a 90° turning section filled with vanes. Air flow passing through the

Figure 2.4 Vertical wind tunnel used by Almeida et al. for experiments on firebrands (Almeida et al. 2009).

vanes flows through a honeycomb to avoid large eddies and then is directed to the working section through a contractor. The author could decrease the flow non-uniformity to less than 0.5%. The same vertical tunnel was also used by Ellis (2013) to study the aerodynamic characteristics of untethered stringy bark of Eucalyptus obliqua. He found that the untethered samples of stringy bark collided with the walls and resulted in the fragmentation or adherence of samples to the wall that affected their combustion. The author carried out modifications to minimise the problem by using multiple layers of screens at the bottom of the work section. Following this

modification, Ellis (2013) presented several experimental formulas to estimate stringy bark firebrands' flameout time, burn out time and ignition duration. Almeida et al. (2009) investigated the effect of wind flow direction on firebrand orientation using a 6.5 m vertical wind tunnel. The samples of Pinus Pinaster cones and eucalyptus globules bark were inserted in the tapered-shape work section of the tunnel (see figure 2.4). The suction blower on the top of the tunnel was capable of providing wind speeds up to 30 m/s. The authors found that the burn-out time of the samples is reliant on their combustion mode (flaming or smouldering) and the orientation of the samples. An empirical model was presented to predict the mass

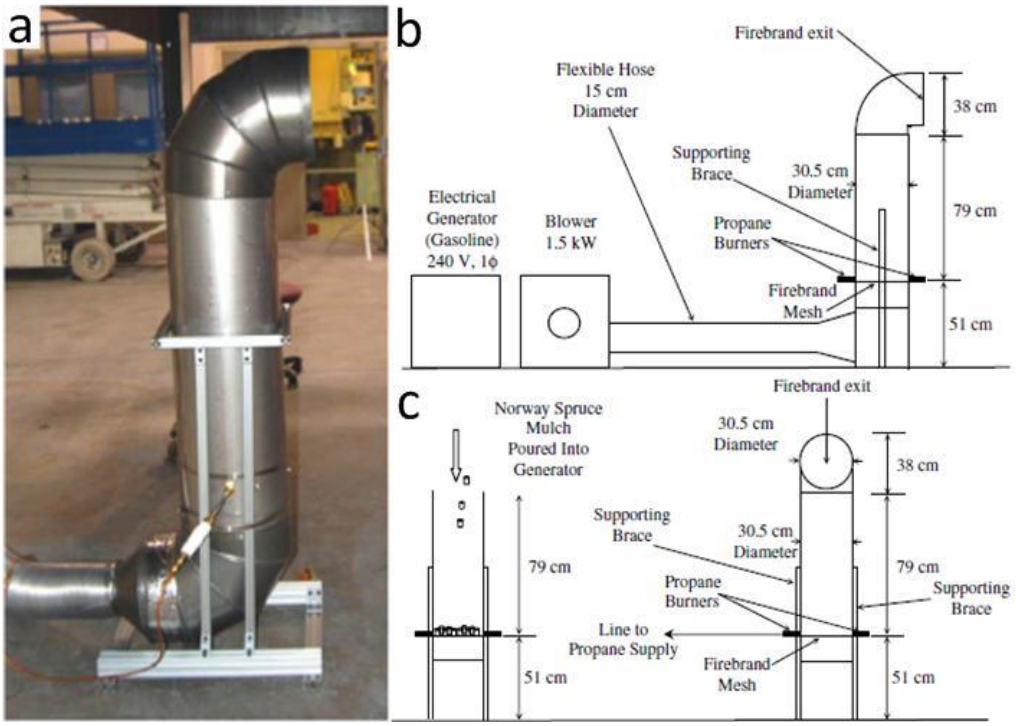

Figure 2.5 full scale NIST firebrand generator (NIST dragon) a) picture of firebrand generator, b) side view scheme, c) cross section scheme (Manzello et al. 2010; Manzello et al. 2011).

loss of the eucalyptus bark and pine cones embers.

The introduction of the NIST firebrand generator by Manzello et al (S. L. Manzello et al. 2008) was a breakthrough in firebrand studies as it made the simulation of actual firebrand attacks possible. The device generates ongoing fire embers with various sizes that are comparable with the sizes of real wildfire firebrands (see figure 2.5). The device consists of two stacked pipes. The upper pipe is removable for placing vegetation on a fine wire mesh mounted at the top side of the lower pipe. Underneath the fine wire mesh, two gas torch burners are inserted from the sides into

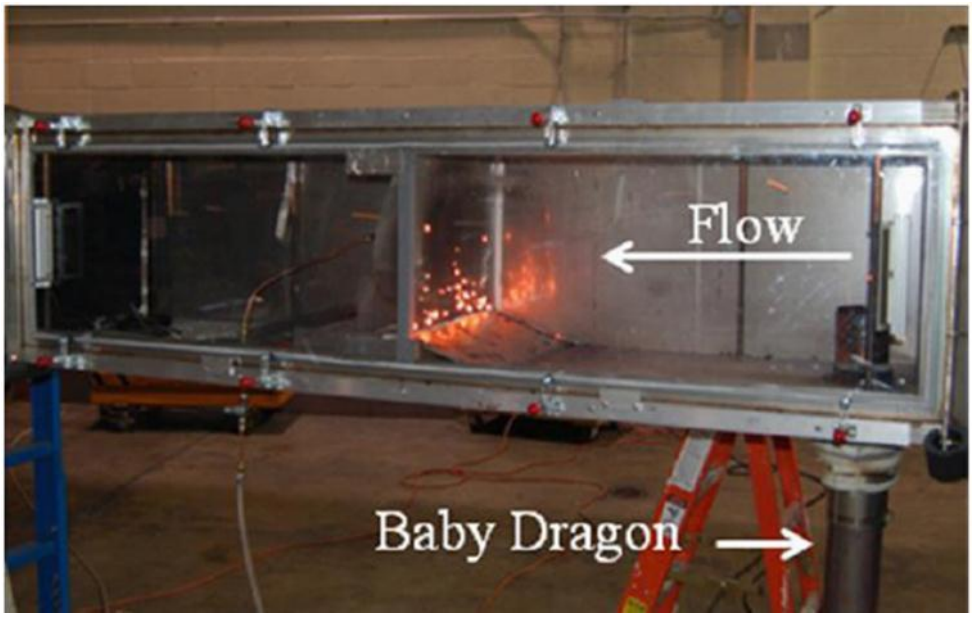

Figure 2.6 picture of reduced scale experiments on mesh screen against firebrand attack in a bench top wind tunnel coupled to Baby dragon (Manzello et al. 2010).

the pipe. An air blower is connected to the pipe through a flexible hose pipe flowing air into the generator which helps lofting of firebrands outward. The so-called NIST dragon was also reproduced in a reduced scale to be utilised in laboratory-scale experiments (see figure 2.6). The reduced scale NIST dragon (baby dragon) was mounted underneath a horizontal wind tunnel with 50 cm×50 cm square test section (Manzello et al. 2011; Manzello et al. 2012). Manzello and Suzuki (2012) also introduced an upgraded version called the NIST continuous feed baby dragon with the capability of generating a constant firebrand shower. The working procedure of the upgraded device is the same as the NIST baby dragon. The upgraded device is fed with a conveyer that delivers the wood cribs in a pre-set time interval to the gates which are connected to the lower pipe of the device. The gates are opened one by one and the wood cribs are poured on the fine mesh in the lower pipe. In this case, the firebrand generator can work for an unlimited period as long as the wood cribs are being supplied by the conveyer. The continuous feed is also assembled on the full-scale NIST firebrand generator (see figure 2.7) to provide extended firebrand attacks (Manzello and Suzuki 2013).

The NIST Firebrand generator was also reproduced by the Institute for Business and Home Safety (IBHS) research centre to investigate the vulnerabilities of house components under firebrand showers (Stephen L. Quarles 2012). The generator was installed as five sets where each set has three stacks extended at three different heights of 1.82 m, 3.35 m and 6.4 m in the research centre wind tunnel. The wind

tunnel has a floor area of 1950.96 m^2 which is facilitated with 105 fans of 1.67 m diameter and provides wind speed up to 59 m/s (category 3 hurricane wind speed) (Harris 2011).

Figure 2.7 Picture of NIST continuous feed firebrand generator for full scale experiments (Manzello & Suzuki 2013).

2.3.3.2. Experimental studies on firebrand trajectories

The early researchers used sample firebrands with an arbitrary wooden machined shape to study aerodynamic and combustion properties of firebrands. Tarifa et al (1967) measured the drag changes of firebrand samples while they were burning in the wind tunnel. The authors used cylindrical and spherical firebrands of five kinds of wood with different sizes and moisture contents. The weight and aerodynamic of fire embers were recorded as a function of time. They showed that the shapes of fire embers have a great effect on their horizontal flying distance. The study discovered that cylindrical fire embers have greater potential to fly more distance in comparison with spherical ones. Also, the type of firebrands has a considerable effect on the flying distance of fire embers. Despite the difficulties in measuring the terminal velocity of untethered firebrands due to the tumbling motion of firebrands, a good agreement was found between untethered and tethered firebrands for aerodynamic drag. It should be noted that tethered firebrands refers to firebrands that are hanged

by a wire in the wind tunnel, while untethered firebrands freely move in the wind tunnel.

Some researchers measured the aerodynamic and combustion properties of a single firebrand using vegetation samples with real shapes. Almeida et al. (2009) studied pine cones and curled Eucalyptus bark firebrands in a vertical wind tunnel which was described in the previous section. The tethered firebrands were exposed to no wind and windy conditions (wind/no wind) at different orientations. The authors found that the combustion duration decreases with the increase of wind speed and is influenced by the orientation. The pine cone firebrands showed a higher combustion duration in comparison with the Eucalyptus bark firebrands. In another study, the authors performed experiments on the effect of firebrand orientation at varying wind speeds for hollow cylindrical Eucalyptus globulus bark (Almeida et al. 2013). They found that apart from wind speed and firebrand orientation, the sign and magnitude of variation of the parameters affect their combustion duration. Ellis (2013) investigated the ignition time, flameout time and burnout times of stringy bark samples with various sizes. He also recorded the remaining mass of firebrands after burn-out time. The author presented several formulas for estimating the combustion of stringy bark firebrands and found a spotting distance of 800 m to 1480 m is the most probable case for this type of firebrand.

In recent years, the development of firebrand generators provided an opportunity to study the flying distance of firebrands in a simulated firebrand shower. The NIST dragon was placed in the Fire Research Wind Tunnel Facility (FRWTF) of the Building Research Institute of Japan. It has a test section of 13.5 metres height, 5 metres width and 15 metres length (Manzello et al. 2008b). The authors used cylindrical and disk wood pieces with different sizes machined from Ponderosa Pine dowels and fed them into the NIST firebrand generator. One hundred and fifty-seven water filled pans (49.5 cm × 29.5 cm) were used to collect the firebrands downstream of the firebrand generator. The mass and surface area of the firebrands were measured after being dried in an oven. Also, the lofting distance of firebrands at no wind and wind speeds of 3 m/s, 6 m/s and 9 m/s were measured. They found a significant effect of wind speed and firebrand sizes on the trajectory distance of firebrands. The flying distance of both cylindrical and disk shape firebrands increased with the increase of wind speed. Harris (2011) used the IBHS facility to

validate a model based on Monte Carlo simulations for flying distance of firebrands. In that work, various sizes of wooden dowels as well as a mix of wood chip and pine barks were fed into the generator to simulate firebrand showers. The firebrands were collected downstream of the generator using 18 water-filled pans at a tunnel wind speed of 8.94 m/s. His study confirmed the important effect of the wind speed on firebrand flying distance. Recently, the NIST firebrand generator was loaded with Poplar wood cubes with a mass of 1.44 g and projected area of 12.7 mm^2, and the firebrands flying distance in no wind and wind conditions were measured (Zhou et al. 2014). Based on their results, the increase of wind speed increases the flying distance and has an effect on their mass and projection area distribution. Also, the shape and density of the loaded wood pieces were important parameters on the mass distribution of firebrands.

2.3.4. Size and mass characteristics of real firebrands

The size of firebrands affect the flying distance of firebrands as discussed previously. In this section, the results of research on measuring the size of real wildfire brands are presented. Firebrands generated from Douglas-fir trees were investigated by Manzello et al (S. L. Manzello et al. 2007). Several Douglas-fir trees with heights of 2.6 and 5.2 metres with a moisture content varying from 10% to 50% were burnt in laboratory conditions. Firebrands were collected using many water-filled aluminium pans surrounding the burning trees. A number of Douglas-fir trees could not produce any firebrands when the moisture content of the trees were above 30%. Also, 83% of the collected firebrands had a mass of less than 0.3 g. For the trees with the same moisture content, the mass distributions of the firebrands were similar except higher trees produced heavier firebrands. Manzello et al. (2008) investigated the size of firebrands generated by the NIST dragon firebrand generator. In their work, Pine dowels were cut in different sizes of cylindrical and disk shapes and were loaded in the generator. Firebrands were collected using arrays of water-filled pans and then were dried in an oven. All collected firebrands had masses less than 0.2 g and surface areas of less than 1000 mm^2. Manzello et al. (2009) measured the size of firebrands generated by burning Korean pine. A 4-metre high Korean pine was burnt in the laboratory, and the firebrands were collected with the same method used in the

Douglas-fir trees experiments (Manzello et al. 2007). Similar to the Douglas-fir trees, the collected firebrands had cylindrical shapes and a large percentage had a mass of less than 0.3 g. The Korean pine could not generate firebrands unless the trees' moisture content was less than 35%. However, Korean pine produced more firebrands compared to Douglas-fir trees and the difference was identified to be the dynamic burning process of the two species.

In Wildland-Urban Interface (WUI) fires, the burning buildings can also be a source of firebrand generation. Hence, some research studies considered the firebrand generation regime of burning structures. Suzuki et al. (2012) collected and measured firebrands generated from a burning house in California. The firebrands were collected by a series of water pans at distances of 4 and 18 metres from the house. The collected firebrands were dried in an oven and then the mass and projected areas of the firebrands were measured. They found that 85% of the firebrands collected at 18 metres and 68% of firebrands collected at 4 metres away from the house had a mass of less than 0.1 g. In terms of firebrands' projected areas, 95% and 96% of the collected firebrands at 18 metres and 4 metres away from the house were less than 10 cm^2, respectively. Firebrand generation from wall and re-entrant corner assemblies were investigated in full scale laboratory tests (Suzuki et al. 2013). The studies were carried out in the Fire Wind Tunnel Facility at the Building Research Institute of Japan that is capable of producing a wind speed up to 10 m/s. The assemblies were burned by a T-shaped burner and the fan started operating on the assemblies immediately after observing the flaming combustion. The results indicated that most collected firebrands in all experiments had a mass less than 1 g and a projected area of less than 1 cm^2. Suzuki et al. (2014) recently studied the firebrand generation from a burning structure in laboratory conditions. The structure consisted of wooden studs and exterior walls as well as a roof that all were made of Oriented Strand Board (OSB). A flashover inside the structure was created using a remote-controlled electric match to ignite a sofa inside the structure at a fixed wind speed of 6 m/s. In this case, more than 90% of the collected firebrands had a mass of less than 1 g and 56% were less than 0.1 g. In terms of firebrands' projected areas, more than 90% of firebrands were less than 10 cm^2.

There are several works on measuring the size of firebrands in a real wildfire. Foote and Manzello used a trampoline sheet of 3.7 metre diameter that was mounted 0.9

metres off the ground during the Angora fire in 2007 (Foote, Liu, and Manzello 2011; Manzello and Foote 2012). The hole areas on the trampolines were measured by means of image processing. They also investigated the burn patterns of firebrands on partly-affected buildings (not destroyed). More than 85% of the holes were less than 50 mm^2 in size. Moreover, inspection of burn patterns on the buildings indicated that the majority of the scorch areas were less than 40 mm^2 with a maximum size of 202 mm^2. Similarly, Rissel and Ridenour (2013) applied trampoline sheets on site during the Bastrop Complex fire, Texas. Seven trampolines with a diameter of 3.8 metres were mounted horizontally 0.9 metres from the ground. After the incident, the trampolines were collected and the sizes of the holes were measured using image processing. The authors reported that more than 90% of holes were less than 50 mm^2 area with a maximum size of 175.80 mm^2. The sizes of firebrands were measured in a prescribed fire in Pineland National Reserve in southern New Jersey (USA) (El Houssami et al. 2015). Twenty water-filled aluminium pans were placed on fire-resistant gypsum boards on the ground in three sites to collect firebrands. Wire nets were placed inside the pans to easily extract the firebrands from the water. Then the collected firebrands were dried in an oven and any mass of firebrands less than 5 mg was not counted in the measurement. It was found that 70% to 89% of firebrands were from the bark slices and the rest originated from branches. Most of firebrands had a mass between 10 mg and 20 mg. However, a few firebrands were found with masses that exceeded 100 mg. Also, about 80% of firebrands had cross-sectional areas less than 20 mm^2.

2.3.5. Effect of firebrands on fuel beds

Firebrands start spot fires when they fall on fuel beds. In this case, the heat transferred by the burning firebrands to the fuel bed increases the temperature of the fuel bed to reach the ignition point. Many previous research studies identified and addressed the parameters that are effective in the ignition of fuel beds. Manzello and his colleagues investigated the effect of firebrand size on the ignition of shredded paper, pine needles and cedar crevices (Manzello et al. 2006). In their work, the fuel bed's moisture content was varied from 0% to 11%. Glowing and flaming firebrands were sourced from machined Ponderosa pine in a disc shape with two diameters (25 mm and 50 mm), and were deposited on different fuel beds at wind speeds of 0.5 m/s

and 1 m/s. The authors reported that the single glowing firebrands were only able to ignite dry shredded paper. Also, they carried out experiments with four glowing firebrands and found that if they had a 50 mm diameter, they could ignite pine needles under 1 m/s wind speed. On the contrary, the single flaming firebrands started fire in all the cases except cedar crevices, however, the cedar crevices ignited in the experiments with three flaming firebrands. The flaming firebrands showed a great potential in inducing ignition on the fuel beds in comparison with glowing firebrands. The authors concluded that the size, number flux and wind speeds are the important parameters in the possibility of fuel bed ignitions. In another study, (S. Manzello et al. (2008) used cylindrical Ponderosa pine firebrands for the ignition of shredded paper, pine needles and hardwood mulch with moisture content varying from 0% to 11%. The sample firebrands were in two sizes: 5 mm diameter and length of 51 mm; and 10 mm diameter and length of 76 mm. All single-flaming cylindrical firebrands caused ignition in all the cases of the fuel beds except for hardwood mulch with 11% moisture content. By comparing the results of the two studies on the two shapes of glowing firebrands, Manzello et al. (2008) stated that the glowing surface area of firebrands and their number are the important parameters to determine whether ignition of fuel beds occurs.

Ganteaume et al. (2009) assessed the flammability of different fuel beds and capability of various flaming and glowing firebrands to ignite them. It was reported that the fuel beds' flammability is related to the type of fuel beds, their moisture content and bulk density. In the case of firebrands, type of firebrands and air flow were found as the effective parameters in their capability to ignite the fuels. The authors reported a higher fuel bed ignition probability with the flaming firebrands, while the glowing firebrands were able to ignite fuel beds only with larger mass and in the presence of air flow over the fuels. They stated that the ignition probability of a fuel bed by glowing firebrands was highly related to the mass of the firebrands and the air flow on the fuel bed which supplied oxygen for the firebrand combustion. In contrast, the main factor in the ignition probability of a fuel bed by a flaming firebrand is the radiative and convective heat transfer which depend on the flame shape rather than particle mass. Ganteaume et al. (2009) found that increasing the airflow up to 4.5 m/s over a fuel bed decreases its time to ignition by deposition of glowing firebrands, and increases the probability of fuel bed ignition. However, the

effect of wind speed higher than 4.5 m/s on the ignition of fuel beds by glowing firebrands was not reported. The effect of glowing firebrands on the ignition of OSB (oriented strand board) and plywood crevices at different angles (60°, 90° and 135°) were studied since both materials are common materials for roofing assemblies (Manzello et al. 2009). They used machined Ponderosa pine in cylindrical shapes with 10 mm diameter and length of 76 mm as firebrands. The cylindrical glowing firebrands were deposited on fuels under two wind speeds of 1.3 m/s and 2.4 m/s. The authors observed ignition of the fuel beds only at the wind speed of 2.4 m/s. It was found that there was a 98°C difference in the maximum surface temperature of glowing firebrand between the two cases of wind speed. They explained that the heat flux between the glowing firebrand and fuel bed is more at higher wind speed (2.4 m/s) as a result of the higher surface temperature of glowing firebrands. It was also stated that the increasing number of glowing firebrand deposition increases the probability of fuel bed ignition due to increasing the heat flux from firebrands to fuel beds.

Ellis (2011) investigated the effect of fuel bed moisture content and their ignitability by samples of stringybark firebrands (with 15 mm width, 50 mm length and 5 mm thickness). The author used pine needle fuel beds with moisture content ranging between 2% and 8%. The fuel beds were tested at no wind and wind conditions (1 m/s) provided by a domestic blower during the experiments. In all the experiments, the flaming firebrands induced flaming ignition on the fuel beds. In the no wind condition and glowing firebrands, there was no observation of flaming ignition of fuel beds. However, for the windy condition, the mass of glowing firebrands and the fuel bed moisture content were found to be significant parameters for a successful fuel bed flaming ignition. The effect of moisture content of fuel beds on their time to ignition by firebrands deposition was also measured by Yin et al. (2012), who used cubes of fire wood (20 mm × 20 mm × 10 mm) with moisture content of 12% to generate glowing firebrands. For the fuel beds, pine needles with moisture content of 24.9–65% at a wind speed of 3 m/s were applied. It was reported that the time to ignition of fuel upon the impact of glowing firebrand was affected by their moisture content. As the moisture content rises, the time to ignition of fuel beds increases.

The ignition possibility of shredded hardwood mulch with various moisture content under wind driven firebrand bombardment was investigated using the continuous

NIST firebrand generator (see section 2.3.2.1) (Suzuki et al. 2014). The fuel beds were placed in a re-entrant corner assembly and was exposed to firebrand showers at two different wind speeds of 6 m/s and 8 m/s. Increasing the number flux of firebrands caused firebrand accumulation on the fuel bed and could even ignite mulch with a moisture content of 74%. In addition to the number flux of glowing firebrands, the authors addressed the great effect of wind speed and firebrand surface contact area as two other important parameters in the ignition probability of mulch beds. Ellis (2015) measured the ignition probability of dry eucalypt forest litters based on the impact of flaming and glowing firebrands. The flaming firebrands were produced by cutting a bamboo stick to samples 50 mm long. By contrast, the glowing firebrands were created as samples 50 mm long and 15 mm wide with thicknesses ranging between 1.3 and 2 mm that originated from shed flakes of Eucalyptus globulus trees. All firebrand samples were oven dried and had moisture content ranging between 3–5%. The firebrands were deposited on fuel beds at their terminal velocity using a wind tunnel with a vertical truncated conical test section. It was reported that the fuel bed moisture content had a significant effect on the fuel bed ignition by flaming firebrands since the reduction in the moisture content increased the probability of ignition. Also, increasing the wind speed up to 2 m/s increased the fuel bed's ignition probability. However, a further increase of wind speed to more

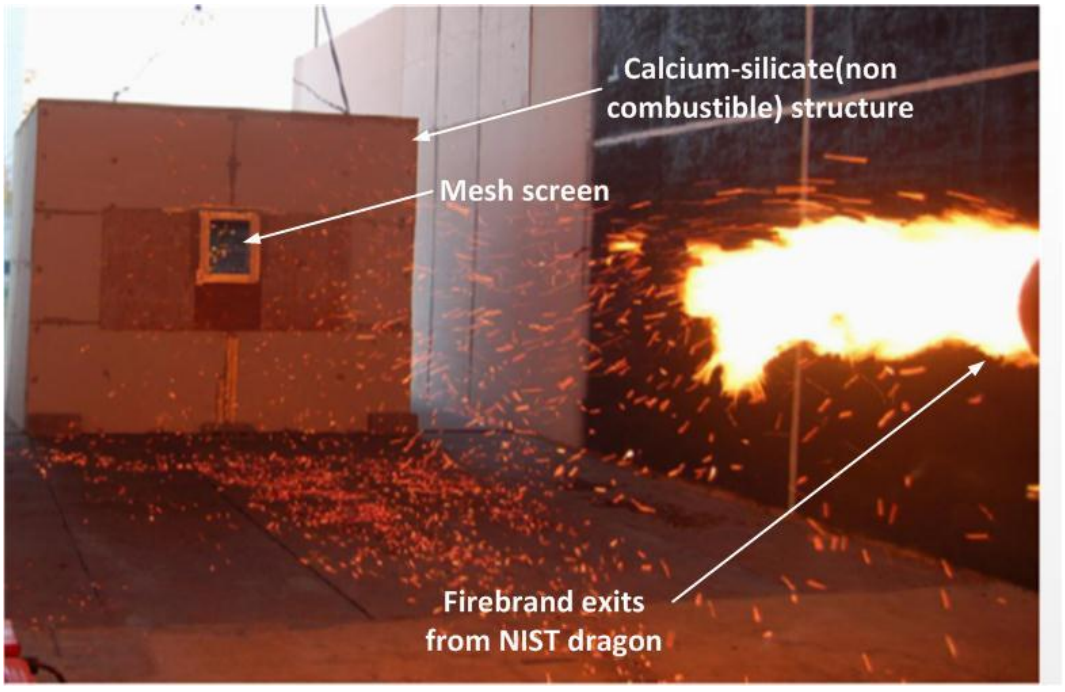

Figure 2.8 picture of full scale experiments on vents mesh screen against firebrand showers using full scale NIST firebrand generator (Manzello et al. 2011).

than 2 m/s had an adverse effect as it increased the rate of heat loss. In the case of glowing firebrands, the authors stated the possible effect of turbulence in addition to the effect of wind speed.

2.3.6. Metal screens versus firebrand attacks

A pioneering work by Manzello and his colleagues following the development of the NIST firebrand generator broke the silence about the blocking mechanism of screens against firebrands for the first time (Manzello et al. 2007). The authors fed 2.1 kg Korean pine mulch in the NIST firebrand generator to produce fire ember showers. Three different screens with opening sizes of 6 mm, 3 mm, and 1.5 mm were mounted on a gable vent of a cubic calcium silicate structure which was erected in the test section at a distance of 7.5 metres from the firebrand generator. The test section has a height of 13.8 metres and a width of 5.0 metres and is located in the Fire Research Wind Tunnel Facility (FRWTF) of the Building Research Institute in Japan. Two pans filled with shredded paper were placed behind the screen in the structure and the wind speed in the tunnel was set at 9 m/s. It was reported that firebrands do not quench at the presence of screens and burn until they can pass through their openings. The passed firebrands could ignite the shredded paper in all the cases.

Four years later, Manzello and his colleagues carried out the same investigation in both laboratory and full scale experiments (Manzello et al. 2011). In full scale experiments, where the layout was the same as their previous investigation (Manzello et al. 2007), different wire screens, with the cell size varying between 1.04 mm and 5.72 mm, were mounted on a vent with an area of 1600 cm^2. In that work, the firebrand generator was loaded with 2.1 kg of Norway spruce mulch and the wind speed was set at 7 m/s. In addition to the shredded paper, cotton and cervices of Oriented Strand Board (OSB) and wood were placed behind the mesh in the structure. Also, in one round of experiments, shredded paper was loaded on the crevice and the behaviour of this fuel bed arrangement behind the mesh was also observed. As per the previous investigation, the study discovered that the firebrands are able to penetrate wire meshes and ignite the materials behind the mesh. The wire mesh could not quench the firebrands and firebrands burned until they could fit the opening size and pass through the mesh. The authors calculated the penetration ratio

of the firebrands for each screen. The penetration ratio (PR) is defined based on the number of firebrands leaving the mesh (FB_l) to the number of firebrands approaching the mesh (FB_a) in a time interval (Δt) and is expressed as;

$$PR = \frac{\sum_{t=0}^{\Delta t} FB_l}{\sum_{t=0}^{\Delta t} FB_a} \times 100 \qquad (2.14)$$

Manzello and his colleagues also measured the retention time of firebrands on the mesh. The retention time is defined as the time interval that an approaching firebrand can burn and fit the mesh opening size. Unsurprisingly, it was found that the penetration ratio rises when the opening size increases, while the retention time of firebrands increases when the opening size reduces. The authors also carried out similar experiments in a laboratory-scale wind tunnel (Manzello et al. 2011). They fitted the small-scale NIST dragon (baby dragon, as discussed in section 2.3.2.1) in a benchtop wind tunnel and set the wind speed to be the same as the full-scale experiments. The mesh area, sizes and fuel beds were the same as full-scale experiments. In order to trap firebrands leaving the mesh and direct them onto the fuel bed, a very fine mesh was inclined behind the first mesh. There was similarity between the full scale and laboratory scale results. Cotton ignited in both full- and laboratory-scale experiments. The crevice was ignited in all cases for all mesh sizes above 1.04 mm. Similarly, the shredded paper ignited in all the experiments except for the minimum mesh size of 1.04 mm. In this case, the ignition was observed for one test in the full-scale experiment out of three attempts; however, no ignition was recorded for the shredded paper in the laboratory tests.

Moreover, firebrand intrusion into the metal mesh screens mounted on eave vents was investigated in the IBHS wind tunnel facility (see section 2.3.2.1) (Quarles 2012). Five sets of firebrand generators were simultaneously loaded with a mix of bark mulch and wood dowels, and the tunnel wind speed was set in the range of 4.5 to 6.7 m/s. The metal screen that covered eave vents of the test building had an opening size just less than 6 mm. Similar to previous investigations, it was found that the screen could not eliminate the firebrand penetration; however, the reduction in the number and size of firebrands was evident when the mesh size reduced.

2.3.7. Summary

The literature review indicated that firebrands can be sourced from any burning vegetation. However, it was indicated that not all firebrands are dangerous since only the firebrands with the ability to burn and fly for a sufficiently-long time present a significant risk. The firebrands can be in a glowing or flaming state of combustion during their impact. The latter is very scarce except in short distance spotting. The review of modelling studies on firebrand spotting mechanisms showed the effect of three forces on the transport of firebrands. Drag, lift and gravity were the forces that determine the ability of firebrands to fly. In addition to the above forces which are dependent on the dimension and mass of firebrands, the combustion rate of firebrands is another important factor for firebrand transportability. The dimensions and mass of firebrands continuously change as they burn. Therefore, the burning rate of firebrands governs the size of firebrands at any stage of their flight path and their burning duration.

The above parameters were subject to many studies to define the characteristics of real wildfire firebrands. The common approach in the experimental studies was the application of a wind tunnel. The firebrands were ignited outside the tunnel and inserted into the wind tunnel to measure the burning rate and also the aerodynamic characteristics of firebrands. The efforts to simulate firebrand attacks led to the introduction of the NIST firebrand generators. The details of firebrand generators, introduced by Manzello and his colleagues, were explained. The NIST firebrand generator is capable of simulating firebrand attacks with firebrand sizes comparable to those in real wildfires. The NIST firebrand generator was also reproduced by the IBHS research centre, with details presented in this chapter.

The experiments on measuring the size of firebrands from burning vegetation, structures or during actual wildfires showed that a great portion of firebrands generated in wildfire incidents have a mass less than 0.2 g and projected area less than 500 mm^2. However, the huge differences in the size of firebrands from various sources were observed.

There are many effective parameters to determine firebrand-induced ignition on fuel beds. The moisture content and type of fuel beds were the effective parameters in the

ignition of fuel beds. It was revealed that flaming firebrands have a greater potential to ignite various fuel beds than glowing firebrands. In the case of glowing firebrands, mass, surface area and number of firebrands as well as the wind speed on the fuel bed were the governing parameters for the probability of fuel bed ignition.

Available studies on the performance of wire meshes during a simulated firebrand attack showed the inability of wire mesh to quench firebrands. Firebrands burn until they can fit the opening size, and ignited different fuel beds. The penetration ratio and retention time for the firebrands were explained. The penetration ratio increases with increasing opening size, while the retention time decreases with the increase of opening size.

2.4. Research gaps

The computational study on the view factor of an object in respect to a fire through metal screens indicates the effect of decreasing a screen's porosity on the reduction of the view factor. The computational study assumed a uniform cell size which is nearly impossible in practice. Even with perfect weaving of wires, still gaps and misalignment can be formed at a later time. As the view factor is highly dependent on the geometry of the screens, the possible deficiencies might change the true view factor. The limitations of previous studies underline the necessities of an experimental study to obtain a more realistic result.

The experiments with the NIST firebrand generator were a great breakthrough on identifying the mechanism of firebrands passing through the screens. However, there are still many uncertainties that need to be addressed by further experiments. The previous investigations were carried out for building vents' mesh screens and were limited to certain mesh sizes and layouts to avoid blocking effective ventilation. However, such limitation is not the case for standalone screen barriers. Based on the literature review in this section, the following research gaps on the passage of firebrands through screens have been identified:

- **Improving the experimental setup**: The NIST baby dragon is a viable design to study screen performance against firebrand attacks for laboratory-scale experiments. However, there is no evidence that the design is capable of working at wind speeds higher than 10 m/s, especially for screens with

low porosity. Therefore, further improvement is required to facilitate the experiments at higher wind speeds, which is necessary in this work. A thorough study on improving the current firebrand generator will be conducted to meet objective 2 (see section 1.8, page 10).

- **Effect of vegetation types other than wooden mulch**: The available studies are unable to explain whether the same mechanism of passage of firebrands can be expected for different types rather than mulch and wood pieces. In practice, a firebrand shower contains a combination of firebrands sourced from various types of vegetation. Based on the literature review, two types of vegetation have been selected to generate firebrands. Eucalyptus leaf has been selected as a source to examine firebrands that are risky for short distance spotting. Leaf firebrands seem to be the hardest firebrands for screens to contain due to their weak structure and intense fragmentation. Therefore, the leaf firebrands have been used in the first series of experiments to represent the worst case scenario to measure the effect of geometries on screen performance against firebrands (without a buffer zone) (section 5.2). The motivation for using hardwood mulch for the second series of experiments is its use in previous studies on metal screens. Mulch firebrands burn longer, have a higher heat release rate and are risky for long distance spotting (as compared to leaf firebrands). Hence, they provide the worst case scenario with respect to embers flying a longer distance across buffer zones and greater likelihood of ignition of fuel beds. This made hardwood mulch the preferred firebrand source for the buffer zone experiments (section 5.3).
- **Effect of high wind speed**: The literature did not address the firebrand behaviour hitting the screen at wind speeds higher than 9 m/s. As this review explained, the wind speed has a great role on firebrand transport, burning rate and even their potential to ignite materials. Also, as discussed in chapter one, most fierce wildfires occur at wind speeds much higher than 9 m/s and therefore it is critical to understand the mechanism of firebrands' passage in that range of wind speeds. The application of a metal mesh as a barrier requires studies of their performance under much higher wind speeds, which was not important in the study of their application for covering house

openings where the wind speed is much lower. Objective 2 in this study focuses on improving the current design of the firebrand generator to facilitate experiments with high wind speeds. Therefore, this study is able to perform experiments with wind speeds greater than previous studies.

- **Effect of screen geometries**: The available literature does not provide information about the performance of screens against firebrand attacks with other possible configurations or geometries. The standalone screens can be designed in various layouts and geometries without the limitations that apply for mesh screens used in building ventilation. These geometries and configurations include screens with different opening shapes, manufacturing type, screen orientations and multi-layer arrangements. The above parameters are addressed in this study through completion of objectives 3-7 (see section 1.8, page 10).
- **Effect of buffer zone**: The previous investigations did not address the effect of the buffer zone between screen and protected object. It is understandable that the investigation focused on building vent screens and the buffer zone was not applicable. As described in this chapter, firebrands have a limited burning time and flying capability. Therefore, it is anticipated that a reduction in the number and capability of firebrands to induce ignition will occur by applying a buffer zone between the object and screen. Objective 8 of this study considers the effect of the buffer zone between the screen and the object on the performance of screens against firebrand attacks (see section 1.8, page 10).

Chapter 3

Direct Radiant Heat Flux (DRHF) through single square woven wire screen

3.1. Overview

One of the objectives of this research study is to find an experimental relation between direct radiant heat flux passing through a woven wire screen and porosity. In the previous chapter, the necessity of further experimental work to validate available computational formulas was explained. The results are presented and discussed in two major sections. In section 3.2, the selection of methodology and design of experimental setup are explained. In section 3.3, the experimental results are presented in four subsections. In subsection 3.3.1, the effect of tunnel vision is investigated by determining its angle for several screens. The passing ratios of light through four applied screens are measured and presented in subsection 3.3.2. In section 3.3.3, the passing ratios are discussed for the sources that are larger than the tunnel vision area, and in section 3.3.4 the experimental passing ratios are compared with the results of the computational equation (Eq.2.3). Finally a formula to estimate IRHF is presented in section 3.3.5. Section 3.4 provides a summary of the chapter.

3.2. Methodology and Experimental setup

3.2.1. Methodology

The wire screens, when exposed to a fire, emit heat due to increased temperature. Therefore, the effect of IRHF produced by hot screens interferes with measurements, and rendering them inaccurate. The alternative approach is to use a light source instead of a heat source. However, based on the Huygens–Fresnel principle, the interference of waves occurs if the waves encounter an obstacle or a slit which is of similar size or smaller with respect to the wavelengths (Tsokos 2010; Serway and Jewett 2010).

It is known that the visible spectrum is between 400 nm and 700 nm (Serway and Jewett 2010), while the wavelength of the infrared ranges between 700 nm to 1 mm (Serway and Jewett 2010). Previous studies show that the effective blackbody bushfire temperature is between 1007 K and 1327 K (Sullivan et al. 2003). Planck's law for spectral radiance measured per unit wavelength (λ) is defined as follows,

$$B_\lambda = \frac{2hc^2}{\lambda^2}\frac{1}{e^{\frac{hc}{\lambda\kappa T}} - 1} \qquad (3.1)$$

where λ is the wavelength, h represents Planck's constant, k stands for Boltzmann's constant, T represents absolute temperature (K), and c denotes the speed of light. Using Planck's law, the peak wavelength of a bushfire is approximately between 2183 nm (at 1327 K) and 2877 nm (at 1007 K). The intensity for wavelengths greater than 25 μm is less than one percent of that of the peak wavelength. Considering that the minimum opening size of the screens used in this work is nearly 40 times this value (0.987 mm, see section 3.2.2.1), no significant interference or diffraction pattern is expected to occur. This can be shown considering the minimum opening size (a) of the screens (0.987 mm) used in the experiments and the peak wavelength of the wildfire, approximately 3 μm. For this case, the diffraction angle using the Huygens principle (Serway and Jewett 2010) from the following formula gives an angle of 0.17°

$$Sin\ \theta = \frac{\lambda}{a}. \qquad (3.2)$$

This is insignificant with respect to the expected tunnel vision angles for this case (68.9°) using the analytical Eq. (2.6) (see section 2.2.2). It should be noted that a

blackbody is a diffuse emitter and light can propagate in all directions and illuminate an object from different angles. Therefore, the projected size of screen cells may fall in a range comparable to the infrared wavelength for the light coming from an oblique angle. In this case, the results obtained in the visible wavelength range may not be applicable for the infrared wavelengths. This possible effect requires investigation in this study.

First the transmittance of light through the screens is determined and then is linked to the view factor. Previous computational work shows that the view factor only depends on the porosity (see section 2.2.2, page 17, lines 22-23). The light passing ratio (PR) is defined as follows,

$$PR(\%) = \frac{I_{screen} - I_{dark}}{I_{no-screen} - I_{dark}} \times 100 \qquad (3.3)$$

where I_{screen} represents the detected light intensity by the spectrometer in the presence of a screen, $I_{no-screen}$ stands for the measured intensity in the absence of the screen, and I_{dark} is the captured intensity in the absence of the light source and screen. Based on the above discussion, an experimental setup with a light source was designed and all mechanical components were manufactured in-house. The side and cross section view of the experimental setup is shown in figure 3.1.

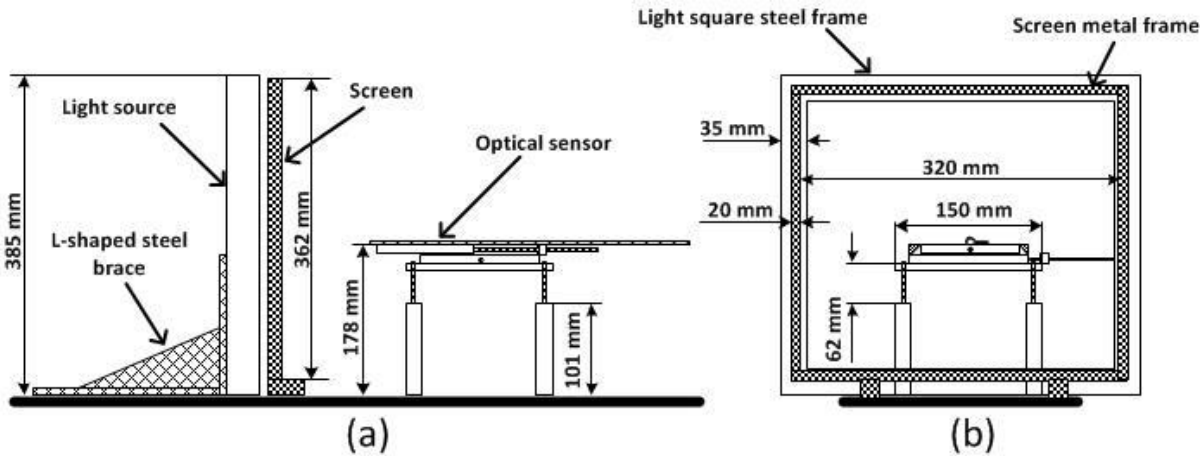

Figure 3.1 the scheme of DRHF experiment setups, a) side view, b) cross section view.

3.2.2. Experimental setup

The experimental setup consisted of a fluorescent light, a fixed frame for holding the screens, a metal board and a Visible-UV spectrometer with an adjustable stand (see

figures 3.1 and 3.2). All components were fixed on a rectangular metal board. The board was a heavy steel board (thickness = 28 mm) with screw holes at an interval of 25 mm in both horizontal directions in order to enable coarse adjustments of the distance between the components.

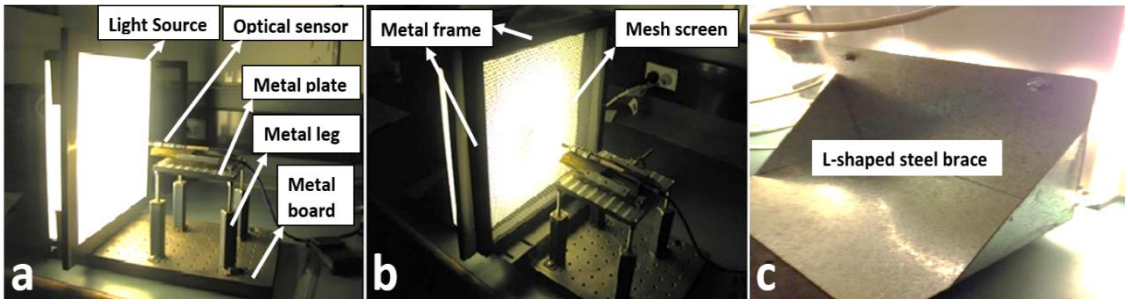

Figure 3.2 a) picture of experiment setup without screen, b) picture of experiment setup with screen, c) picture of L-shaped steel brace.

The light source and screen were set in parallel to each other and the optical sensor was mounted on the right hand side of the screen in figure (3.1a) perpendicular to the surface of both light source and screen (see figure 3.2). In the following sections, the details of experiment components and their layouts are presented.

3.2.2.1. Light source

The available commercial light sources in the market are dominated by technologies including incandescent lighting, Light Emitting Diodes (LED) and fluorescent lighting. Incandescent light sources such as bulbs and halogen lamps generate a considerable amount of heat due to the glowing filament in the lamps and these emit both infrared and visible waves. In contrast, LED and fluorescent lamps mostly emit light within the UV-visible spectrum range and both have a higher luminosity efficiency. The advantage of fluorescent light over LED is the reflective coating inside the tube reflecting the infrared spectrum back to the tube and makes infrared emissions by fluorescent lamps nearly zero (Ganslandt and Hofmann 1992). Besides this, LED lamps are concentrated and effective for point illumination while fluorescent lamps have diffusive light radiation in all directions (Ganslandt and Hofmann 1992). Fires are diffuse emitters (Hurley et al. 2016) and it seems fluorescent lamps are an appropriate choice from among the available lamps to represent diffuse emitters.

A square flat ceiling fluorescent light source (Auriga, Eglo) with a size of 310 mm was selected to be used in this work. The fluorescent light source included a square

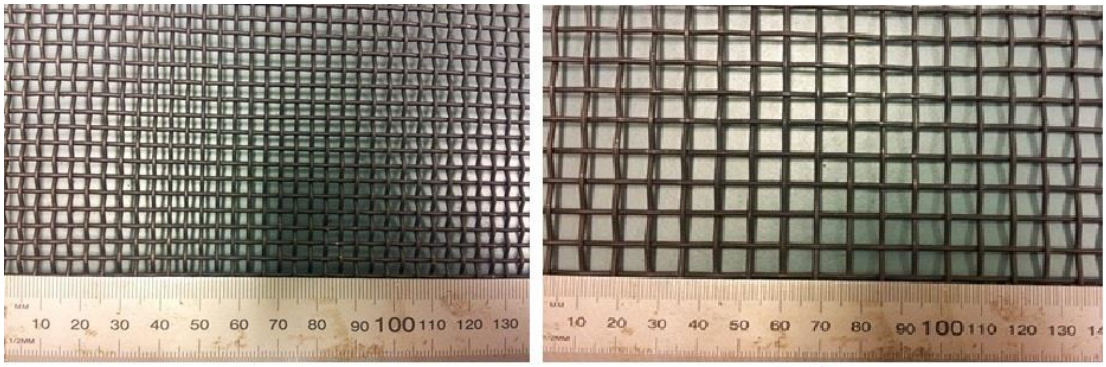

Figure 3.3 Applied square woven wire screen with porosity of a) 54%, and b) 66%.

steel frame (see figure 3.2a) and a circular fluorescent tube covered by a square semi-transparent glass deflector to improve the uniformity of the emitted light. The light source was secured to the metal board by an L-shaped steel brace (See figure 3.2c).

3.2.2.2. Screens

Four commercial square woven wire screens were applied in these experiments. The details of the woven wire screen geometrical properties are listed in Table 3.1. All screens were blackened to eliminate or reduce possible contribution of indirect radiation (reflection and scattering) (see figure 3.3). The screens were placed in front of the light source and held by a 32 cm x 32 cm metal frame (see figure 3.2b). The screens were fixed between the frame and a square bracket was tightened with bolts. At the base of the frame, two steel legs were welded to the frame. The legs were fixed to the required position on the metal board using screws.

Table 3-1 details of square woven wire screens applied in DRHF measurement experiment.

No	Cell size (mm)	Wire diameter (mm)	Porosity
1	1.53	0.54	41%
2	4.3	1.15	54%
3	6.25	1.5	58%
4	8.4	1.56	66%

3.2.2.3. Ultraviolet- Visible (UV) Spectrometer

A UV spectrometer (USB 4000, Ocean Optics) consisting of a fibre-optic sensor and a detector was used. Figure 3.4 provides the layout of the USB 4000 spectrometer light detection procedure. The fibre-optic sensor is connected to the detector via an SMA 905 connector (No. 1 in figure 3.4). The light is transmitted to the detector past

a dark piece of material which contains a rectangular aperture (slit) (No.2 in figure 3.4). The slit regulates the amount of light entering the detector and controls the resolution. Then it passes through to the filter (No. 3 in figure 3.4), which restricts the light to certain wavelength regions. The light is directed to the collimating mirror (No. 4 in figure 3.4) and then reflects to the grating groove (No. 5 in figure 3.4) where the light is diffracted into several beams. Then the light is reflected to the focusing mirror (No. 6 in figure 3.4), where the first-order spectrum is propagated towards the L4 detector (No. 7 in figure 3.4).The visible detector (No. 8 in figure

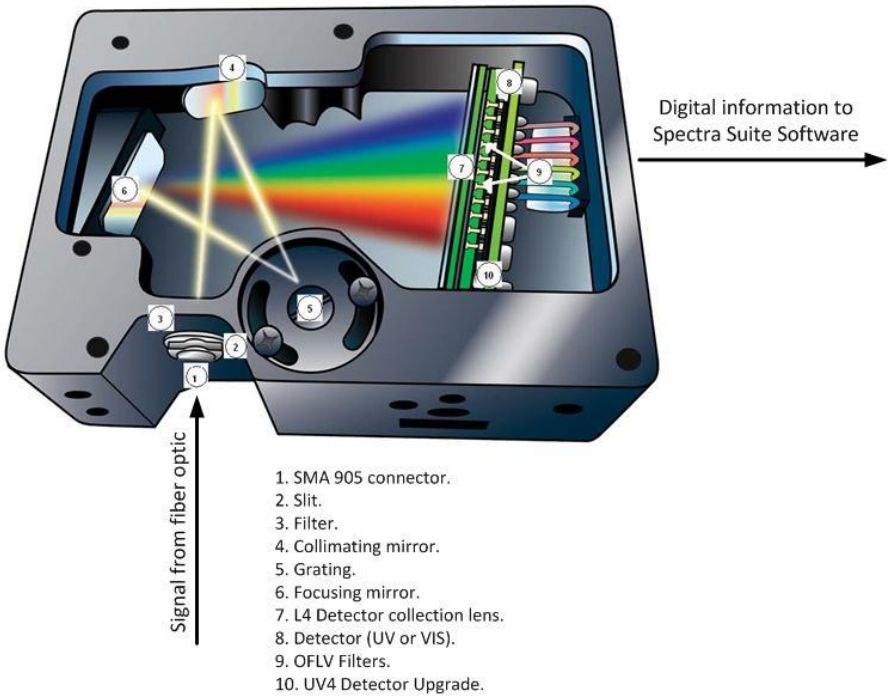

Figure 3.4 The scheme of USB 4000 (ocean optic) light detection procedure (Ocean Optics 2008).

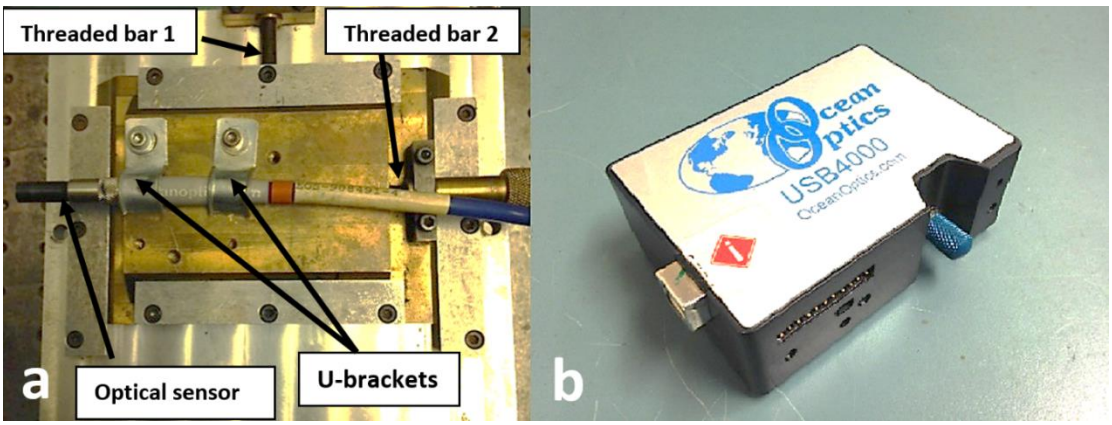

Figure 3.5 Setup of USB 4000 spectrometer applied in this study a) layout of optical sensor on metal plate, and b) picture of ocean optics USB 4000 spectrometer

3.4) collects the light, recording it as pixels and then converts it to digital responses. The Variable Longpass Order-sorting Filters (OFLV) (No. 9 in figure 3.4) block the second- and third-order lights (unwanted portions of the light spectrums) and the UV4 Detector (No. 10 in figure 3.4) is an optional feature that increases the performance of the spectrometer for wavelengths less than 340 nm. At the final stage, the digital information is transmitted to the software application via a USB port.

Table 3-2 details of spectrometer specifications applied in DRHF measurement experiment.

Specifications	Details
CCD detector	Toshiba TCD 1304AP (3648-element linear silicon CCD array
Detector range	200-1100 nm
Signal-to-noise ratio	300:1 (at full signal)
Dark noise	50 RMS counts
Integration time	3.8 milliseconds to 10 seconds

The fibre-optic sensor was placed in front of the light source where a screen was placed in between the light and sensor (see figure 3.1a). Table 3.2 lists the specification of the applied spectrometer. The optical sensor was laid on a metal plate using two u-brackets (see figure 3.5a) and the metal plate was fixed to the base board using four metal legs adjustable in the vertical direction. The metal plate included two threaded bars that provide fine adjustments of the fibre optic sensor in both horizontal directions, whereas the metallic legs gave the opportunity of fine adjustment of the sensor in the vertical direction. Consequently, the position of the

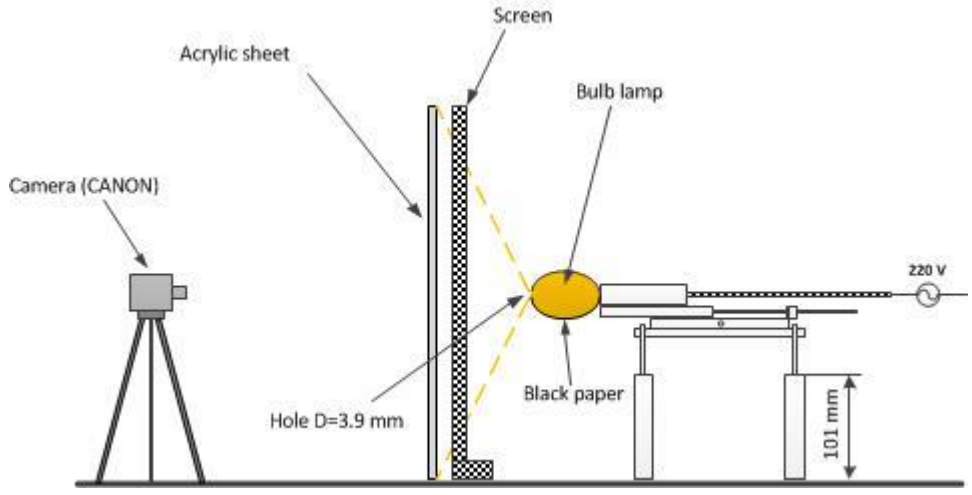

Figure 3.6 Experiment layout for detecting tunnel vision angle.

fibre-optic sensor can be adjusted in all directions with an accuracy of 100 microns. The sensor was co nnected via the USB 4000 spectrometer (see figure 3.5b) to a laptop computer running the commercial Spectra Suite software which enables users to monitor the spectrum and to analyse an individual wavelength.

3.2.2.4. View factor and tunnel vision angle

To observe the tunnel vision area and measure the angle, four screens with different porosities were placed between a bulb lamp, and a semi-transparent sheet of acrylic which was in contact with the screens. Figure 3.6 displays the experimental layout for the tunnel vision detection. The bulb lamp was covered with paper, and a hole with a diameter of 3.9 mm was cut in the middle of the cover. The diameter of the hole was the same size as the diameter of the optical sensor of the spectrometer used in this work. The lamp was fixed on the stand, and a camera was placed on the back side of the acrylic sheet to capture the images of tunnel vision effect. The lamp was moved to find the best distance for the clearest image. Finally, the diameter of the

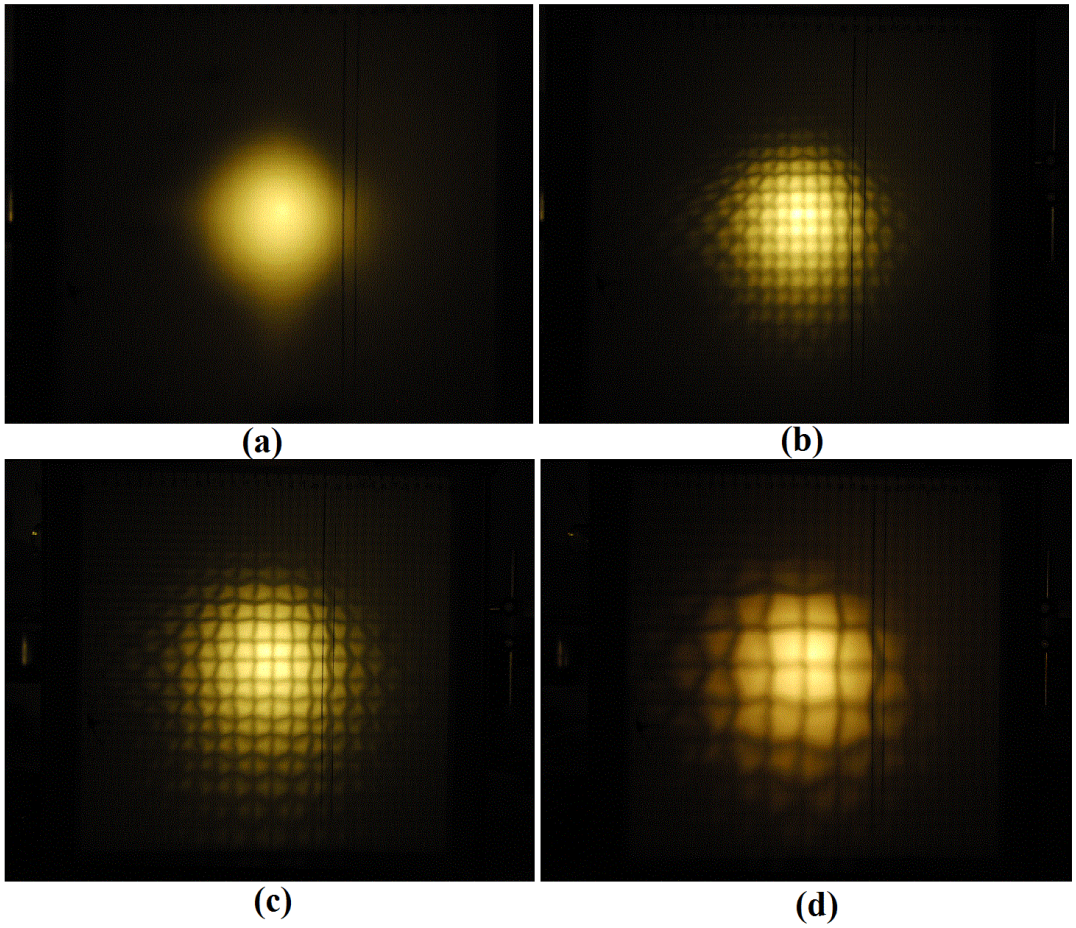

Figure 3.7 captured tunnel vision area for square woven wire screens with porosity of a) 41%, b) 54%, c) 58%, and b) 66%.

illuminated area on the sheet, and distances among the lamp, screen and acrylic sheet were recorded.

3.3. Results and discussion

3.3.1. Tunnel vision effects of screens

3.3.1.1. Tunnel vision detection

The tunnel vision effect of the screens is evident in the photographs shown in figure 3.7. The photo shows that the centre of the image is bright, but as the distance from the centre of the image increases, the illumination decreases. At the edge of the visible part of the image, the diameter of the wires appears to be greater than their actual size. Due to the growing apparent size of the diameters on the sheet, they overlap, and as a result, the dark shadow section appears. The diameter of the bright and nearly circular section depends on the screen porosity and the distances between the sheet, screen, and light source.

Table 3 3 The details of measured view factors for applied woven wire screens.

Porosity (%)	**41**	**54**	**58**	**66**
Distance of light to acrylic sheet (mm)	49	55	52	41
Radius of tunnel vision (mm)	85	157.5	157.5	157.5
Angle of tunnel vision (degree)	60.04	70.75	71.72	75.4
View factor ($\boldsymbol{VF}$)	0.7505	0.8913	0.9017	0.9422

3.3.1.2. Tunnel vision angle measurements

Table 3.3 lists the measured radius and angle of tunnel vision for the applied wire screens. The tunnel vision angle is calculated in degrees based on the measured values. The measured angle has a maximum theoretical uncertainty of 3.3% based on 2 mm uncertainty in the distance measurement, maximum of 5 degree misalignment between the light source and screens and uncertainty of 1 mm in measurement of the radius of the visible circle.

The results show that the angle of tunnel vision increases as the porosity increases. This was expected based on analytical solution (sees section 2.2.2) and the

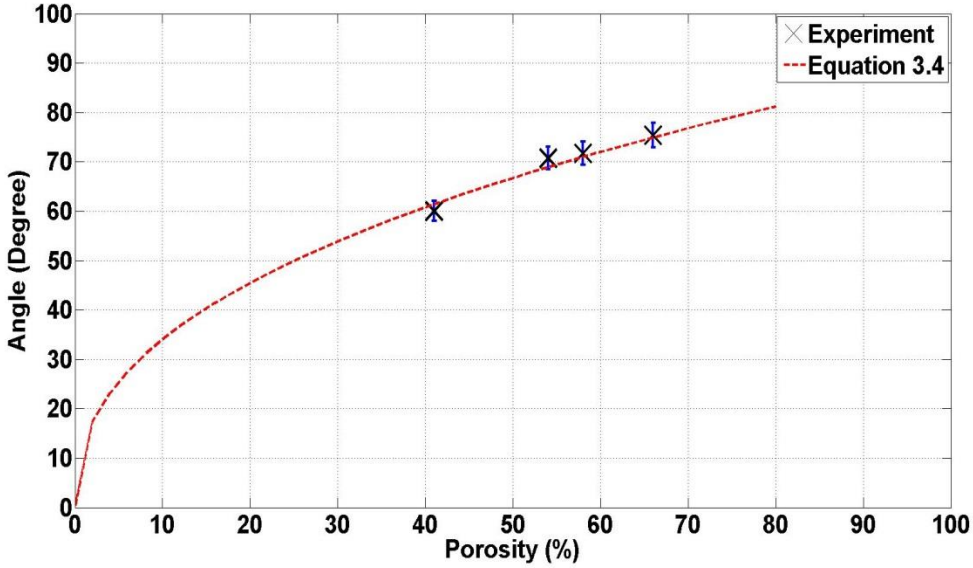

Figure 3.8 the change of experimental tunnel vision angle and estimation by equation (3.4)

experimental results can be expressed by an exponent formula which brings ease to the calculation of tunnel vision angle of plain woven screens with square shape cells in the range of porosities of 41%-66% as follows,

$$\alpha_{TU} = 13p^{0.418} \qquad 41\ \% \leq p \leq 66\%, \quad \lambda/L << 1 \qquad (3.4)$$

Where p represents the porosity, α_{TU} stands for tunnel vision angle in degree, L stands for screen cell size, and λ represents the light wavelength. Figure 3.8 shows the experimental results and those obtained from the proposed formula (3.4). The maximum difference between the above formula and experimental results are 2.6% at 54% porosity. Taking into account the uncertainty of the experiment, the maximum error of the formula is 6.2%, using the square root of the mean square error.

3.3.2. Light passing ratio of screens for a light source with size corresponding to tunnel vision area

It was found that the light behind a screen cannot be seen at angles greater than a certain value. The light passing ratio of screens is expected to change with the size of the light source. When the light source and screen sizes are greater than the tunnel

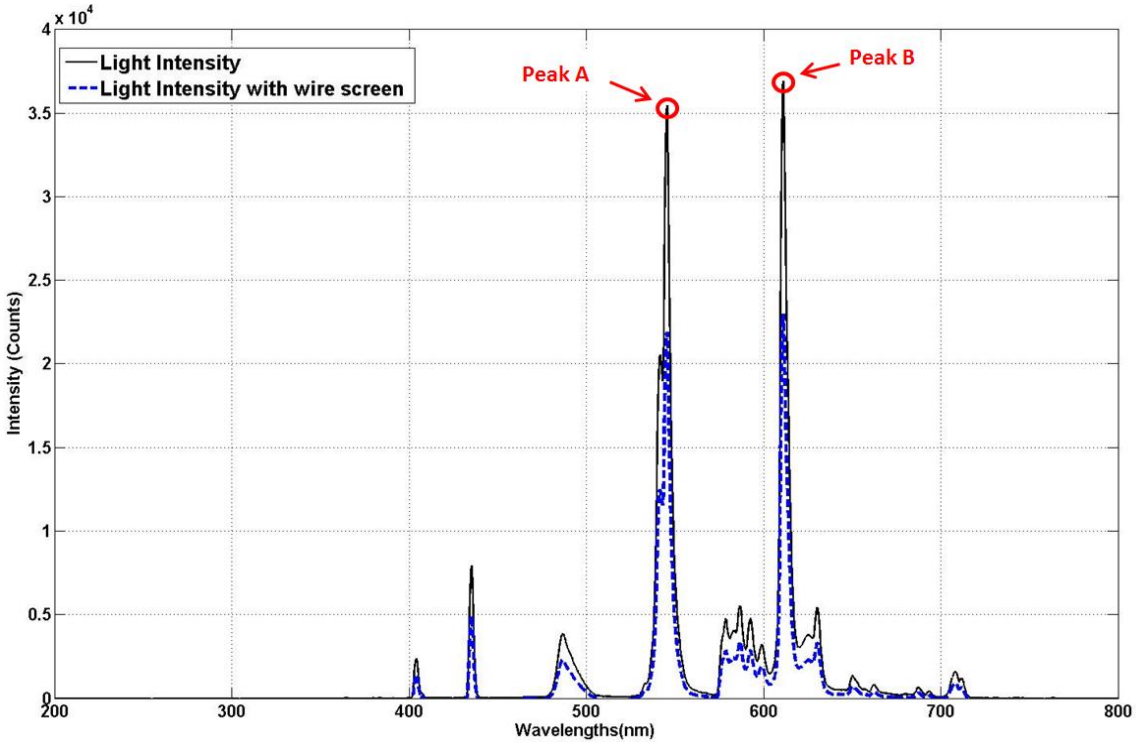

Figure 3.9 the light intensity distribution with and without 66% screen porosity.

vision area (L_v), the intensity of the light reaching the object in the presence of the screen remains unchanged by a further increase of the size of the light source. In contrast, in the absence of the screen, the overall light reaching the object increases as the size of the light source increases. Considering formula (3.3), this leads to a smaller passing ratio. Therefore, it is necessary to specify the size of the screen and light source before investigating the passing ratio.

3.3.2.1. Light passing ratio acquisition

Figure 3.9 shows the spectrum of the light source detected by the spectrometer used in this study. The figure indicates seven peaks in the wavelength range of 200 nm to 800 nm, where most of the peaks have intensity of near or less than 5000 counts. The measurement of uncertainty associated with those peaks reaches beyond 10%, considering that noise intensity ranged between 400-600 counts. Therefore, the two peaks with the maximum intensities were selected in this study in order to increase the signal-to-noise ratio and to minimise error. The selected wavelengths were 545.51 nm (peak A) and 611.01 nm (peak B). The woven wire screens were positioned between the light source and the sensor of the spectrometer. The fibre-optic sensor of the spectrometer was placed at the distance measured between the small light source and screen in section 3.3.1.2. After measuring the intensity at the two wavelengths (I_{screen}), the screen was replaced with a black paper having a circular

hole of the same size of the tunnel vision area. After positioning the black paper, the new measured intensities were recorded as $I_{no\text{-}screen}$. In addition, the intensity captured by the sensor in the dark room (I_{dark}) was measured. It should be noted that the reflection and emission from the screen can contribute to the measured intensity. The screen was exposed to the light for about 1 hour to reach its steady temperature in order to remove those contributions. The measured intensity after turning off the light source was registered as the dark intensity. The contribution of reflection of blackened screens was tested separately and was found to be negligible. The light passing ratios at the two peaks were calculated using equation (3.3). The final passing ratios are the average of the passing ratios obtained at the two peaks. The results are presented in table 3.4. The detailed results for the screen with the porosity of 66% are shown in figure 3.9.

3.3.2.2. Experiment uncertainties

The sources of uncertainty in the experiment are spectrometer noise at the highest intensity (4.4%); spectrometer noise in the dark room (1.6%); maximum of 5 degree misalignment for the screen, light source and sensor (1.7%); intensity drift during experiment (0.08%); maximum of 1 mm error in distance measurement (1.7%); error in measurement of the porosity (1.3%); and non-uniformity of light intensity within the visible area (5.2% ,12.6% across the whole light source). This leads to an uncertainty of 7.5% in measurement of light intensity in the presence of the screen, and an uncertainty of 7.4% in the absence of the screen, which gives an overall uncertainty of 10.5% for the passing ratio.

Table 3-3 the measured peak wavelengths and averaged passing ratios versus porosities.

Porosity (%)	Passing Ratio at Peak A	Passing ratio at Peak B	Passing ratio
41	27.8%	27.7%	26.7 %
54	42.1%	41.9%	42%
58	49.6%	49%	49.6%
66	63.2%	59.6%	61.3%

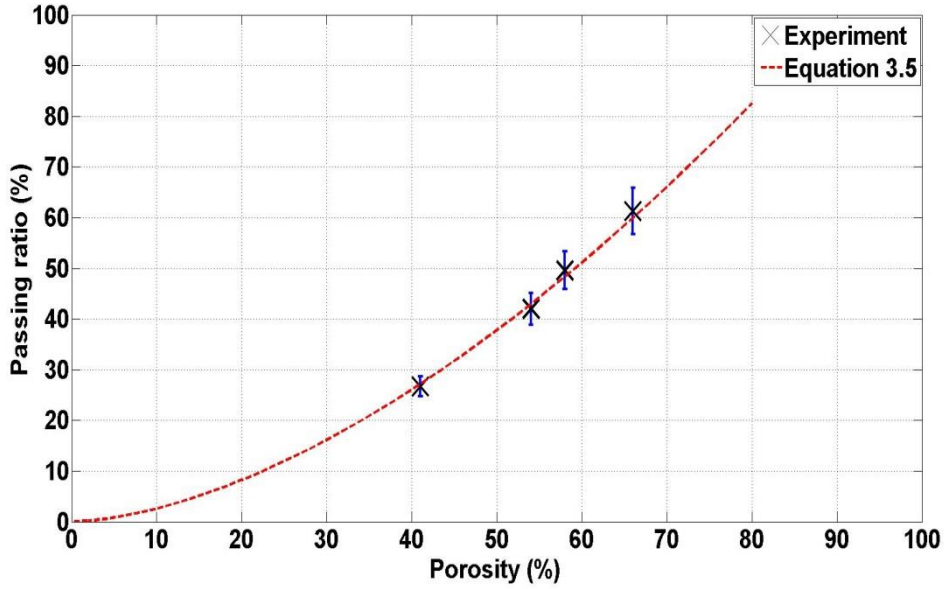

Figure 3.10 the change of experimental passing ratio and estimation by equation (3.5)

3.3.2.3. Light passing ratio versus screens porosity

Based on the results listed in table 3.4, it can be deduced that the passing ratio of light through a screen is independent of the light wavelength or has a very limited impact. The passing ratio of the 41% porosity screen is 27.8% at peak A, but it drops to 27.7% at peak B. A similar trend also was observed for the screen with porosities of 54% and 58% in which the passing ratio varied from 42.1% to 41.9% and 49.6% to 49%, respectively. The maximum difference in passing ratios of peaks A and B is for the screen with 66% porosity. In this case, the passing ratio decreases from 63.2% at peak A to 59.6% at peak B which represents a 3.6% difference. The results show a decreasing trend as the wavelength increases. The result is not conclusive since the changes are less than the uncertainty associated with these measurements. However, these results suggest that change in the wavelength range of 545.51-611.01 nm is ineffective or insignificant on the passing ratio.

The average experimental passing ratios are listed in the last column of table 3.4 According to the table, the passing ratio increases as the porosity increases, but it is always less than the porosity. The difference between the two values decreases as the porosity increases. The difference is 13.2% at the porosity of 41%, 12% at the porosity of 54%, 8.7% at the porosity of 58%, and 4.6% at the porosity of 66%. This indicates that the effectiveness of screens in blocking light due to tunnel vision is particularly important at lower porosities. For similar reasons as equation (3.4) (see

section 3.3.1.2), a formula for determining the light passing ratio has been proposed as follows,

$$PR_{TU} = 0.05676p^{1.662} \qquad 41\% \leq p \leq 66\%, \qquad \lambda/L << 1 \qquad (3.5)$$

The maximum relative error of the equation (3.5) with respect to the experimental results is 2.3%. Therefore, the maximum relative error of formula (3.5) is expected to be 10.7%. Figure 3.10 sh ows the experimental results and the fitting curve (equation 3.5). The condition $\lambda/L << 1$ implies that formula (3.5) is only valid if the cell size is not comparable to the wavelength as discussed in section 3.2.1.

3.3.3. Light passing ratio of screens for a light source greater than tunnel vision area size

The previous section provides an efficient means to calculate the light passing ratio through screens when the light source is exactly the size of the tunnel vision area. However, in practice such a condition is extremely unlikely. To calculate the passing ratio of screens for a light source greater than the tunnel vision area size, first the view factor of tunnel vision area (VF_{TU}) needs to be calculated. In the case of a circular object, the view factor can be calculated as (Lienhard 2011),

$$VF_{TU} = \frac{1}{2}\left[X - \sqrt{X^2 - 4\left(\frac{R_2}{R_1}\right)^2}\right] \qquad (3.6a)$$

where,

$$X = 1 + (1 + R_2^2)/R_1^2 \qquad (3.6b)$$

and,

$$R_1 = \frac{r_1}{h}\ ;\ R_2 = \frac{r_2}{h}. \qquad (3.6c)$$

Here h represents the distance between two parallel circles, r_1 the radius of the object, and r_2 the radius of the tunnel vision area. The view factor of a light source

with respect to a sensor (VF_s) depends on their shapes and distances and can be calculated using conventional formulae in heat transfer.

The view factor of the light source with respect to the sensor (VF_s) also should be calculated. Assuming a uniform intensity light source and Lambertian distribution and in the absence of the screen, the light intensity striking the sensor increases as,

$$I_{A>L_{v-no\ screen}} = I_{LV}\frac{VF_S}{VF_{TU}} \qquad (3.7)$$

Here, $I_{A>Lv\text{-no screen}}$ stands for the light intensity of the source greater than the size of tunnel vision area. Therefore, in this case, the light passing ratio of the screen ($PR_{S>Lv}$) can be calculated as,

$$PR_{S>L_v} = PR_{TU}\frac{VF_{TU}}{VF_S} \qquad 41\% \leq p \leq 66\% \qquad (3.8)$$

Substituting the value of PR_{TU} from equation (3.5), we obtain the formula for the light passing ratio as follows,

$$PR_{S>L_v} = 0.05676p^{1.662}\ \frac{VF_{TU}}{VF_S} \qquad 41\% \leq p \leq 66\%,\ \ \lambda/L << 1 \quad (3.9)$$

One interesting point of equation (3.9) is that by increasing VF_S, the passing ratio decreases. This indicates that screens are more effective for a larger light source. This is particularly interesting in the context of blocking the radiant heat flux of large bushfires.

Table 3-4 extended passing ratios of infinite source size versus view factor correlation (equation (2.3)).

Porosity (%)	41	54	58	66
Passing ratios$_{\text{Extended to infinite source}}$(%)	20.03	37.4	44.7	57.7
Passing ratios$_{\text{Viewfactor correlation}}$(%)	27.9	42.7	47.4	57.1

3.3.4. Light passing ratio of screens for an infinite light source

As discussed in section 2.2.2, equation (2.3) is a correlation between the view factor of an object to an infinite fire through an infinite screens with screen porosity ranging 25–90%. To verify the correlation with light passing ratio, the results of the experimental work must be extended for an infinite light source. When the light source and screen are so large or the object is so close to the screen that the screen and source can be regarded as infinite, the view factor of the light source can be assumed to be one (VF_S=1). In that case, the light passing ratio of the screen can be calculated through equation (3.9) as,

$$PR_{inf.} = PR_{TU} \times VF_{TU} \qquad 41\% \leq p \leq 66\% \qquad (3.10)$$

By substituting the value of PR_{TU} from equation (3.5), the above formula can be rewritten as follows,

$$PR_{inf.} = 0.05676p^{1.662} \times VF_{TU} \qquad 41\% \leq p \leq 66\%, \quad \lambda/L << 1 \quad (3.11)$$

The view factors of tunnel vision area were calculated based on equation (3.6), and are listed in the last row of Table 3.3. The light passing ratios versus porosity for an

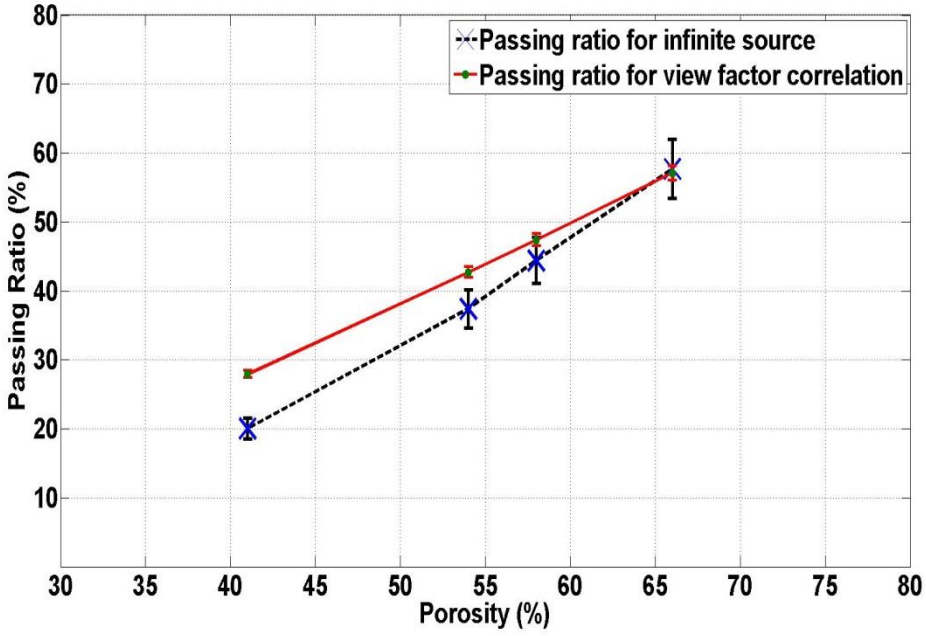

Figure 3.11 the change of passing ratio extended for infinite light source and computational equation (2.3)

infinite light source were calculated based on equations (3.11) and (2.3) and are listed in table 3.5. Figure 3.11 provides the opportunity for comparing the results.

The results show that equation (2.3) overestimates the light passing ratio of an infinite screen in front of an infinite light source with one exception at the porosity of 66%. The difference between the predictions of equation (2.3) (view factor correlation) and equation (3.11) (empirical equation) decreases as porosity increases. The experimental light passing ratio at the porosity of 41% is 20.9% whereas the computational formula (equation 2.3) gives a ratio of 27.9%, showing a difference of 7%. The difference decreases to 5.3% and 3% at the porosities of 54% and 58%, respectively. The minimum difference is 0.7% at the highest porosity of 66%.

3.3.5. Indirect radiant heat flux

Justification for extending the result obtained with light to fire RHF was provided in section 3.2.1. The emission from a screen to an object can be calculated using conventional formulae once the screen temperature and the view factor of the screen with respect to the object are known. The screen temperature is affected by many factors such as wind speed, conductivity of the screen, the relative size of the screen and the fire behind the screen. The view factor of the screen (VFscreen) with respect to the object is the difference between the fire view factor with respect to the object without and with a screen

$$VF_{screen} = VF_S - VF_{TU} \tag{3.12}$$

Having the view factor of a screen with respect to an object, screen temperature (T) and emissivity (ε), the indirect radiant heat flux emitted towards the object can be calculated as follows,

$$q_{IRHF} = VF_{screen}\varepsilon\sigma T^4 \tag{3.13}$$

3.4. Summary

This chapter reported the experimental investigation on the direct radiant heat flux through four square woven wire screens with porosities ranging 41–66%. The methodology and rationale of its selection were discussed at the beginning of this chapter. A light source was chosen instead of a heat source since it eliminates the effect of indirect radiant heat flux emitted from a hot screen. In this case, the

effectiveness of the screen was defined based on the ratio of the light intensity with a screen to the light intensity detected in the absence of a screen. An experimental setup was designed and manufactured which included four square woven wire screens, a light source and a UV-Visible spectrometer that were mounted on a heavy metal board. The mechanical components were designed in order to provide any coarse adjustment. The initial analysis of light spectra was carried out using the Spectra Suite software. Also, an experimental layout was developed to determine the tunnel vision angle.

The tunnel vision effects of woven wire screen were documented. The angle of tunnel vision with respect with screen porosity was measured and a correlation between the angle and screen porosity in the range of 41–66% was presented in this chapter. The angle of tunnel vision increased with the growth of screen porosity. Then, the light passing ratios of four square woven wire screens were measured for the light with the same size of tunnel vision area. The passing ratio decreased with the decline in porosity. The result revealed that the light wavelength ranging from 545.51 nm to 611.01 nm does not have a significant effect on the light passing ratio of screens with openings greater than 0.987 mm. It suggests that the results can be generalised to a broader range of wavelengths, such as the wildfires' wavelengths.

Furthermore in this chapter, the light passing ratios were extended for the source with size greater than the screen tunnel vision area. It was found that the screens are more effective when the source increases, such as wildfires, owing to tunnel vision effect. The results were extended for an infinite light source and compared with the available computational formula. It showed a good agreement particularly at high screen porosities. Finally, the effect of IRHF was discussed and a solution to estimate IRHF was presented.

Chapter 4

Development and characterization of Ember Shower Simulator (ESS)

4.1. Overview

In chapter two, the NIST Baby Dragon firebrand generators was presented as an effective method to carry out laboratory scale experiments for the evaluation of screen performance against firebrand attacks. However, as it was mentioned, there was no indication that the design can be employed for the experiments with low porosity screens at the high wind speed desired in this work. At the beginning of this chapter, the reasons for the development of a new ember shower simulator is explained and followed by the details of the new design (section 4.2.1). Section 4.2.2 illustrates features of the manufactured device which was called the "Ember Shower Simulator" (ESS). Following that, the instrumentation installed in the ESS is detailed in section 4.2.3 and a method to visualise and count the firebrands is presented in section 4.2.4. The details of the fabricated L-shaped stand to capture firebrands outside the ESS and the feeds applied in the simulator are given in sections 4.2.5 and 4.2.6, respectively.

The second part of the chapter presents the characteristics of the ESS. Section 4.3 contains the performance of the ESS which is identified through several experiments. It includes the details of velocity and temperature distribution within the ESS, firebrand flow characteristics, and generated firebrands' mass and projected area and finally the firebrands' number flux. At the end of the chapter, a summary underlines the significant features of the ESS and its performance.

4.2. Development of Ember Shower Simulator

The application of wind tunnels was a popular experimental approach in firebrand related studies. As discussed in chapter two (literature review), the wind tunnel approach to study the firebrand transport has been used by many researchers since the early sixties. In many of those studies, the firebrands when inserted were tethered or sometimes untethered in the wind tunnel and the combustion and aerodynamic properties of the fire embers were monitored. It is evident that the use of wind tunnels is a valuable approach to study the characteristics of a single firebrand. However, this approach does not replicate actual firebrand attacks in terms of intensity.

The great evolution in the existing experimental approach to firebrand-related studies was carried out by Manzello et al. (2008) and their presentation of the NIST dragon, the details of which were provided in the literature review (section 2.3.4). The NIST dragon firebrand generator is able to generate an ongoing firebrands' shower that has been applied in full and laboratory scale experiments. However, as mentioned in section 2.4, the wind speed applied in both scales' experiments was less than 10 m/s. It was discussed that the only facility capable of simulating a firebrand attack at full scale and with wind speed greater than 10 m/s is the IBHS wind tunnel with the cloned NIST firebrand generator (see section 2.3.2). The size of the wind tunnel appears to have a smaller impact on results as discussed in chapter 2 since similar results in the laboratory and full-scale experiments were reported for NIST dragon. This provides an opportunity to downsize the wind tunnel and to reduce the experimental costs in obtaining the initial results. However, as a final step, the initial results should be verified by full-scale experiments. As will be discussed

in section 4.2.1, the NIST baby dragon cannot be coupled to a wind tunnel operating at a high wind speed and/or used for testing a low-porosity screen due to the possibility of reversed flow at the inlet and the subsequent safety hazard. This requires a new design of the laboratory-scale fire embers shower simulator, which is able to work in a wider range of wind speeds and to test low-porosity screens.

4.2.1. Design of Ember Shower Simulator (ESS)

4.2.1.1. Limits of current design (NIST baby dragon)

The existing firebrand shower simulator for use at a laboratory scale is the NIST Baby Dragon or other simulators of similar design. The design consists of a wind tunnel and a firebrand shower generator. The generator includes a separate blower which provides an easy way to regulate the wind speed over the feeds. The blower is the Achilles's heel of the design when it is coupled to a wind tunnel operating at a relatively-high wind speed. A firebrand simulator similar to the Baby Dragon was manufactured. A strong reverse flow was observed that scattered firebrands in the laboratory when a low porosity screen (41%) at a wind speed of 12 m/s was tested. A preliminary computational model of the Baby Dragon showed that this reverse flow is due to the increase of the back pressure before the screen and the problem cannot be avoided just by changing the area ratio of the contractor. The reversed flow is the consequence of the pressure build-up at the test section under the above-described conditions. The built-up pressure may exceed the maximum pressure supplied by the blower, which in turn reverses the flow in the generator.

The limit can be explained by imagining a non-porous sheet with an area equal to that of the test section (a complete blockage). The blockage causes the flow to be diverted from the wind tunnel to the firebrand generator and then to the outside air (see figure 4.1). The reversed flow carries the generated firebrands in the generator to the outside and thus is a fire hazard in non-fire proof laboratories. The combination of extended Bernoulli's, the Darcy Weisbach and the major and minor loss equations all losses equations gives the pressure difference between a point before the screen and a point at the exit of the wind tunnel as $K.V^2$ where V is the velocity and K is a

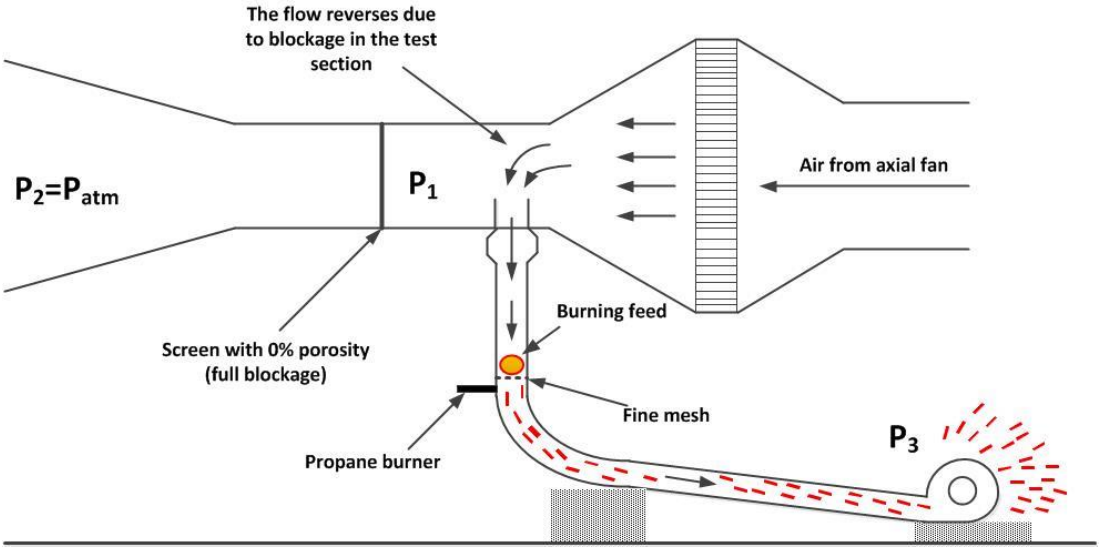

Figure 4.1 the scheme of reverse flow in NIST baby dragon due to test section blockage

coefficient depending on many factors such as the porosity of the screen between the two points. Previous studies have shown that the pressure loss between the two sides of a screen increases (or K increases) as the porosity decreases such as the porosity of the screen between the two points. Previous studies have shown that the pressure loss between the two sides of a screen increases (or K increases) as the porosity decreases(Sharifian and Buttsworth 2007). As the pressure at the exit of the wind tunnel is constant (Patm), the built up pressure behind the screen is the ΔP between these points. The reversed flow slightly lessens if a tiny hole is punched in the sheet (decrease of K). At this point there are four ways to eliminate the reversed flow. The first is to increase the number of the holes (decrease of K), which indicates that the design can only operate at porosities higher than a specific value corresponding to the wind speed in the wind tunnel. The second way is to reduce the flowrate in the tunnel to a value equal to or less than the value that can pass through the hole (decrease of V). This demonstrates that the wind speed cannot exceed a certain limit value which depends on the porosity. The third solution is to adjust the blower flow in a way that only stops the reverse flow. This third solution is obviously impractical as it does not provide firebrands in the test section and requires individual adjustment for each experiment. The fourth way is to select a blower that can supply a pressure higher than the built-up pressure. This delicate job is also a safety hazard as the flow containing glowing firebrands may reverse back from the inlet of the wind tunnel.

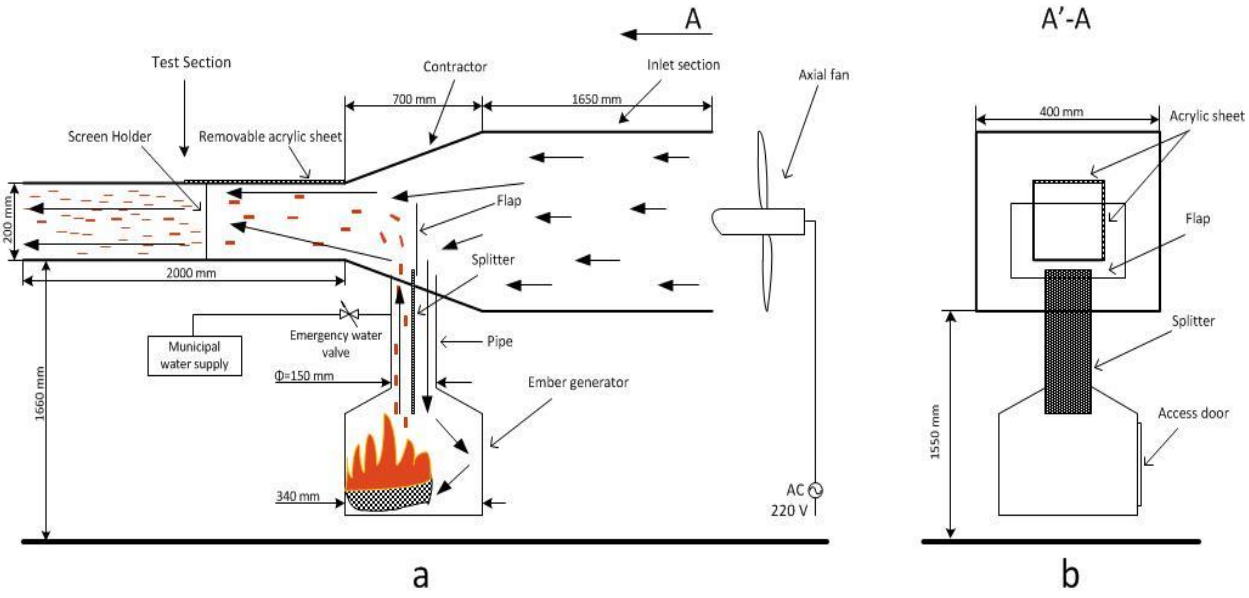

Figure 4.2 the scheme of the Ember Shower Simulator (ESS), a) Side view, b) Cross section view

The NIST design can be perfectly used in full-scale wind tunnels at any wind speed and for all screens regardless of their porosities. The reason is that the firebrand generator is placed inside the full-size wind tunnels and therefore its inlet pressure is equal to the built-up pressure. As the outlet pressure of the blower is always higher than the inlet pressure, no reversed flow is expected. This is a key element in the design of an ember generator coupled to a benchtop wind tunnel designed to work at high wind speeds and/or with low porosity screens. If the design uses the flow behind the test section as the inlet to the ember generator, it will be a self-adjusting system.

4.2.1.2. New design

Figure 4.2 shows the side and cross-sectional views of the design which was named the "Ember Shower Simulator" (ESS). The design consists of a wind tunnel including an inlet duct, a contractor and a test section as well as a fire ember generator mounted underneath the tunnel. The fan blows air into the wind tunnel and the air passes through the contractor prior to entering the test section (see Figure 4.2a). In the middle of the contractor, a vertical pipe connects the firebrand generator to the underneath of the tunnel. The vertical pipe is divided into two sections lengthwise by a partition called a "splitter" to direct a portion of the airflow in the wind tunnel to the ember generator through one half and driving the burning firebrands to the test section in its other half. The splitter also forms a suction region

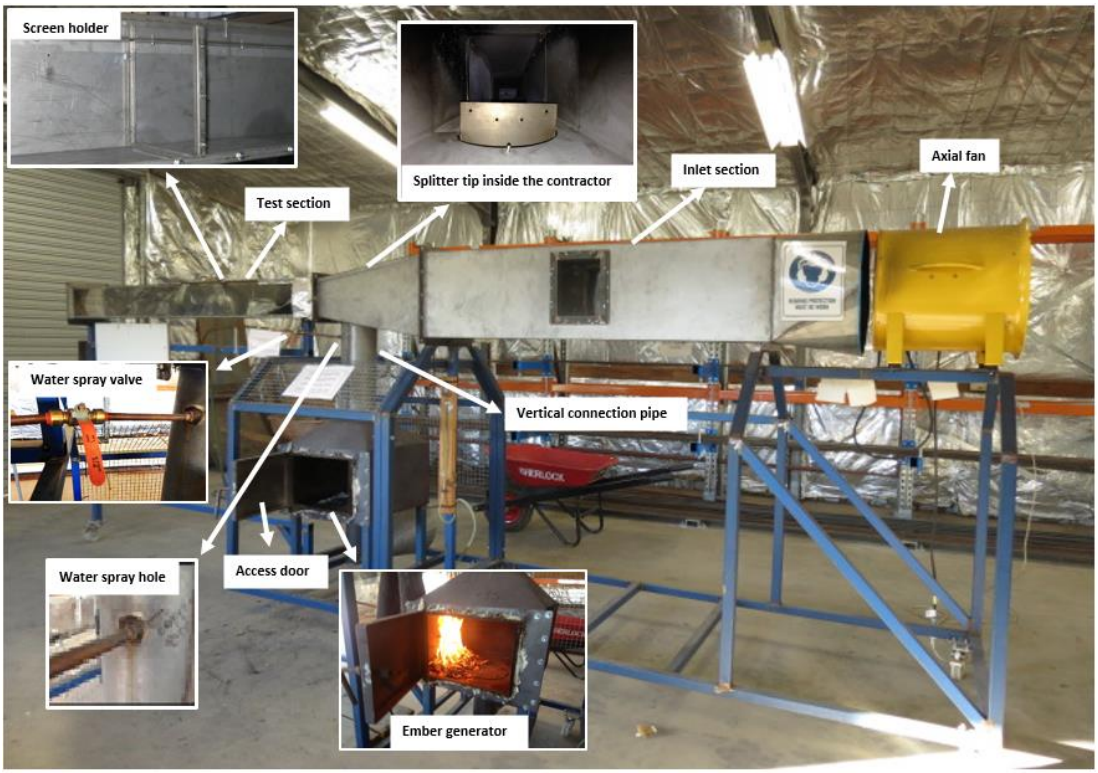

Figure 4.3 Picture of fabricated Ember Shower Simulator (ESS).

above the exit part of the vertical pipe which helps to lift the firebrands up from the generator to the tunnel.

The design does not include a blower to adjust the air speed in the ember generator. However, the ability to control wind speed in the ember generator for both designs is essential because, as a previous study concluded, the firebrands produced would be forced out of the generator earlier than planned, resulting in flaming firebrands when the wind speed exceeds a certain value. Therefore the ability to adjust the wind speed in the generator is essential to provide control over the state of combustion. Therefore, the tip of the splitter located in the wind tunnel was designed to be short, but it can be bolted to flaps with different heights to regulate the amount of air being diverted down and thereby can control the wind speed inside the generator. The lofted firebrands mix with the airflow in the wind tunnel which was not diverted down into the ember generator, and then enter the test section prior to exiting the wind tunnel.

The design can still cause reversed flow when a non-porous sheet is placed in the test section, but it is not a safety concern. In this case, the inlet air of the tunnel circulates

in the inlet section and does not reach the ember generator section; therefore the reversed flow does not contain glowing firebrands.

4.2.2. Manufacturing the ESS

Figure 4.3 is the picture of manufactured Ember Shower Simulator by the workshop at University of Southern Queensland. The apparatus consists of a fire ember generator and a wind tunnel. The wind tunnel includes a fan, an inlet duct, a contractor and a test section.

4.2.2.1. Fan and Inlet duct

An axial fan (FANMASTER, Australia) was mounted at the inlet of the wind tunnel duct. The fan is capable of blowing air at the wind speed of 5.25 m/s (0.84 m^3/s) at the wind tunnel inlet with a cross-sectional area of 1600 cm^2 made of zinc-coated steel sheeting. The dimensional details of the inlet duct are indicated in figure 4.2a. The wind speed inside the wind tunnel can be adjusted by pulling the fan away from or towards the wind tunnel inlet.

4.2.2.2. Contractor

The air blown into the inlet duct passes a contractor before the test section. The contractor is made of zinc-coated steel sheeting with a cross section of 1600 cm^2 at the inlet duct side and 400 cm^2 at the test section side. At the bottom of the contractor, a pipe with a 150 mm diameter that connects the fire ember generator to the wind tunnel is mounted. The pipe is divided into two section by a thin metal sheet (splitter) welded axially inside the pipe to direct a portion of air into the fire ember generator from one side and loft burning embers into the tunnel from the other side (see figure 4.2a). It is possible to change the wind speed inside the generator by mounting a flap with different heights in the contractor that changes the portion of air flowing down to the generator. Three flaps with heights of 50 mm, 100 mm and 150 mm were built using the same material as the splitter. The flaps can be bolted to the tip of the splitter and cover the entire width of the contractor at that point (see figure 4.3).

4.2.2.3. Ember generator

The firebrand generator box is made of steel sheets with a thickness of 3 mm and its square-shaped cross-section is 340 mm long. An access door made of steel was mounted on the front side of the ember generator to place the feeds inside the generator. The feeds to the ember generator can be any type of vegetation. They are ignited by an external ignition source (torch ignitor). After observing a stable flame core, the access door is closed and the fan starts operating. The air diverted into the ember generator not only lofts the generated firebrands into the wind tunnel, but also supplies the required oxygen for combustion. The top of the generator is conical in shape to facilitate the firebrands' passage into the vertical pipe.

4.2.2.4. Test section

The test section is a square duct with a cross-sectional area of 400 cm^2 and a length of 2000 mm. The top and one side of the test section were made using transparent acrylic sheets for monitoring purposes. In addition, one metre of the top surface of the test section is detachable for mounting screens and cleaning ashes. The screens are slightly stretched and secured by a fixed frame called the screen holder (see figure 4.3) at a distance of 800 mm away from the inlet of the test section. The maximum wind speed in the unfilled test section is approximately 21 m/s (0.84 m^3/s). The airflow and firebrands exit the test section at a distance of 1200 mm from the screen.

4.2.2.5. Emergency water spray

In the case of an emergency which requires an immediate response, municipal water can be sprayed on the fire in the combustion chamber through a hole in the top of the discharge side of the vertical pipe (see figure 4.3). A one-inch copper pipe, which is welded to the hole, delivers the municipal water to the hole (see figure 4.3).

4.2.3. Instrumentation

4.2.3.1. Video camera

In order to measure the penetration ratio for each experiments, a high speed video camera (CASIO EXILIM EX-FH20) capable of capturing frames with a maximum speed of 1000 frames per second (fps) is used to monitor the glowing firebrands at both sides of the screens. Figure 4.4 shows a picture of the camera and table 4.1 lists its specifications. The video camera was placed outside the tunnel next to the screen

in the test section. The camera was mounted on a tripod and a thick sheet covers its surroundings to reduce the light noise during the experiment.

Figure 4.4 high speed camera (CASIO, EXILIM EX-FH20).

In some experiments, an additional camera was necessary to monitor the experiment. The camera (CANON Power Shot SX40 HS) takes photos and records videos on a standard frame rate of 30 fps. In both cases, the data was recorded on Secure Digital (SD) memory cards and then the captured videos were exported to the computer for further analysis.

Table 4-1 Details of high speed camera specifications applied in fire ember studies experiment.

Specification	Details	
Brand	CASIO	
Model	EXILIM EX-FH20	
Recorded image	**Resolution**	**Recording speed**
	1280×720	HD 30 fps
	480×360	210 fps
	224×168	420 fps
	224×56	1000 fps
	480×360	30-210 fps (Switchable)
	640×480	30 fps
Effective Pixels	9.10 Megapixels	
Imaging element	Size: ½.3-inch square pixel high speed CMOS ,total pixels 10.29 Megapixels	

4.2.3.2. Hot-wire anemometer

A hot-wire anemometer is a sensor that measures the fluid velocity based on heat convection. Figure 4.5a shows the scheme of hot wire anemometer circuits. The resistance wire, R(T), at the head of the sensor is heated above ambient temperature. The resistance of the wire is kept constant using an amplifier. The flow passing over the wire cools the wire and changes its resistance temperature. To keep the resistance constant, the current is fed into the sensor by an amplifier. The input current determines the velocity.

In this study, a hot-wire anemometer, KM 4007 manufactured by Comark Ltd (UK), is utilised to measure the wind velocity. In order to measure the wind speed at the test section of the wind tunnel, the transverse area of the test section was divided into nine zones and the wind speed at the centre of each zone was measured using the hot-wire anemometer. The uncertainty related to the hot anemometer is 2.7% for the lowest wind speed and it is 1.3% related to the manual mounting of the probe based on 10 mm deviation from the point of measurement.

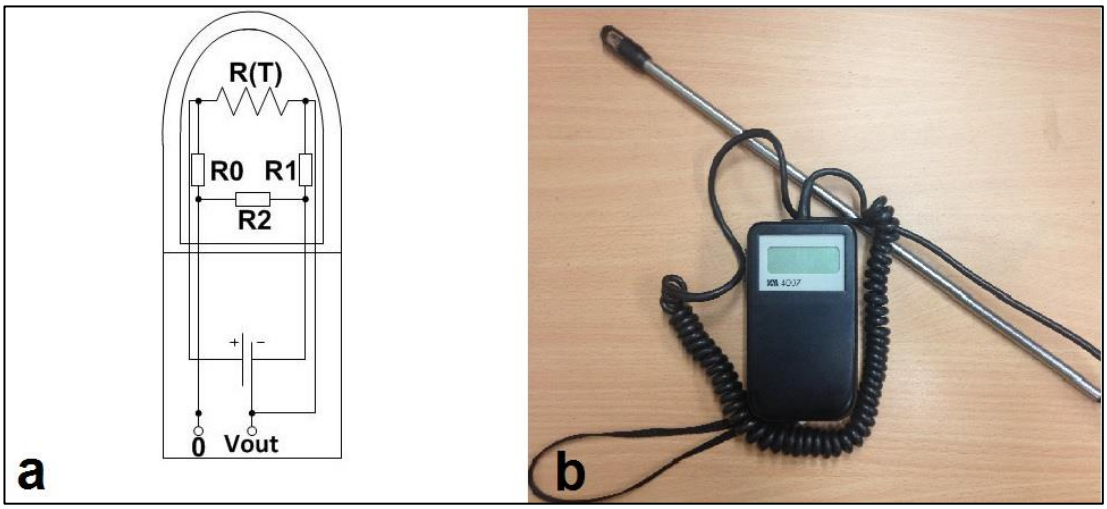

Figure 4.5 Hot-wire anemometer a) the scheme of the anemometer circuit (Lomas 2011), b) a photograph of the anemometer.

4.2.4. Data Acquisition

The initial visual investigation was carried out using Adobe Premier Pro, and then the counting process of glowing embers took place in MATLAB. The initial observations indicated that the high turbulence near the screen complicates the counting process. Therefore, the counting process took place a short distance away

from the screens. The firebrands are counted within a virtual strip. The width of the strip has a major impact on the accuracy of the counting. If the virtual strip is too narrow or too wide, the outcome could be no-counting or double-counting, respectively. The width of the strip is initially estimated based on the frame rate of the camera and assuming an identical speed for firebrands and wind speed. For instance, for a wind speed of 14.5 m/s and a frame rate of 420 fps, the maximum width of a strip to avoid double counting should be 35 mm (14500/420). However, firebrand lengths differ and their speeds are not equal and not necessarily the same as the wind speed. After comparing the results of manual and automated counting processes, the best width was found to be 2 mm, which showed a maximum of 5% difference between the two counting methods.

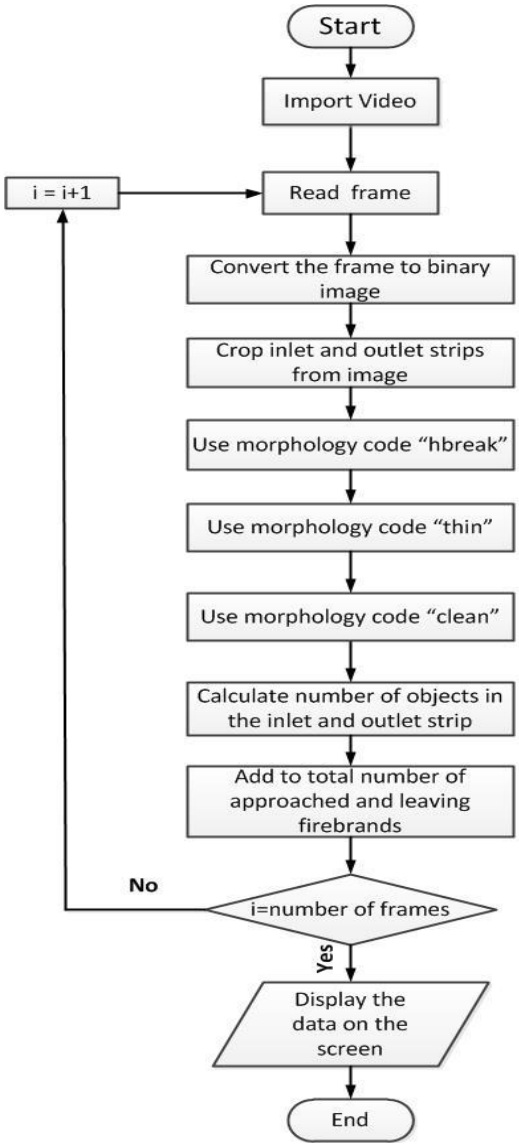

Figure 4.6 The algorithm of MATLAB script for fire ember counting.

The captured videos were imported into MATLAB for firebrand counting purposes. The counting of glowing firebrands in MATLAB was carried out using the image processing toolbox. A MATLAB script was developed using the morphology toolbox to count the firebrands in each frame. Figure 4.6 shows the algorithm of the script for counting the firebrands. A loop repeats the reading step for each frame. During the reading process, the frame is converted to a binary image and the strip is cropped from the image. Morphology operators improve the counting process of the strips. First, the morphology code 'hbreak' is used to separate fire embers in the strips if they are too close to each other. Then, the morphology code 'thin' is applied to narrow the fire embers pixel region in order to improve the separation. Finally, the scattered pixel points are cleaned in the strips using the morphology code 'clean'. The number of fire embers is detected and is added to the previous total number of the detected embers for each strip. The loop repeats for subsequent frames and finally the penetration ratio is determined based on the total number of fire embers in both the inlet and outlet strips.

4.2.5. L-shaped stand

A special stand was fabricated to capture firebrands at the outlet of the ESS. The design helps to investigate the characteristics of firebrands generated by the ESS and also assesses the capabilities of the firebrands that pass the screen and ignite various fuel beds. Figure 4.7 shows the layout of the L-shaped stand and the ESS. The stand is fabricated of plywood sheets were that joined in an L-shaped layout. The height of the stand was the same as the height of the ESS outlet. The layout directs the firebrands downwards onto a sheet made of

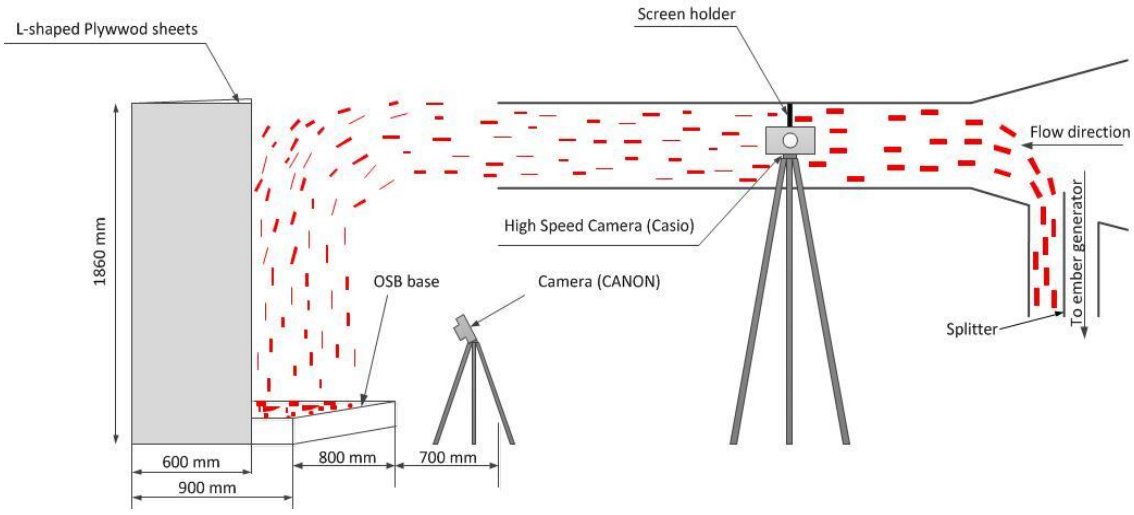

Figure 4.7 Layout of L-shaped stand and Ember Shower Simulator (ESS).

Oriented Strand Board (OSB) which is located at the base of the L-shaped stand. The high speed camera (CASIO) monitors the firebrands inside the tunnel, while the second camera (CANON) monitors the firebrands falling on the OSB base at a standard frame rate of 30 fps.

4.2.6. ESS feeds

Two different types of vegetation were used to generate embers: Eucalyptus Leaf and Hardwood Mulch. Dead leaves were collected from beneath Eucalyptus Populnea trees (Myrtle species) located at the University of Southern Queensland (see figure 4.8a). The moisture content and size of leaves were measured for twenty randomly-selected leaves. The average weight of a single Eucalyptus leaf was recorded as 0.255 g and the moisture content was 27% based on an oven-drying technique. The oven-dry method calculates the moisture content based on the dry mass of the object in the oven to the initial mass of the object. Also, the average length and width of the leaves were measured as 71.9 mm and 59.1 mm, respectively. Moreover, hardwood mulch is provided *pro bono* by Toowoomba city council and is a mix of local recycled trees. Figure 4.8b shows the hardwood mulch used in these experiments. The mass and projected (cross-sectional) area of the hardwood mulch varied in the range of 0.04 grams to 5 grams and 600 mm^2 to 20,000 mm^2. Likewise NIST firebrand generator, ESS is a wind-driven firebrand generator that wind speed over feed plays crucial role in determining the size and number of generated firebrands. It should be noted that the size of the feed does not determine the size distribution of generated firebrands. The size distribution of firebrands before and after the screen is an important parameter to assess the performance of the screen. Therefore, the size distribution of generated firebrands should be measured and compared with the size of real firebrands as is presented in section 4.3.

Figure 4.8 Vegetation used in the ESS. a) Dead leaves of Eucalyptus trees and, b) mix of hardwood mulch.

4.3. Performance of Ember Shower Simulator

Several experiments were carried out to assess the performance of the manufactured ESS. The experiments aimed to identify the velocity and temperature characteristics in the test section, mass, projected area and mass flux of the generated glowing firebrands as well as the glowing firebrand flux. Three sets of experiments were performed using the flaps of different heights; the flap details were given in section 4.2.2.2. Each set of experiments was carried out under three wind speeds – low, medium and high – which brought the total number of experiments to nine.

An 800 gram load of hardwood mulch was fed into the ember generator in the experiments. In order to collect firebrands, the L-shaped stand was placed outside the tunnel. The firebrands were captured using five water-filled aluminium pans on the OSB base (see figure 4.9). The water-filled pan technique is the most common technique used in many previous research studies discussed in section 2.3.3. In this section, only the high speed camera (CASIO) was used to count the firebrands in the tunnel and most of the recordings lasted 491 seconds due to the memory limitations of the camera at a frame speed of 420 fps with image resolution of 168 x 224 pixels. In a few experiments, the whole process was recorded using a lower image resolution. The combustion of the feed lasted for 10 to 15 minutes depending on the wind speed in the firebrand generator.

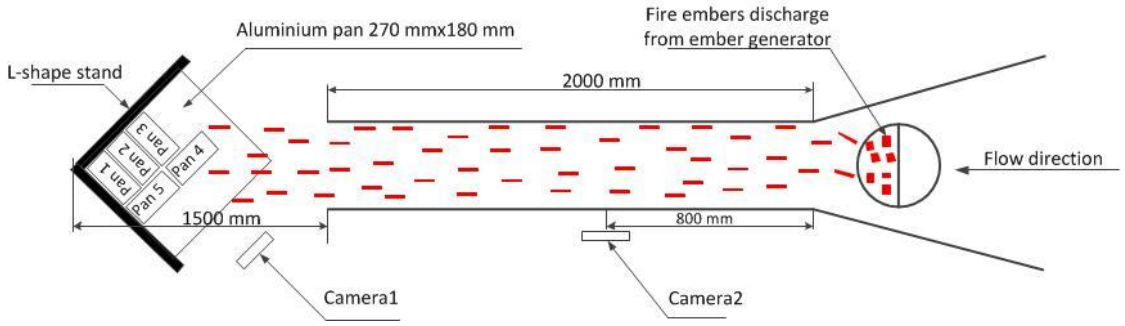

Figure 4.9 Top view of layout of water filled pans, L-shaped stand and the ESS

4.3.1. Velocity characteristics

An important parameter of the ESS is the air velocity characteristics inside the test section. The validity of the results produced by the ESS depends on the reliability of reported wind speeds. Therefore, velocity characteristics, such as wind speed uniformity and turbulence

intensity inside the test section, require investigation. For this, a hot-wire anemometer probe was inserted into the test section at a distance of 150 mm before the screen holder (650 mm after the inlet of the test section). The velocity was recorded at three different heights of 50 mm, 100 mm and 150 mm from the test section floor. The velocity measurements were also performed at the outlet of the test section. The measurements at the outlet were carried out with a 3×3 grid of locations across the sections that were equally spaced vertically and horizontally from each other and from the walls. The measurement was repeated several times with and without screens. It was found that the velocity non-uniformity slightly decreases when a screen is used. Therefore, the results presented here are in the absence of a screen which represents the worst case scenario. The measurements were recorded for 420 seconds at a frequency of 1 Hz. The streamwise turbulence intensity was calculated as the root mean square of turbulent velocity fluctuations in the streamwise direction (u_{rms}) to the average velocity (u_{ave}) (Cebeci 1974):

$$T(\%) = \frac{u_{rms}}{u_{ave}} \times 100 \qquad (4.1)$$

The root mean square of the fluctuations (u_{rms}) is calculated as follows,

$$u_{rms} = \sqrt{\sum \frac{(u_i - u_{ave})^2}{(n-1)}} \qquad (4.2)$$

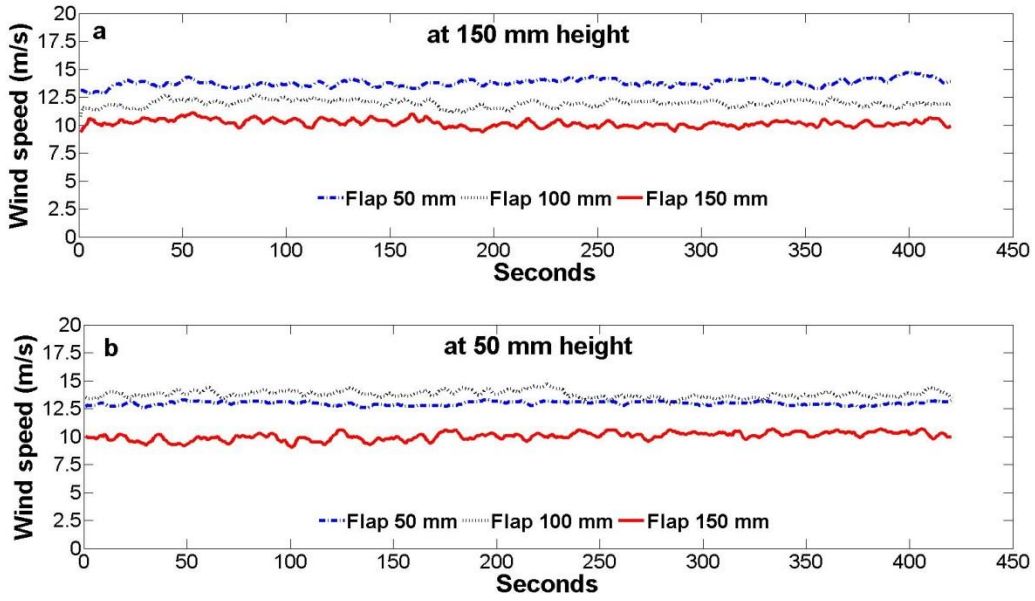

Figure 4.10 The temporal velocity behaviour for the applied flaps measured a) at 150 mm height from the tunnel floor b) at 50 mm height from the tunnel floor.

where u_i stands for the instantaneous velocity sample and *n* is the number of samples.

Figure 4.10 shows the instantaneous velocity for the three flaps of 50 mm, 100 mm and 150 mm at two heights of 50 mm and 150 mm. According to figure 4.10a, the velocity at the height of 150 mm decreased as a higher flap is used. At the height of 50 mm (Figure 4.10b), the velocity in the case of flap 150 mm was the lowest. However, at this height, the velocity in the case of flap 100 mm was slightly higher than that of flap 50 mm. This could be explained considering that a higher fraction of the flow in this case was directed to the ember generator compared to flap 50 mm. Therefore, for flap of 100 mm and at the height of 50 mm, the effect of the flow from the ember generator was still present even though the average velocity was less than that of flap 50 mm.

The turbulence intensity at the distance of 150 mm before the screen holder and at the three heights of 50 mm, 100 mm, and 150 mm was calculated based on the measured instantaneous velocities in absence of a screen. The turbulence intensity increases as the height of the flap increases. The maximum turbulence intensity for flap of 50 mm was measured as 2.4% and increased to 3.7% for flap of 150 mm.

The non-uniformity of wind velocity field at the three heights was also quantified at the inlet and outlet of the test section. The results show that the non-uniformity both at the inlet and outlet increases as the flap height increases. At the inlet of the test section, the overall variation of the velocity as the root-mean-square (RMS) percentage of the mean velocity was $\pm$ 2.5% for the flap of 50 mm and $\pm$ 9.5% for the flap of 150 mm. It should be noted that the maximum non-uniformity was 3.5% for flap 50 mm and 14.2% for flap 150 mm. Based on the results at the three heights (and for each height three points) at the outlet of the test section, the overall variation of the velocity as the root-mean-square percentage of the mean velocity was $\pm$ 6.3% for flap of 150 mm. In this location, the maximum non-uniformity was $\pm$ 10.3%, which shows that the negative impact of flaps on the air flow decreases as the distance between the flap and the location increases.

In the absence of information on flow characteristics of NIST wind tunnels, only a comparison can be made between the ESS and common wind tunnels used in fire research. Ellis (2000) addressed a ±4% variation of wind speed in the work section of a vertical wind tunnel designed by Knight at a wind speed of 5 m/s. Weise (1994) designed and constructed a wind tunnel to study fire behaviour at various slopes. The author noted a 15% non-uniformity

of the flow in their experiments. They suggested an acceptable level of non-uniformity of less than 5% in fire behaviour research (Weise 1994; Weise and Biging 1996). Sullivan et al. (2013) designed and constructed a wind tunnel called "CSIRO Pyrotron" to study the behaviour of free-burning fires. The authors reported a maximum non-uniformity of less than 5% at their lowest speed in the tunnel's work section. Taking into account the non-uniformity suggested in previous work, the mean non-uniformity of 2.5% measured for the flap of 50 mm is acceptable. The level of mean non-uniformity for the flap of 150 mm exceeds the recommended value but still is less than the reported values in some previous work.

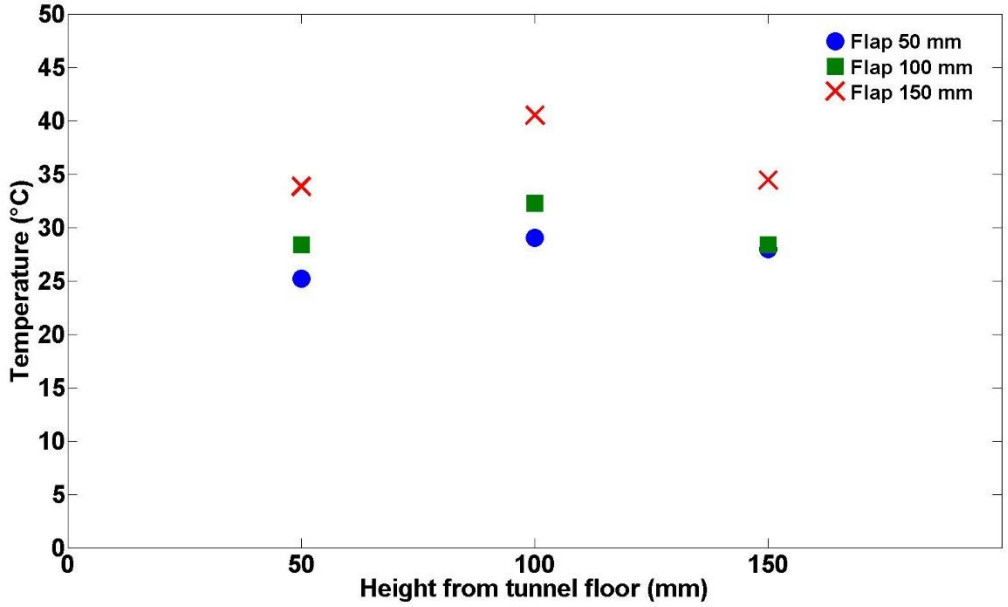

Figure 4.11 Temperatures profile inside the test section at a room temperature of 19°C for the three flaps of 50 mm, 100 mm, and 150 mm.

4.3.2. Temperature characteristics

The temperature inside the test section has an effect on the velocity measurements, and the burning and motion of firebrands. It is expected that the temperature inside the test section will be affected by the mix of hot air coming from the ember generator with cold air coming from the inlet of the wind tunnel. The mixing ratio varies for different flap heights and wind speed settings. Therefore, the temperature characteristics should be identified for the various flap and wind speed settings.

The temperature of the wind flow at the distance of 150 mm before the screen holder and at the three heights was measured. T-type thermocouples were placed at the three heights, and

data collection was performed at a sampling frequency of 1 Hz. Figure 4.11 shows the highest measured temperature non-uniformity which occurred at the lowest velocity setting (corresponding to Figure 4.10). As with the previous section, only the maximum temperature non-uniformities are presented which were obtained when no screen was used. According to figure 4.11, the temperature at all heights increases as flap height increases. This trend was expected as a higher portion of flow is directed to the ember generator when a higher flap is used. The interesting point when considering a single flap is that the highest and lowest temperatures occur at the centre and the lowest measured height (height of 50 mm) of the test section, respectively. The higher temperature at the height of 150 mm compared to that of flap 50 mm can be speculated upon by the lower density of warm air and the lower conductivity of acrylic sheets used as the top surface with respect to zinc alloy steel used for the bottom surface of the test section. The maximum temperature non-uniformity of 4.3°C was recorded for the flap of 150 mm. The maximum temperature non-uniformity decreases to 2.6˚C for the flap of 100 mm and to 1.7°C for the flap of 50 mm.

4.3.3. Firebrand size measurement

Once the collected wet firebrands were filtered and dried, they were weighed using a scale precise to 0.0001 grams. A script was developed in MATLAB to determine the projected area of the firebrands. Photos of the collected firebrands were taken (see figure 4.12a) and were then processed using the script (see figure 4.12b). The script calculates the pixel area of firebrands and then the areas are converted to mm^2 using a scale factor on the photos. The script is able to determine the projected area of the firebrands with a high degree of accuracy,

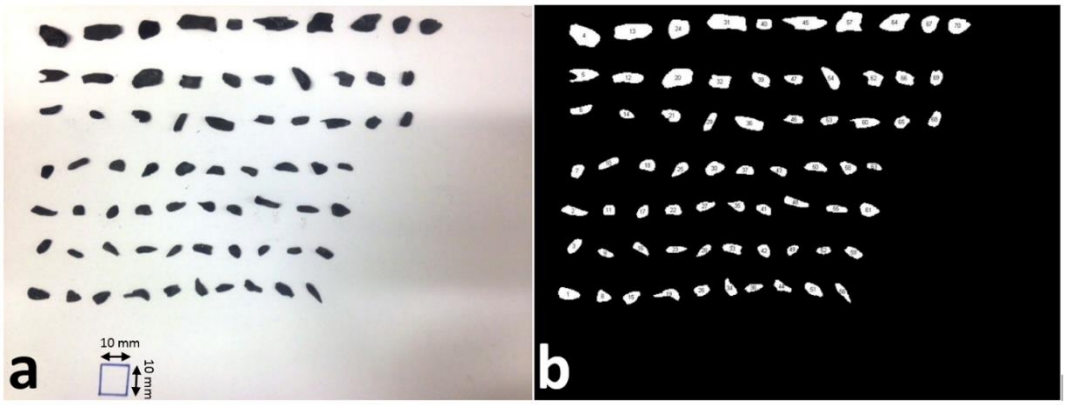

Figure 4.12 Image of collected firebrands in experiments with flap of 100 mm and wind speed of 10.7 m/s: a) actual photo; b) binary image.

depending on the resolution of the photos.

4.3.4. Firebrand flow characteristics

The experimental work shows that the firebrand shower simulator can work with a wide range of porosities and wind speeds without any reverse flow jeopardising safety. The lowest porosity tested was double-layer identical screens with a porosity of 43% (0.987 mm aperture, wire diameter 0.54 mm). The maximum wind speed associated with the different flaps varied (see table 4.2). The velocities are the average of nine measurement points at the outlet of the test section (as described in section 4.3.1).The decrease of velocity with the height of the flap shows it has a substantial contribution to the total head loss in the device. Table 4.2 also shows the range of wind speeds observed for each flap by sliding the fan backward or forward. Lower wind speeds than those presented in table 4.2 are obtainable by partially blocking the gap between the inlet of the wind tunnel and the fan. Higher wind speeds cannot be generated without utilising a larger or a higher speed fan. The wind speeds were categorised as low, medium and high for each flap in the absence of any screen in the test section, as listed in table 4.2.

Table 4-2 Range of wind speeds tested in the ESS for different flaps.

Flap Height (mm)	Wind Speeds (m/s)		
	Low	Medium	High
50	13.4	16.0	18.0
100	10.7	12.7	14.6
150	7.3	9.2	10.9

The flow of firebrands generated by the ESS is not steady, showing random fluctuations on a time scale of several seconds. Therefore, the total numbers of the firebrands at time intervals of one minute were calculated and are presented in figure 4.13. The total number of glowing firebrands observed at the test section changed for different amounts of feed placed in the generator but, in all cases, the pattern shown in Figure 4.13 remained the same. The firebrand flux started from zero, increased to a maximum and eventually fell off back to zero at the end of the experiment. A steadier flow of the firebrands is expected if a continuous feeding system similar to the study of (Suzuki and Manzello 2011) is integrated with the design.

4.3.5. Mass and projected area of firebrands

Table 4.3 lists the average and maximum mass and projected area of the collected firebrands during the nine experiments. For a specific flap, increasing the wind speed at the test section increases the size and mass of the generated firebrands. Another way to increase the mean mass and mean projected area of the firebrands is to increase the height of the flap. The only direct comparison available in Table 4.3 is for the 100mm-flap at a wind speed of 10.7 m/s, where the mean mass and mean projected area increased from 0.79 milligrams and 4.81 mm^2 to 3 milligrams and 16.11 mm^2 for the 150mm-flap at a wind speed of 10.9 m/s. The reason for the different average size and mass of the firebrands is believed to be the speed of the wind in the ember generator. A higher wind speed in the wind tunnel or a higher flap causes a higher wind speed in the ember generator which in turn carries larger and heavier firebrands into the test section.

Table 4-3 Mean and maximum of mass and projected area of collected firebrands in the different experiments

Flap Height (mm)	Wind speed(m/s)	Mass (milligram)		Projected area (mm^2)	
		average	*maximum*	*average*	*maximum*
50	13.4	0.27	6.7	2.60	36.6
	16.0	0.69	15.6	4.90	82.8
	18.0	1.90	44.4	9.50	161.2
100	10.7	0.79	17.0	4.80	70.3
	12.7	2.60	57.2	12.70	240.3
	14.6	3.00	118.0	13.70	197.7
150	7.3	0.40	13.0	2.60	105.5
	9.2	1.30	23.4	7.20	137.6
	10.9	3.00	62.1	16.10	259.0

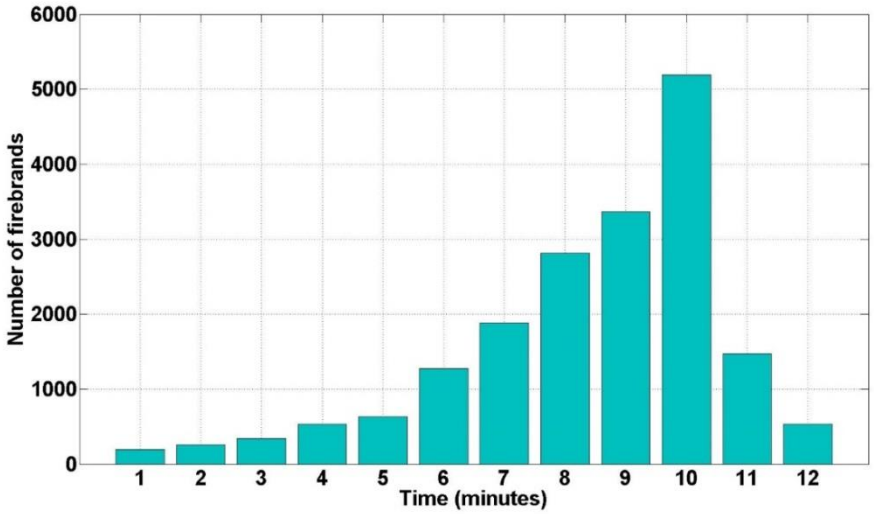

Figure 4.13 Number flux of firebrands generated by the ESS with wind speed of 16 m/s at the test section and flap height of 50 mm.

Table 4.4 shows the projected area distribution of the produced firebrands collected from the flow exiting the wind tunnel. The measurements showed that all generated firebrands for the 50 mm flap at the low wind speed (13.4 m/s) had a size less than 50 mm^2. The size of the firebrands increased as the wind speed increased for all the flaps utilised in this study. Another way to increase the projected area of the firebrands was to use taller flaps. For instance in the case of the 100mm-flap at a wind speed of 10.7 m/s, 99.5% of the firebrands had a size less than 50 mm^2, but this ratio decreased to 93.0% for the 150mm-flap at a wind

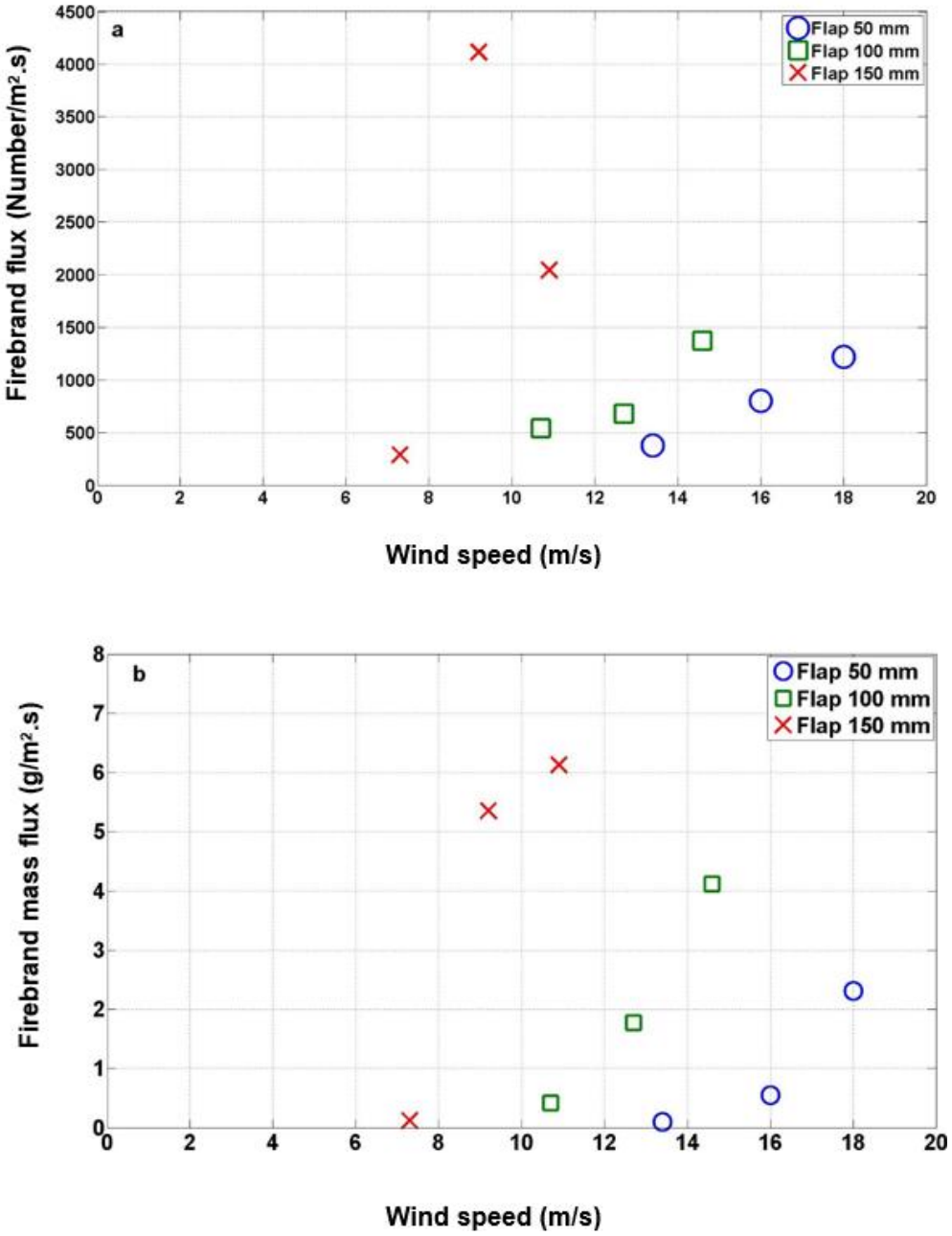

Figure 4.14 a) Number flux of collected firebrands at different flaps versus wind speeds; b) Mass flux of collected firebrands at different flaps versus wind speeds

speed of 10.9 m/s.

Table 4-4 Firebrand size distribution collected at the exit of the wind tunnel.

Projected area, A_p (mm^2)	Firebrand size distribution (%)								
	Flap 50mm			Flap 100mm			Flap 150mm		
	13.4 (m/s)	16.0 (m/s)	18.0 (m/s)	10.7 (m/s)	12.7 (m/s)	14.6 (m/s)	7.3 (m/s)	9.2 (m/s)	10.9 (m/s)
$A_p<50$	100.0	99.9	96.7	99.5	96.1	93.9	99.9	98.2	93.0
$50 <A_p< 100$	0.0	0.1	2.6	0.5	3.2	4.9	0.0	1.5	5.5
$A_p >100$	0.0	0.0	0.7	0.0	0.7	1.2	0.1	0.3	1.5

4.3.6. Firebrand number and mass flux

The glowing firebrand number flux (or simply "firebrand flux") is defined as the number of firebrands passing through the unit area per unit of time. The flux is related to the amount of feed placed in the generator and the wind speed in the firebrand generator, and was not constant throughout any one experiment. However, an average value for each experiment was calculated based on the total number of generated glowing firebrands in the experiment and the overall duration of the experiment (492s). The average glowing firebrand flux for each experiment is displayed in figure 4.14a and table 4.5.

Table 4-5 Number and mass fluxes of firebrands in different experiments

Glowing firebrands	Flap 50 mm			Flap 100 mm			Flap 150 mm		
	13.4 (m/s)	16.0 (m/s)	18.0 (m/s)	10.7 (m/s)	12.7 (m/s)	14.6(m/s)	7.3 (m/s)	9.2 (m/s)	10.9 (m/s)
Number flux (Number $.m^{-2}.s^{-1}$)	378	804	1220	540	681	1374	288	4415	2043
mass flux ($g.m^{-2}.s^{-1}$)	0.10	0.55	2.31	0.42	1.77	4.12	0.12	5.35	6.13

The results show that for the two flaps with the height of 50 mm and 100 mm, the number of produced firebrands increased with the increase in wind speed. A similar trend can be observed for the 100mm-flap. However, in the case of the 150 mm flap, the number flux initially increases to a peak and then decreases. This particular case is discussed later (see section 4.3.5). A photo of the firebrands in this case is presented in figure 4.15. The results also showed that the ESS can produce a wide range of firebrand number fluxes with a maximum of 4415 firebrands.$m^{-2}.s^{-1}$ for an 800 gram load of hardwood mulch.

An approximate way to calculate the glowing firebrand mass flux is to multiply the firebrand number flux by the average mass of firebrands for each experiment. The results obtained using this technique should be considered as indicative because the average mass of glowing firebrands is taken to be equal to the average mass of glowing firebrands that fell into the collecting pans. This was not the case because our observations showed that the percentage of tiny firebrands that fell into the collecting pans was smaller than large firebrands. Consequently, the calculated value tends to be larger than the actual value, particularly for experiments in which large firebrands are produced.

The glowing firebrand mass fluxes were calculated based on the above-mentioned technique and the outcomes are presented in table 4.5 and figure 4.14b. The results show that the ember generator produces the firebrand mass flux in a wide range from 0.10 $g.m^{-2}.s^{-1}$ to 6.13 $g.m^{-2}.s^{-1}$. According to the results, the mass flux increases by either increasing the wind speed or the height of the flaps.

Figure 4.15 Collected firebrands in experiments with flap of 150 mm and high wind speed.

An important characteristic of the ember generator is the mass ratio of generated glowing firebrands to initial mulch. The total mass of glowing firebrands can be calculated by multiplying the mass flux, the duration of the experiment and the area of the test section. The results are presented in table 4.6. According to the results, the total mass of the generated firebrands changed from a minimum of 1.964 grams to a maximum of 120.393 grams, corresponding to mass ratios of 0.2% and 15.0%, respectively. A further experiment is

required for a better understanding of the large difference between the minimum and maximum ratios. In a supplementary experiment, a 65.27 gram load of the same hardwood mulch used in the previous experiments was completely burned to ashes without allowing the ashes to escape from the container. The final mass decreased to about 2.60 grams, representing a decrease of 96%. The results of this experiment are used to illustrate the main results in section 4.3.7.

Table 4-6 Total estimated mass of generated firebrands in experiments

Flap height (mm)	Wind speed (m/s)	Mass of generated glowing firebrands (grams)
50	13.4	1.964
	16.0	10.802
	18.0	45.369
100	10.7	8.249
	12.7	34.763
	14.6	80.917
150	7.3	2.357
	9.2	105.074
	10.9	120.393

4.3.7. Discussion

The initial tests of the ESS demonstrate the capability of the design to work under various wind speeds and screen porosities. The reverse firebrand flow was not observed, in spite of using double layer low porosity screens that covered the entire test section. The maximum wind speed in the test section was 21 m/s in the absence of any screen in the test section. The flap causes some turbulence and non-uniformity both on temperature and velocity of air flow in the test section. The maximum spatial velocity non uniformity was measured to be 9.54% at the inlet of the test section and 6.34% at the outlet of the test section for the 150 mm flap. The temperature inside the test section reached a steady value after about 2 minutes of the fan running. The maximum temperature non uniformity of 4.7˚C was determined at the inlet of the test section for the 150 mm flap. These results call for awareness in the selection of the flap. A high flap produces a higher wind speed in the ember generator as well as higher non uniformities at the test section, which may not be compatible with the requirements of some applications. Generally speaking, non-uniformity greater than 10% is not acceptable, but it reduces to 5% for some applications. In the absence of any information on non-uniformity of the Baby Dragon, the 2.5% non-uniformity caused by the 50 mm flap appears to be acceptable. A comparison between non uniformities at the inlet and at the outlet of the test

section shows that by increasing the distance between the flap and the test section, a better uniformity is achievable. However, this increase may have a negative impact on firebrand flow due to their possible quenching over a longer distance.

The results demonstrated that in the case of the 150 mm flap, contrary to the other cases, the flux of the glowing firebrand at the highest wind speed (10.9 m/s) decreased compared to the flux at the medium wind speed (9.2 m/s). This can be explained in two ways. First, from table 4.3, it can be seen that the mean mass (3.0 milligrams) and projected area (16.10 mm^2) at the highest wind speed are higher than those (1.3 milligrams, 7.20 mm^2) at the medium wind speed. This led to the increase in the mass flux, despite the lower number flux (see figure 4.14). An alternative way to explain the decrease of firebrand flux at the highest wind speed is to examine the difference between the estimated total mass of the firebrands in the two cases (Table 4.6). According to the table, the total mass of the generated firebrands was 120.393 grams at the corresponding maximum wind speed and 105.074 grams at the medium wind speed. As only negligible amounts of mulch remained in the generator at the end of the experiments, it can be concluded that a higher percentage of firebrands were not properly burned or not burned at all in the case of the maximum wind speed at the 150 mm flap. Figure 4.15 appears to further support the argument. Therefore, it is reasonable to conclude that for the 150mm flap, increasing the wind speed from medium to high leads to producing a comparatively lower number but larger-sized firebrands in the earlier stages of combustion. Therefore, the wind speed in the generator must be limited with short flaps if only the glowing firebrands are required.

The supplementary experiment showed that the mulch lost 96% of the initial mass when it was completely burnt. Thus, it was expected that the final mass of the 800 gram mulch would become at least 32 grams. Table 4.6 shows that in five cases out of the nine, the final mass was greater than 32 grams. This demonstrates that the firebrands were not completely burned. However, in four cases, the final mass of the glowing firebrands were less than 32 grams, which shows that a percentage of the firebrands were completely burned before approaching the test section. It should be noted that observation in these cases ruled out the alternative possibility of unburned firebrands passing through the test section. Three of the cases were at the low wind speed for the three flaps and the fourth case was for the 50 mm flap at the medium wind speed. These results lead to the conclusion that the wind speed in the generator in these cases was not sufficient to lift heavy firebrands, only the small size or fully-burned

firebrands and ashes. This demonstrates that the ESS is able to produce a variety of different sizes and masses of firebrands in different stages of combustion.

The results show that the size of the firebrands is slightly smaller than firebrands in actual wildfire events. It should be noted that the projected area in this work and the surface area reported in the literature review from laboratory studies (section 2.3.3) are not quite the same but the difference is not significant for the firebrands produced in this work (see figure 4.12a). Previous studies revealed that about 85% to 90% of the firebrands produced in actual wildfire events have a size less than 50 mm^2, which is less than the minimum ratio of 93% measured in this work. This shows that the firebrands produced by the ESS nearly simulate an actual or a slightly worst-case scenario in terms of firebrand penetration through screens.

4.4. Summary

An experimental apparatus was designed and manufactured at the USQ workshop in order to simulate a firebrand shower. The design of the Ember Shower Simulator was inspired by the NIST laboratory scale firebrand generator (NIST baby dragon) and adapted with particular improvements that enable experiments with low-porosity screens at high wind speed up to 21 m/s. The simulator consists of a wind tunnel and an ember generator that was mounted underneath the wind tunnel. An L-shaped stand was fabricated to direct and collect firebrands outside the tunnel. The quantity of fire embers at two sides of the wire screen was recorded with a high-speed camera. The initial visual investigation of recorded videos was carried out in Adobe Premier Pro and the number of fire embers was counted in MATLAB using the image processing toolbox.

The performance of the ESS was assessed through several experiments. The flaps on the splitters were major source of flow non-uniformity inside the test section. The turbulence intensity had a maximum of 3.7% in the test section. A comparison between the non-uniformity of ESS and common wind tunnels used in previous fire research showed that the mean non-uniformity measured for ESS is within the acceptable range reported in previous works. The temperature inside the test section had a maximum variance of 4.2°C when the highest flap (150 mm) was mounted on the splitter. The mass, projected area and mass flux as well as firebrand flux were presented. It was found that the simulator is capable of working with various wind speeds and producing different sizes of firebrands. The size distribution of the generated firebrands was biased towards producing smaller sizes than addressed by

literature. It showed the ability of the ESS to simulate the worst-case scenarios in terms of performance of the screen in containing firebrand showers.

Chapter 5

Performance of screens to contain firebrands

5.1. Introduction

In the previous chapter, the design and development of ember shower simulator was explained and the performance of ESS was assessed by several preliminary experiments. This chapter aims to report the results of experimental works carried out to fulfill the objectives set in section 1.8 in relation to screen performance against firebrand attacks. Objectives 3 to 7 assess the effect of screen geometries on the performance of screens against firebrands and objective 8 looks at the combined effect of buffer zones and metal screens on screen performance. This chapter presents the results of this experimental work in two parts. Section 5.2 explains the experimental results for the effect of screen geometries on screen performance to contain leaf firebrands. It begins with the assessment of uncertainty in the experimental outcomes from Eucalyptus leaf firebrands prior to assessing the impact of screen geometry: opening size, wire diameter, screen manufacturing type and opening shape as well as firebrand flow orientation. Then, in section 5.3, the experimental work to evalute the combined effect of a buffer zone and screens with different opening size on protecting an object against firebrand attacks is presented. Sections 5.4 and 5.5 provide a summary of notable results and a list of conclusions, respectively.

5.2. Effect of screen geometry on screen performance to contain firebrands

5.2.1. Preliminary Experiments

Several preliminary experiments were performed to determine the minimum number of leaf embers required for repeatable results and to assess the possible effects of the intensity of the ember shower and ambient conditions on the results. The reasons for selecting Eucalyptus leaves as a source for firebrands for this experiment is provided in section 2.4, page 39.

Initial experiments showed that good repeatability could not be achieved only by increasing the time of the experiment or the number of embers without adopting a special procedure. In an experiment in which approximately 20,000 embers were recorded, the penetration ratios (see section 2.3.6) for twenty clusters of 1000 embers were measured and the results demonstrated a variance of ±38.4%. The change of average size of approaching embers during the experiment was identified as the main reason for the high variance. It was found that a smaller variance could be achieved if the results for the entire embers produced in an experiment were compared with those of the next experiment. The results of three consecutive experiments in which approximately 20,000 embers were produced showed a variance of ±3.0%. Taking into account the uncertainty of 5.0% in the counting process, the procedure was accepted and utilised for the remaining work.

Table 5-1 the penetration ratio (Eucalyptus leaf fragmentation ratio) for different ember shower intensities using a square woven wire screen with porosity of 54% and opening size of 3.15 mm at the wind speed of 14.5 m/s.

Exp .No	Intensity ($\frac{firebrands}{s.m^2}$)	Penetration ratio
1	2380	2.62
2	6716	2.80

The effect of the intensity of the ember shower on the measured penetration ratio was assessed at two intensities of 2380 ($\frac{firebrands}{m^2.s}$) and 6716 ($\frac{firebrands}{m^2.s}$) (see table 5.1). The intensity was increased by mounting a higher flap while the wind speed (14.5 m/s) at the test section and the amount of leaves (producing around 20,000 embers) at the generation section were kept unchanged. The comparison between the results of the two successive experiments shows a variance of ±3.3%. Taking into account the uncertainty of the counting and the results of two consecutive experiments with approximately 20,000 embers at an identical

intensity having a variance of ±3.0%, the effect of the intensity of the ember shower was marked as minor.

Four preliminary experiments on different days were performed to estimate the possible effects of ambient conditions on the results (see table 5.2). The penetration ratio showed a variance of ±6.8%. The main experiments were performed on different days and ambient conditions could not be controlled. The maximum overall uncertainty of the results was calculated using the root mean square values. The maximum overall uncertainty was 8.9% based on 5.0% uncertainty of counting, 6.8% uncertainty of ambient conditions, 2.1% uncertainty of measuring mesh size and porosity, and 2.1% uncertainty related to wind speed measurements.

Table 5-2 The effect of ambient conditions on penetration ratio (Eucalyptus leaf fragmentation ratio) of a square woven wire screen with porosity of 66%, opening size of 6.85 mm, and wire diameter of 1.54

Date	16 April	10 June				11 June	23 June
Temperature(C)		24	18	17		19	
Relative Humidity (%)				62	73.5	70.5	47
Penetration ratio				2.98	2.6	2.95	2.92

5.2.2. Effect of opening size

The uncertainties of experiments provided in section 5.2.1.The impact of screen opening sizes and porosities on the penetration ratio was investigated, and the results are listed in table 5.3. The wind speed was set as 14.5 m/s inside the test section, while no flap was mounted on the splitter. The load of Eucalyptus leaves placed in the ember generator of ESS was 160 g for all experiments, then ignited with an external source. This experiment condition was the same for all experiments with Eucalyptus leaf firebrands.

Table 5-3 The Eucalyptus leaf fragmentation ratio of four square woven wire screens with different porosities, opening sizes and wire diameters at the wind speed of 14.5 m/s

Exp. No	Opening size (mm)	Wire diameter (mm)	Fragmentation ratio
1	0.99	0.54	1.29
2	1.61	0.57	3.07
3	6.85	1.56	2.96
4	11.15	1.51	2.29

The experiments show that no firebrands remain on the arrival side of the screen after terminating the experiment regardless of the opening size, but the number of embers on the downstream side and retention time change. This observation shows that the approaching firebrands shatter into pieces and produce secondary firebrands, and the secondary firebrands, being smaller than the opening size, pass through the screen. Therefore, the penetration ratio exceeds one. The results show that it is more relevant to call the ratio defined in section 2.3.6 a fragmentation ratio instead of a penetration ratio for leaf embers.

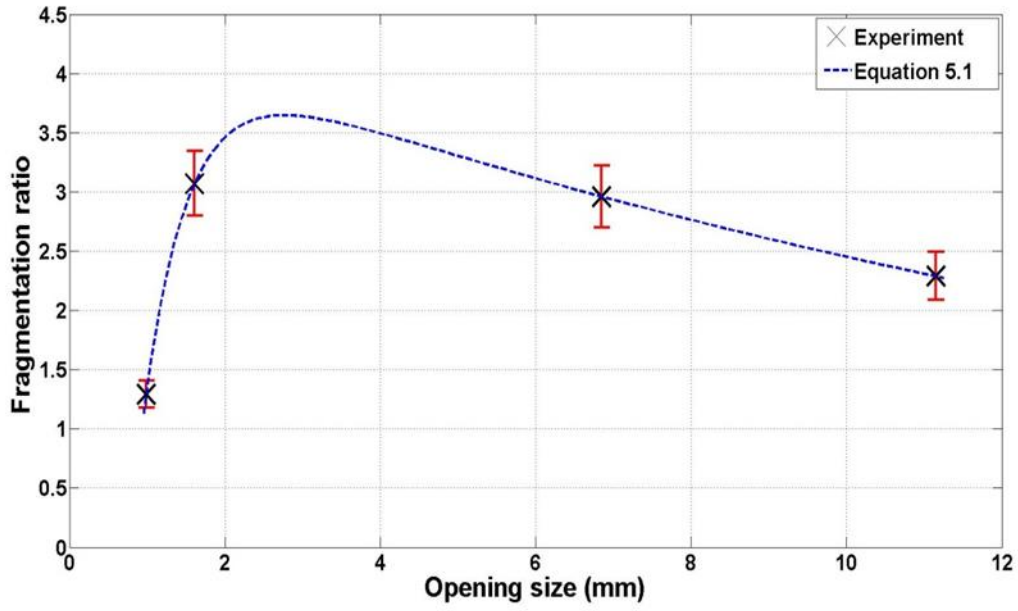

Figure 5.1 Eucalyptus leaf fragmentation ratio versus opening size of square woven wire screens at the wind speed of 14.5 m/s.

According to figure 5.1, the fragmentation ratio of burning embers sharply increased from 1.29 at the minimum opening size of 0.99 mm to a maximum measured value of 3.07 at the opening size of 1.61 mm, and then moderately decreased to 2.29 at the maximum opening size of 11.15 mm. Figure 5.2 contains four snapshots from the videos showing the behaviour of embers in the test section for four screens with different opening sizes. The retention time and the number of secondary embers for the minimum opening size screen of 0.99 mm (figure 5.2a) is the highest. Due to the high retention time which gives sufficient time for a high percentage of embers to burn out and quench, many embers passing through that screen are not glowing/flaming, thus the fragmentation ratio of the burning embers is a minimum. As the opening size increases, the retention time sharply decreases (see figure 5.2b) and a higher percentage of secondary embers are still burning, consequently the fragmentation ratio of the burning embers increases. By further increasing the opening size (see figure 5.2c), the

effect of the number of passing embers becomes dominant and the fragmentation ratio decreases. It should be noted that the size of embers passing through the screens always increases as the opening size increases. The retention time becomes negligible for openings greater than 1.61 mm.

Based on the experimental results, the correlation of opening size (a) and fragmentation ratio (FR) was developed as,

$$FR = 4.455\,\mathrm{e}^{-0.05969a} - 16.4e^{-1.752a} \qquad (5.1)$$

Equation 5.1 has a maximum 1.15% error with respect to experimental results at an opening size of 0.99 mm. Figure 5.1 indicates the experimental results and the estimation of formula

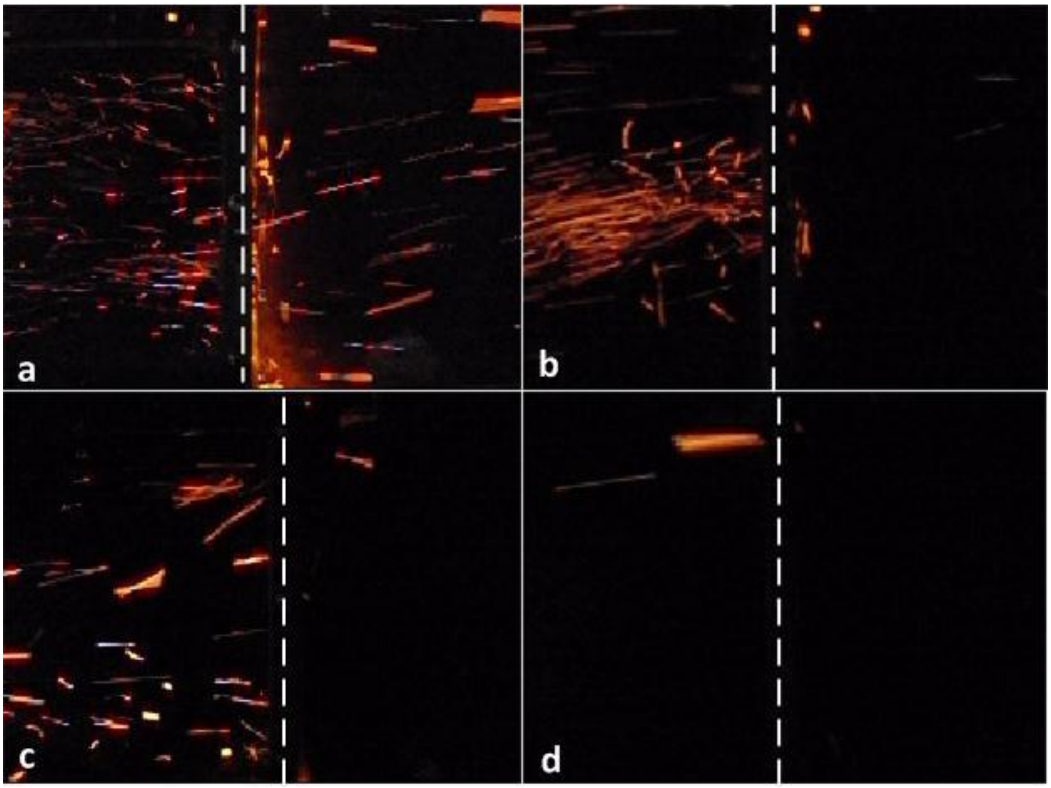

Figure 5.2 Four selected frames of the captured video showing approaching and leaving Eucalyptus leaf embers during the experiments with square woven wire screens at the wind speed of 14.5 m/s. The dashed white line is screen; the flow direction is screen. a) Screen with an opening size of 0.99 mm, wire diameter of 0.54 and porosity of 41%; b) screen with an opening size of 1.61 mm, wire diameter of 0.57 mm and porosity of 54%; c) screen with an opening size of 6.85 mm, wire diameter of 1.56 mm and porosity of 66%; and d) screen with an opening size of 11.15 mm, wire diameter of 1.51 mm and porosity of 78%.

5.1.

Leaf embers showed fragmentation ratios of greater than one due to the production of secondary fire embers. Secondary fire embers are produced because of the weak structural strength of burning leaves that lead them to shatter into small pieces on their arrival at screens. The fragmentation ratio experienced a sharp increase from the minimum opening size (0.99 mm) up to opening size of 1.61 mm and then gradually decreases for opening sizes greater than 6 mm. The main cause of experiencing this steep increase in fragmentation ratio was the effect of retention time that was tremendous for the opening size of less than 1.61 mm for leaf embers. The retention time increased with the reduction of opening size and therefore many of the embers quenched before passing the screen. This is in agreement with the previous work by Manzello et al. (2011), who showed that the retention time of firebrands (wood mulches derived from Norway Spruce trees) behind screen increases with the decrease of the mesh size (see section 2.3.6). By decreasing the mesh size, firebrands stay behind the screen until their size fits the mesh size and some reach their burnout time and then quench before passing the screen.

5.2.3. Effect of wire diameter and porosity

The opening size and porosity of common commercial screens increase simultaneously. In the previous section, the effects of the opening size have been investigated but it should be noted that the porosity also increased. Therefore, it is not entirely clear that the obtained results are indeed due to opening size. The porosity has been reported as the key factor determining the drag force on the screen (Sharifian 2010) and the capability of screen in limiting the radiant heat flux of wildfires (Sharifian and Buttsworth 2008, Sharifian and Buttsworth 2010). To break the trend between the increase of opening size and porosity, two screens with approximately the same porosity but different opening sizes were tested. The first screen has an opening size of 1.61 mm and porosity of 54.5% and the second screen has an opening size of 3.15 mm and porosity of 53.7% (see table 5.4).

Table 5-4 The leaf fragmentation ratio of two square woven wire screens with porosity of 54% and different opening sizes and wire diameters at the wind speed of 14.5 m/s.

Screen	Opening size (mm)	Wire diameter	Porosity	Fragmentation ratio
1	1.61	0.57	54.5%	3.07
2	3.15	1.15	53.7%	2.76

This result can be explained by considering the wire diameters of screens, which are related to porosity and cell size (see section 2.2.2, Eq. 2.5). The first and second screens have wire diameters of 0.57 mm and 1.15 mm, respectively. From figure 5.1, a fragmentation ratio of 3.62 for the second screen could be reasonably expected if its wire diameter was equated with the first screen and consequently the porosity was increased to 71.7%. The difference between the experimental result (2.76) and the expected result (3.62) is 31.1% which is far greater than the estimated experimental uncertainty of 8.9%.

The observation showed that there are two reasons for the decline of the fragmentation ratio from the expected value. A larger diameter wire blocks a higher percentage of the firebrands and considerably increases the retention time. In addition, as their contact surface area with the firebrands is greater, they do not cause breakage of firebrands as much as thinner wires do. Therefore, the wire diameter (or porosity) is one of the key factors influencing the fragmentation ratio.

5.2.4. Effect of screen type

The screens are categorised based on the way they have been woven or manufactured. The possible effect of screen types on the fragmentation ratio was investigated by the use of two different types of screens. The first type was the woven wire screen with an opening size of 6.85 mm and porosity of 66%. The second screen was a flat screen with 6.82 mm opening size and nearly the same porosity of the woven wire screen. The two screens were tested with conditions as explained in section 5.2.2 and their fragmentation ratios were measured.

Table 5-5 The Eucalyptus leaf fragmentation ratio of two different types of screens with identical porosity at the wind speed of 14.5 m/s

Screen type	Opening size(mm)	Wire diameter(mm)	Fragmentation ratio
Woven	8.41	1.56	2.96
Flat	8.34	1.52	2.38

Table 5.5 lists the details of experiments and results, and figure 5.3 shows snapshots of the firebrands' behaviour during the observation. The results show that the fragmentation ratio of the flat screen is lower than that of the woven wire screen. The fragmentation ratio of the woven wire screen is 2.96, while this ratio declined to 2.38 (19.6% decrease) for the flat screen. The reason is similar to what was explained for the impact of the wire diameter. The distances between openings of a flat screen are flat and have a larger contact area with embers than those of the woven wire screen, thus the embers split into fewer pieces which reduces the fragmentation ratio.

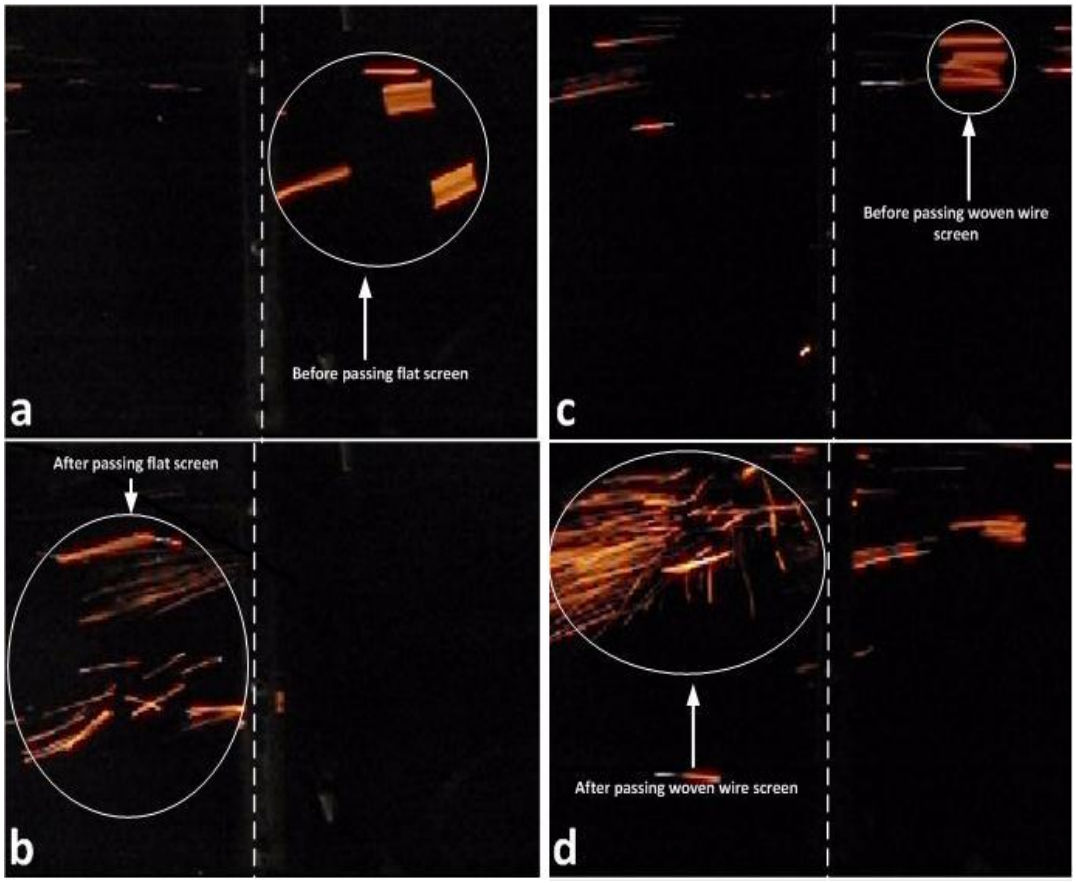

Figure 5.3 The photos of Eucalyptus leaf embers before and after passing through two types of screens with porosity of 66% at the wind speed of 14.5 m/s; a) Approaching embers to a square flat screen with an opening size of 6.82 mm and gap size of 1.52 mm; b) Leaving secondary embers from the screen described in (a); c) Approaching embers to a square woven wire screen with an opening size of 6.85 mm and wire diameter of 1.56 mm; and d) Leaving secondary embers from the screen described in (c).

5.2.5. Effect of Opening shape

The possible effect of opening shape on the fragmentation ratio was investigated using three flat screens with approximately the same porosity and opening shapes of square, circular and rectangular. The experimental conditions were the same as explained in section 5.2.2. The square cell shaped screen had a mesh size of 8.34 mm and an opening size of 6.82 mm, while the rectangular cell shaped screen had a mesh size of 10.5 mm×5.35 mm with an opening size of 8.65 mm×4.52 mm. The circular cell shape screen had a cell diameter of 9 mm and an opening diameter of 8.3 mm. The porosity of the square, rectangular and circular shape screens were 66.9%, 69.5% and 66.8%, respectively.

Table 5-6 The Eucalyptus leaf fragmentation ratio of three flat screens with different opening shapes and sizes at the wind speed of 14.5 m/s.

Mesh shape		Opening size (mm)	Pitch Length (mm)	Fragmentation ratio
Square		6.82	8.34	2.38
Rectangular	Warp	8.65	10.5	2.57
	Weft	4.52	5.35	
Circular		8.3	9	2.42

Table 5-7 The Eucalyptus leaf fragmentation ratio of a square wire woven screen with a porosity of 54%, opening size of 3.15 mm, and wire diameter of 1.15 mm in three different orientation at the wind speed of 14.5 m/s

Opening size	Wire diameter	Orientation (°)	Fragmentation ratio
3.15 mm	1.15 mm	45	1.63
3.15 mm	1.15 mm	90	2.76
3.15 mm	1.15 mm	135	2.04

Table 5.6 lists the details of the screens' dimensions and measured fragmentation ratios. The measured fragmentation ratios show negligible changes in all three experiments. While the fragmentation ratio of the square mesh shape is 2.38, it is 2.43 for the circular screen (+2.1%) and 2.57 for rectangular screen (+7.9%). The change of the ratio is less than the uncertainty of the experiment (8.9%), therefore the results are not conclusively different.

5.2.6. Effect of screen orientation

All applied screens in previous experiments were normal to (90°) the firebrand flow direction. This investigation was carried out by applying two different orientations in addition to the vertical position used previously. The wire screens were positioned at a 45° angle with respect to the firebrand flow and then laid back with a 135° angle. The selected woven wire screen had a cell size of 4.3 mm and porosity of 54%.

The experimental results are detailed in table 5.7. The results show that tilting the screen has a significant impact on the fragmentation ratio. For the wire screen with the 45° orientation (tilted forward), the fragmentation ratio decreased remarkably from 2.76 for the vertical screen to 1.63 (41% decrease). For the wire screen with the 135° orientation (45° tilted backward), the fragmentation ratio is 2.04, which shows a 25% increase with respect to the 45° degree screen and 26.1% decrease with respect to the vertical screen. Figure 5.4 indicates the experimental results and estimation of fragmentation ratios by the best fitted curve.

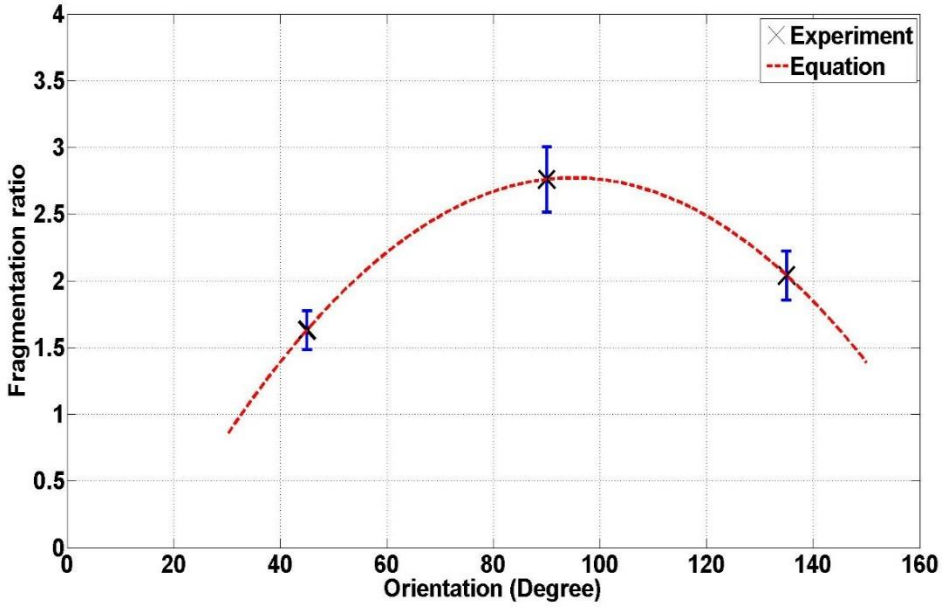

Figure 5.4 Eucalyptus leaf fragmentation ratio versus orientation angle for a square woven wire screen with opening size of 3.15 mm, wire diameter of 1.15 mm and porosity of 54% in wind speed of 14.5 m/s.

The reduction of the fragmentation ratio for tilted screens was further investigated by reviewing the captured videos. The observation for the 45° orientation shows that the number of trapped embers behind the screen increases in comparison with that of the vertical screen. The possible reasons are the decrease of the projected area of screen openings and reduction of the perpendicular wind force against the screen to push the embers through the screen. In

addition, the observation shows that in the case of the 45° screen, some embers move downward and accumulate at the bottom of the screen on the upstream side (see figure 5.5a). These embers spend some time behind the screen before passing through the screen. Due to the delay, the retention time increases which gives sufficient time for some embers to quench. For the case of the 135° screen, the number of trapped embers behind the screen is similar to the 45° screen, but embers are inclined to slip upward on the screen (see figure 5.5b). The slippage on the screen causes some embers to shatter and find an opportunity to pass through the screen

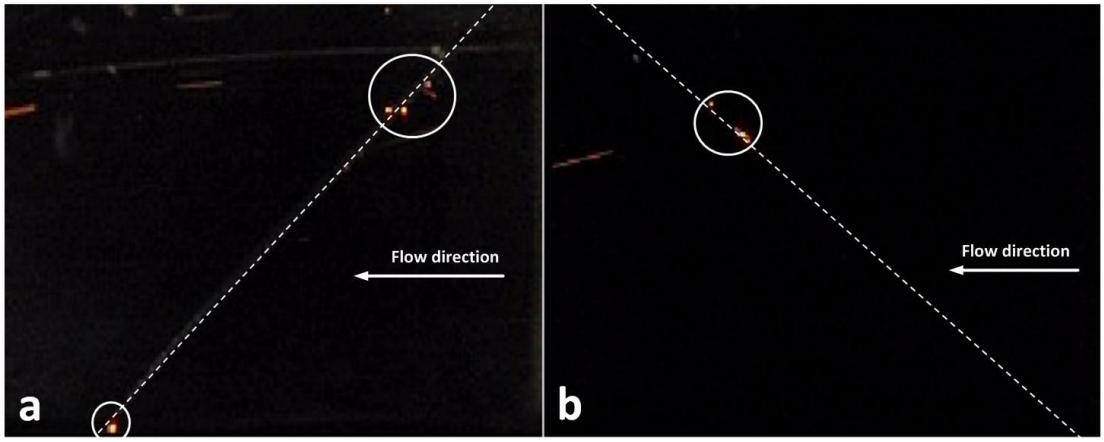

Figure 5.5 Two captured frames during experiment on a square woven wire screen with opening size of 3.15 mm, wire diameter of 1.15 mm and porosity of 54% for two different orientation angles; a) 45° degree orientation; and b) 135° degree orientation.

.

5.3. Combined effect of buffer zone and woven wire screens on mitigating associated risk of firebrand attacks

Three experiments including one in the absence of a screen and two others using screens with aperture sizes of 1.61 mm and 1 mm were performed. All experiments were conducted several times to check the repeatability of the experiments. The experimental equipment consisted of the ESS and L-shaped stand (see section 4.2.5). The fuel beds consisted of oven-dried cotton cloths that were cut and placed in two aluminium pans. The pans were positioned on the L-shaped stand outside the ESS. Also, a water-filled aluminium pan was placed near the fuel bed to capture the firebrands for further analysis. A buffer zone with an arbitrary size of 4.48 m between the screen fuel beds was applied. It is the average distance on streamlines and the maximum distance that a representative glowing firebrand could still reach the fuel

bed with current setup. Figure 5.6 shows the experimental layout including aluminium pans on the L-shaped stand and ESS. In all the experiments, the average wind speed in the wind tunnel was set at 10 m/s, and an identical load (0.5 kg) of oven-dried hardwood mulch out of a fully mixed pile was deposited into the fire ember generator. Hardwood mulch was used because preliminary experiments showed that a lower percentage of smouldering hardwood mulch (in comparison to leaf firebrands) extinguishes during passage through the buffer zone. (see section 2.4, page 39). Three cameras were applied in these experiments. Camera 1 (CASIO, see section 4.2.3.1) was used to monitor the firebrands before and after the screen at the frame rate of 420 fps, similar to the previous application in section 5.2. Also, camera 2 (Canon, see section 4.2.3.1) was placed near the L-shaped stand in order to monitor the fuel beds and Camera 3 was mounted behind the L-shaped stand towards the exit of the ESS. Cameras 2 and 3 had the same brand and model and recorded the videos at a standard frame rate of 30 fps.

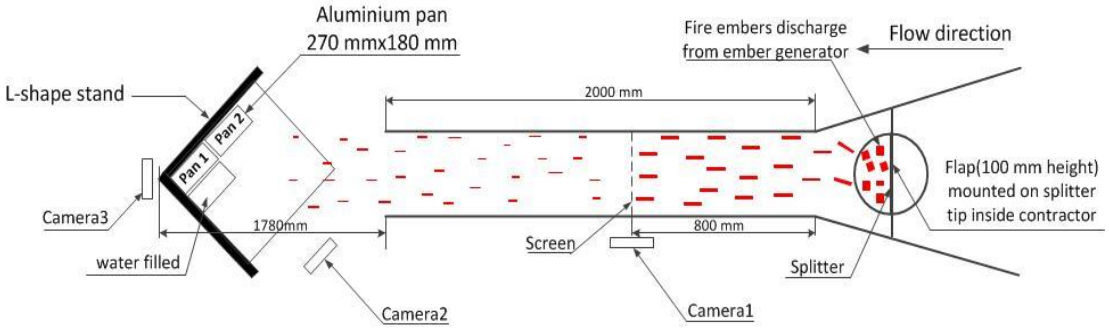

Figure 5.6 Top view of the experimental layout showing ESS and fuel bed positions.

5.3.1. Fuel bed ignition

The results showed that, in all the three cases, the fuel beds can be ignited. The word ignition refers to smouldering combustion throughout this study as in no case was a stable flaming combustion observed. Figure 5.7 shows the ignited points for the cotton cloth fuel bed in pans 1 & 2 in the absence of a screen and in the case of using the screens with the opening sizes of 1.61 mm and 1 mm in the first round of the experiments. All experiments were repeated at least three times and yielded similar results. The detailed results of the first round of the experiments performed with cotton cloth and the overall results of all experiments are listed in table 5.8.

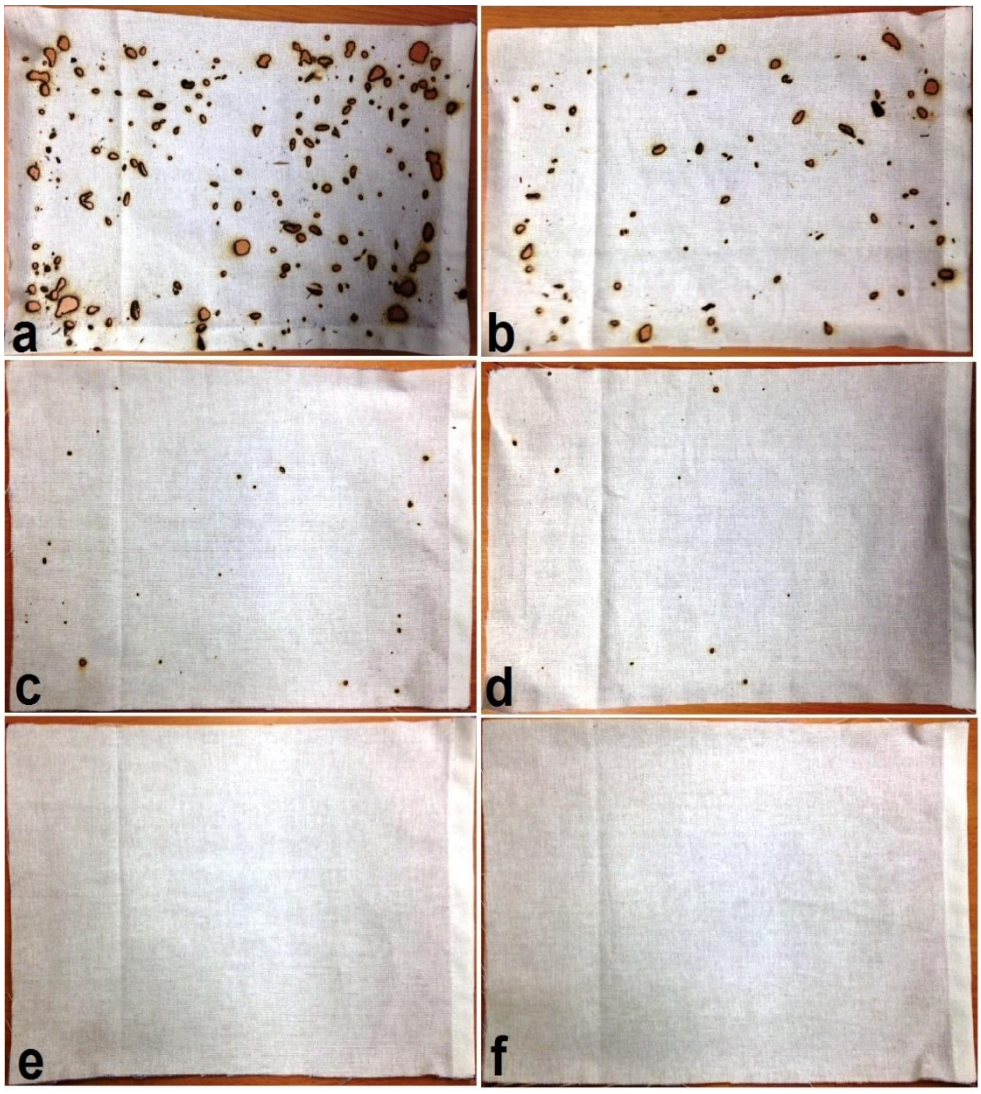

Figure 5.7 Pictures of cotton fuel beds captured after the first round of the experiments: a) Pan1 after no-screen experiment, b) Pan 2 after no-screen experiment, c) Pan1 after 1.61 mm-screen experiment, d) Pan2 after 1.61 mm-screen experiment, e) Pan1 after 1 mm-screen experiment, and f) Pan 2 after 1 mm-screen experiment.

Table 5-8 Number of ignited points detected on the fuel beds at wind speed of 10 m/s.

Case	Number of ignited points on fuel beds (first round)	Range of ignited points on fuel beds in all the experiments
No screen	304	90-304
Screen: 1.6 mm openings	47	17-47
Screen: 1.0 mm openings	0	0-7

According to the data in table 5.8, the number of ignited points decreased for the screen with smaller openings. In the absence of a screen, the number of the ignited points was 304 for the cotton cloth fuel beds. When the screen with the opening size of 1.61 mm was used, the number significantly reduced to 47. The screen with the openings of 1 mm had the best performance. In that case, the number of ignited points dropped to zero in the first round of the experiments. However, in some later rounds, the fuel beds were ignited. The full range of the ignited points observed in the repeated experiments are presented in table 5.8.

Table 5-9 Fragmentation ratios and numbers of firebrands at two sides of the screen holder at wind speed of 10 m/s.

Case	Number of		fragmentation ratio	overall range of fragmentation ratio
	approaching firebrands	leaving firebrands		
No screen	8266	8455	1.02	1.02-1.03
Screen: 1.6 mm openings	5131	6560	1.28	1.23-1.28
Screen: 1.0 mm openings	7746	7456	0.96	0.85-0.96

The results presented in table 5.8 are the most the most interesting from a practical point of view from among all the results presented in this work. They show the number of ignited points of the fuel beds for the same amount of burning feeds. However, they do not provide much insight into the above experiments. Therefore, for a better understanding, the whole process was broken down into four steps. The first step is the path between the ember generator and the first virtual counting strip located 90 mm before the screen holder; the second step is the path between the first counting strip and the second virtual counting strip located 110 mm after the screen holder. The next step is the path between the second counting strip and the fuel beds, while the final step is the state of the fuel bed before and after the exposure to the firebrand shower.

5.3.2. Firebrands from ember generator to the screen holder

The number of generated firebrands was expected to be similar in all experiments as the mass of hardwood mulch (0.5 kg) and the wind speed in the test section were identical. However, the recorded numbers of firebrands showed a level of discrepancy greater than the uncertainty of the counting process (5%). For example, in the first round of the experiments (table 5.9), the number of the firebrands approaching the test section were 8266, 5131, and 7746, showing an uncertainty of 24% around the mean value (6699 ± 1568). In addition, the flow of the generated firebrands was not steady and uniform. Figure 5.8 shows the number of firebrands at both sides of the screen with opening size of 1 mm versus time. The figure shows that the number of the firebrands observed in the test section started from a low value, and progressively increased to reach a maximum before decreasing toward zero at the end of the experiment. This typical performance of the ESS was observed in all the experiments. In addition, the size of the firebrands at the test section were not uniform, and the measured projected area varied from a minimum of 2 mm^2 to a maximum of 40 mm^2. Figure 5.9 shows a typical collection of the firebrands at the test section before the screen holder.

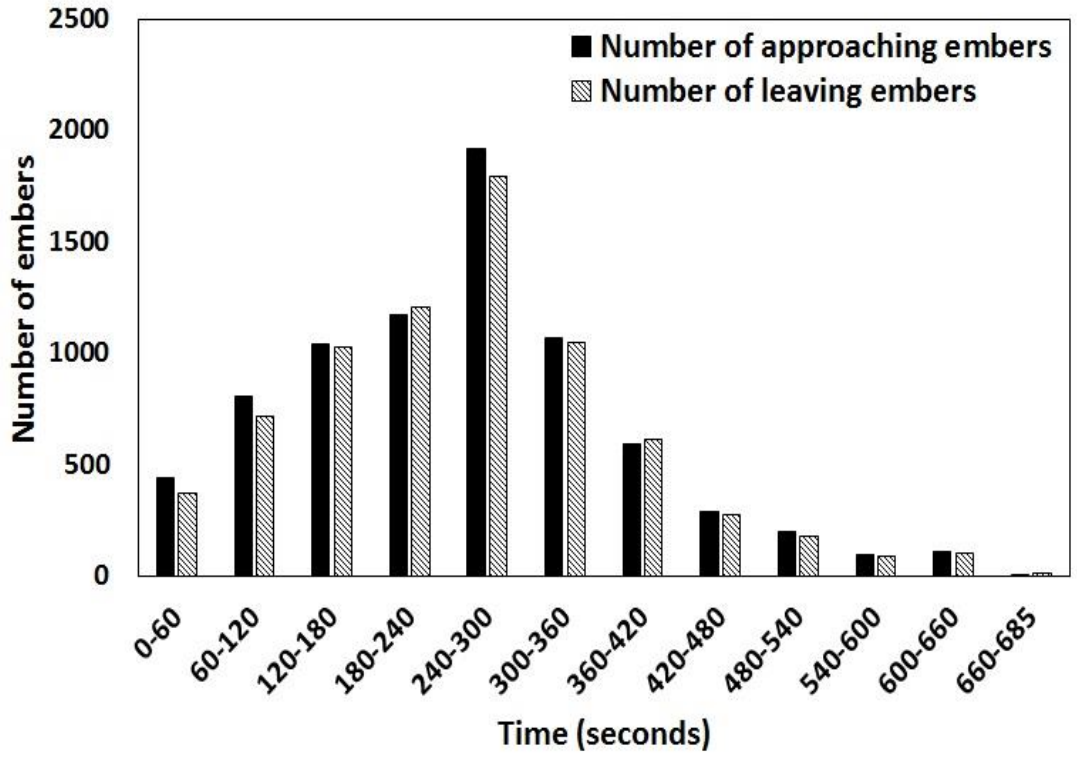

Figure 5.8 Typical number of firebrands at both sides of the screen with opening size of 1 mm.

Several factors can be the cause of variance in the number of generated firebrands in the experiments. The ESS does not provide any control on wind speed inside the generator, while the wind speed in the test section can be controlled. The pressure drop inside the filled test section is compensated for by moving the fan toward the duct inlet, which increases the speed inside the generator. Therefore, the variation of wind speed inside the generator can be the main cause of discrepancies. The hardwood mulch is mixed as homogenous batches, however some inaccuracies during the mixing process are expected. Other factors such as a variance in the flaming period of feeds before operating the fan or possible inaccuracy of placing the feeds at the same spot inside the generator for consecutive experiments can be taken into account as possible reasons. In addition, the moisture content of oven-dried batches possibly varied at the time of transferring feeds from the oven to the experiment site.

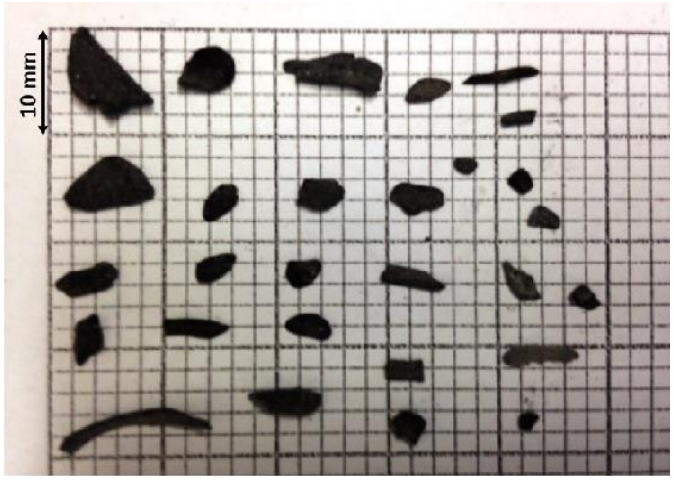

Figure 5.9 Firebrands collected inside the test section of the wind tunnel before screen holder.

5.3.3. Firebrand movement between the two sides of the screen holder

The present results show that the approaching firebrand flux does not appear to affect the fragmentation ratio. Figure 5.8 shows that at the fourth timeslot (180–240 s), in which the number of approaching firebrands was 466 (flux of 194 firebrands/m^2.s), the fragmentation ratio was 1.16. At the highest intensity, which occurred in the sixth timeslot (300–360 s), the number of approaching firebrands was 1125 (flux of 469 firebrands/m^2.s) and the fragmentation ratio was 1.33. During the seventh time slot in which the number of approaching firebrands was 827 (345 firebrands/m^2.s), the fragmentation ratio was 1.37.

Therefore, the fragmentation ratios of mulch firebrands are independent of their intensities at least when the flux is less than 469 mulch firebrands/m^2.s and for the conditions of these experiments. Similarly, it was shown (see section 5.2.1) that the fragmentation ratio does not appear to be related to the leaf firebrand flux.

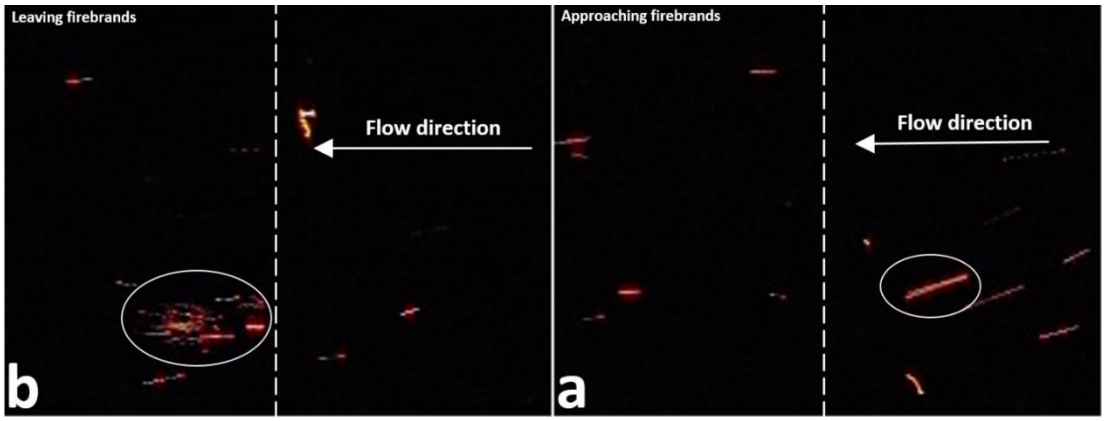

Figure 5.10 Shattering mechanism of a firebrand passing through the screen with opening size of 1.61 mm a) before the impact, and b) after the impact.

Table 5.9 lists the fragmentation ratio measured in the first round and the overall range of the ratio measured in all the experiments, where in the absence of a screen, the ratio varied from 1.02 to 1.03. A ratio greater than one was not initially expected. In practice, it was observed that some firebrands hit the sides of the tunnel and shattered into smaller pieces, something that is not expected to occur in wildland fires. However, due to the 5% uncertainty of the counting process, the result is not conclusive. The application of the screen with openings of 1.61 mm increased the ratio to between 1.23 and 1.28. In this case, it was observed that a fair percentage of approaching firebrands shattered into smaller pieces after hitting the screen (see figure 5.10), similar to what was reported for leaf firebrands (see section 5.2.2).

The secondary firebrands were smaller in comparison with those in the case of no screen, but still maintained their illumination. The shattering process was not reported in other studies (Manzello et al. 2010, Manzello et al. 2011), perhaps due to a lower wind speed (7 m/s) or a different type of mulch (Norway spruce). Instead, the firebrands paused before the screens, which was also observed in this work for the 1.61 mm screen. Figures 5.11a, 5.11b, and 5.11c show the pausing mechanism of firebrands taken by camera 3. Figure 5.11a shows the size of a firebrand when hitting the 1.61 mm screen. Figure 5.11b shows that the firebrand became smaller in size but still burning after 5 seconds. Figure 5.11c shows that it completely burnt to ash six seconds after the impact.

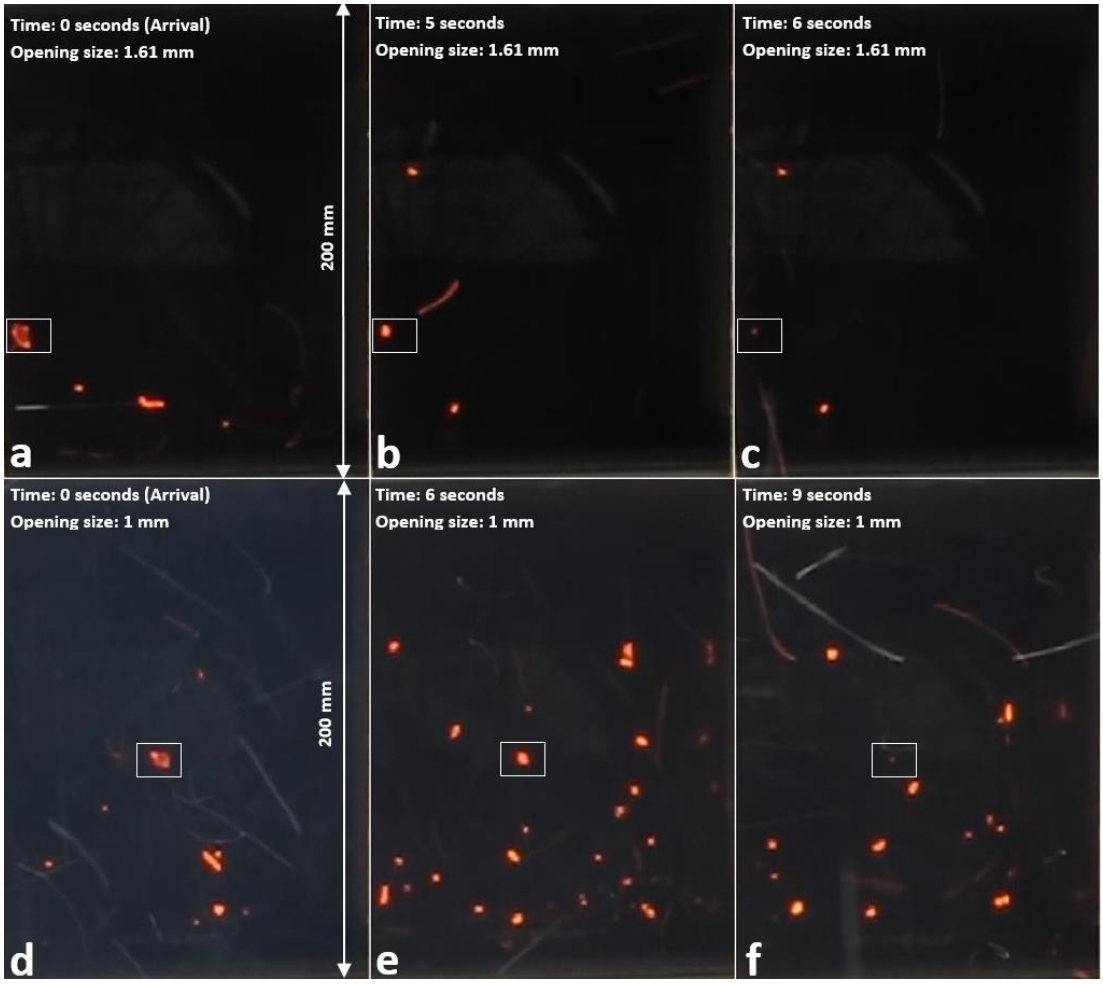

Figure 5.11 Front view of pausing mechanism of firebrands behind screens. a) A firebrand at the time of impact with the 1.61 mm screen, b) the firebrand of (a) after five seconds, c) the firebrand of (a) after six seconds. d) A firebrand at the time of impact with the 1.00 mm screen, e) the firebrand of (d) after six seconds, f) the firebrand of (d) after nine seconds.

The fragmentation ratio decreased to values in the range of 0.85 to 0.96 when the screen with the openings of 1 mm was utilized (Table 5.9). Based on the observation, a sizeable

percentage of approaching firebrands paused behind the screen until they completely burnt and fitted the screen openings (see figures 5.11d, 5.11e, and 5.11f). The figures show the size of a firebrand at the time of the impact, and six seconds and nine seconds afterwards. The shattering mechanism was still observed but to a lower extent, and the loss of illumination was evident.

The pausing mechanism was observed by Manzello et al. (2011), and the retention time of the firebrands behind the screen was reported. The delayed mechanism might be explained through the fact that a smaller opening provides a better support for susceptible firebrands.

5.3.4. Firebrands after the screen holder to the fuel bed

Table 5.10 presents the number of glowing firebrands after the screen and the number of firebrands that approached and made contact with the fuel beds. In the absence of a screen, the number of glowing firebrands which made contact with the fuel beds was the highest, and subsequently decreased as the aperture size decreased. The firebrand survival ratio is defined as the number of the glowing firebrands making contact with the fuel beds divided by the number of the glowing firebrands leaving the screen holder (counted in the second virtual strip, section 4.2.4).

Table 5-10 Number of firebrands detected after screens and on fuel beds, and firebrand survival ratio at wind speed of 10 m/s

Case	Number of firebrands after the screen (first round)	Number of firebrands on the fuel beds (first round)	Survival ratio (first round)	Overall survival ratio
No screen	8455	407	4.8%	4.5%-4.8%
Screen: 1.6 mm openings	6560	98	1.5%	1.1%-1.5%
Screen: 1.0 mm openings	7456	3	0.0%	0.0%-0.4%

However, it should be noted that some firebrands were not caught by the L-shape stand (around 40%), many quenched in their path to the fuel beds, or some flew over the fuel beds without making any contact. Therefore, the survival ratio defined here is a comparative ratio and is only valid under the conditions of this study. Figure 5.12 shows the size of firebrands reaching the fuel beds during the first round of experiments. As expected, the size decreased as the opening size of the screen decreased. It can therefore be concluded that the survival ratio decreases as the opening size decreases.

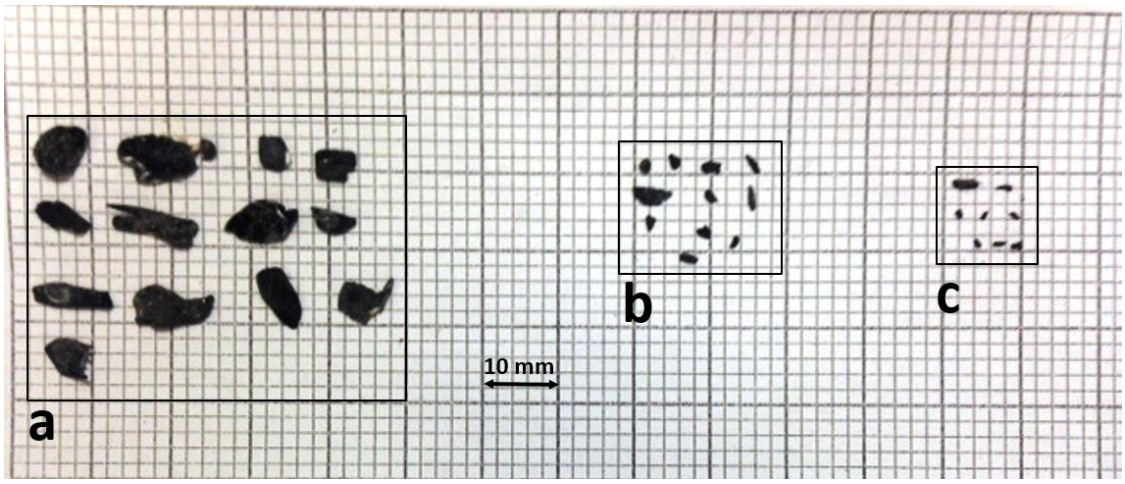

Figure 5.12 Firebrands collected near fuel beds during the first round of the experiments; a) without screen, b) screen with 1.61 mm opening size, and c) screen with opening size of 1 mm

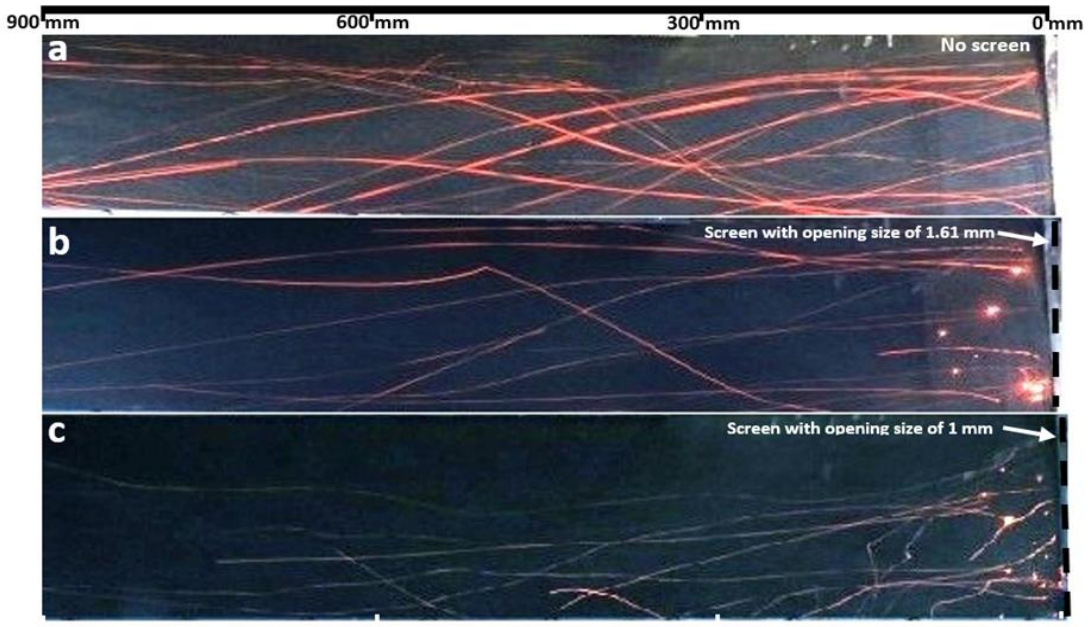

Figure 5.13 Captured pictures of firebrand traces in the test section of the wind tunnel at wind speed of 10 m/s under the experimental conditions of; a) no-screen, b) screen with the opening size of 1.6 mm, and c) screen with the opening size of 1 mm.

The above discussion suggests that the chance of firebrands becoming quenched along the buffer zone of 4.48 m significantly increases as the size of the screens' openings decreases. For further exploration, in separate runs after the main experiments, the movement of the firebrands in the test section was recorded with a long exposure time of 250 ms for the first camera. The resulting images are displayed in figure 5.13.

Figure 5.13a shows that most firebrands maintain their illumination along the wind tunnel in the absence of a screen. Figure 5.13b shows that in the case of 1.61 mm-screen, a lower percentage of the firebrands remain alight at the end of the tunnel compared to the previous case. Figure 5.13c shows that for the case of 1 mm screen, the tunnel is conspicuously darker than the two previous cases. Therefore, firebrands passing through the screen with the opening size of 1 mm have the highest likelihood of being quenched by the screen and also in their path to the fuel bed.

5.3.5. State of the fuel bed before and after the exposure

The firebrand hazard ratio was defined, which is the number of burnt marks on the fuel beds to the number of the firebrands making physical contact with it. Table 5.11 presents the firebrand hazard ratio measured in the first round of the experiments, as well as the range of the ratio measured during all the experiments.

Table 5-11 The number of firebrands that made contact with the fuel beds, the number of ignited points on fuel beds, and the hazard ratio of firebrands at wind speeds in the range of 0.5 m/s to 1.1 m/s.

Case	Number of		Firebrand hazard ratio (first round)	Overall firebrand hazard ratio
	firebrands on fuel beds	ignited points on fuel beds		
No screen	407	304	74.7%	32.5%-74.7%
Screen: 1.6 mm openings	98	47	48.0%	9.1%-48.0%
Screen: 1.0 mm openings	3	0	0.0%	0.0%-23.1%

The results show that as the size of screen aperture decreases, the ignition capability of the passing firebrands diminishes. It should be noted that the ratio of zero was found only three

times among seven experiments performed on the 1 mm screen. The overall results show that the firebrands were still capable of igniting the fuel beds.

5.3.6. Further discussion

The results show that the ESS did not generate a steady firebrand shower. However, by comparing the results at different stages of the experiments, it was shown that the intensity of the flux of firebrands does not appear to have a major impact on the fragmentation ratio. It should be recognized that these results are only valid for the range of the flux used during the experiments (less than 466 firebrands.m^{-2}.s^{-1}). A lower fragmentation ratio at higher firebrand fluxes, particularly for screens with smaller apertures, is not unexpected due to possible blockage of the openings by firebrands during the retention time.

The results show that two mechanisms of pausing and shattering cooperated during the passage of firebrands through the screens. The percentage of firebrands pausing behind the screen decreases as the opening size increased. It was also observed that a higher percentage of firebrands shattered into smaller pieces when the screen with larger openings was used for the opening size of range 1 –9.64 mm. These two mechanisms are expected to operate in parallel for other screens, at different wind speeds, and other types of feeds but in different proportions, thus resulting in different fragmentation ratios. According to the results presented in section 5.2.2, the passage of leaf firebrands through a screen with an opening size of 1 mm at wind speed of 14.5 m/s reported a fragmentation ratio of 1.29, which is considerably different from the results of this study. This indicates that, for a particular screen, a higher fraction of shattering mechanism occurs at higher wind speeds and/or for more susceptible firebrands. Therefore, the fragmentation ratios found in section 5.3.1 are only accurate under the specific conditions for which the testings were performed, but they can still be taken as indicative under different conditions.

Based on the current study, no conclusions, positive or negative, can be drawn for the cases without a buffer zone. The results show that a screen is significantly effective in reducing (but not eliminating) the intensity of firebrand showers at a distance of 4.48 m, but the intensity of secondary firebrands may increase without including a buffer zone. For instance, the fragmentation ratio and the size of the secondary firebrands reduced for a 1 mm screen opening size compared with those of 1.61 mm screen. However, during a wildland fire event, several types of firebrands simultaneously exist under varying wind speed conditions. Taking

into account that the fragmentation ratio is greater than one for a high wind speed and/or a vulnerable firebrand, the actual combined fragmentation ratio may exceed one. A fragmentation ratio greater than one indicates a higher firebrand shower intensity. However, the higher intensity does not necessarily lead to a worse condition, because the sizes of the secondary firebrands are smaller than those of the approaching ones.

The results appear to show that screens with smaller openings are more effective in lowering the intensity of firebrand showers than those with larger openings. However, care should be taken to extend these results to the real world. In the wind tunnel condition, all approaching firebrands are enforced to pass through the screen. In the real world due to build-up of a stronger stagnation pressure behind the screen with smaller openings, a higher percentage of firebrands may pass around or over the screen. Therefore, the use of screens with smaller openings may not be the best option.

5.4. Summary

The performance of screens in containing firebrands was evaluated, and the results were presented in this chapter. The preliminary experiments with firebrands sourced from Eucalyptus trees leaf indicated an 8.9% uncertainty for experiments. The effect of screen geometry on their performance to contain leaf firebrands were investigated. The results revealed two important mechanisms of firebrands: retention time; and shattering of firebrands. The impact creates smaller firebrands called secondary firebrands. The number of secondary embers was a function of screen opening size and its wire diameter. Due to the shattering mechanism and larger number of firebrands on the downstream side of screens, fragmentation ratios were greater than one in all cases. The number of glowing secondary firebrands for screens with opening size greater than 1.61 mm decreased as the opening size increased, and consequently the fragmentation ratio decreased. For screens with an opening size less than 1.61 mm, the retention time had a major impact on the fragmentation ratio. As the retention decreases, fewer embers completely burn out before fitting the size of opening, and therefore, the fragmentation ratio increases. The retention time for leaf firebrands became approximately zero when the opening size exceeded 1.61 mm, and thus only the number of secondary firebrands influenced the fragmentation ratio.

The diameter of the screen wires (or porosity) and the type of screen had impacts on the fragmentation ratio. For two screens with nearly the same porosity and varied opening size, a thinner wire that had a smaller contact area was able to produce more secondary firebrands;

thus, the fragmentation ratio increased. The application of flat screens showed a reduction in the fragmentation ratio since they provide more contact area with firebrands and therefore produce a lower number of secondary firebrands. It was also found that the opening shape did not have a major impact on the fragmentation ratio.

The orientation of the screen with respect to wind direction had a considerable impact on the fragmentation ratio. A tilted screen had a smaller fragmentation ratio as both the projected area and perpendicular wind force that pushed the leaf embers through the screen decreased. A screen leaning forward had a better performance in terms of fragmentation ratio than a leaning back screen as it pushed the embers downward and increased the retention time.

The performance of two screens with openings of 1.61 mm and 1 mm and a buffer zone of 4.48 m in order to protect fuel beds were investigated and compared with those in the absence of a screen. Similar to leaf firebrands, hardwood mulch firebrands passed the screen via the mechanisms of shattering and retention behind the screens. In comparison with leaf firebrands, mulch firebrands shattered with less severity, and, therefore, the fragmentation ratios were much lower than those of leaf firebrands. The screens with the opening size of 1.61 mm and 1 mm were effective in reducing the number of ignition points on fuel beds. The effect of the buffer zone was significant since many of firebrands quenched along the buffer zone. The number of extinct firebrands along the buffer zone increased as the opening size reduced to 1 mm. It was found that larger firebrands had a greater tendency to ignite the fuel beds.

5.5. Conclusions

Based on the results presented in this chapter, a list of conclusions can be made as follows:

- Hardwood mulch and Eucalyptus leaf Firebrands pass through screens via two mechanisms: shattering (firebrands shatter into small pieces and then pass the screen) and retention of firebrands (firebrands keep burning or quench behind the screen to fit the size of the screen opening).
- Shattering of firebrands is related to the screen opening size and wire diameter.
- The retention time of firebrands behind the screen increases with the decrease of opening size.
- Flat screens reduce the shattering of firebrands and consequently the fragmentation ratios of leaf firebrands in comparison with woven wire screens.

- The opening shape has a negligible effect on the number of secondary leaf firebrands and consequently the fragmentation ratio.
- The orientation of screens with respect to the firebrand flow direction significantly reduces the fragmentation ratio of leaf firebrands.
- The effect of a buffer zone between screen and object is significant in reducing the number of firebrands that could reach the object. Many firebrands quench within the buffer zone after leaving the screen.
- Screens with a smaller opening size remarkably reduce the number of glowing firebrands that reach the object.
- Screens with a smaller opening size considerably reduce the number of ignited points on the fuel bed with a buffer zone of 4.48 m.
- A buffer zone and screen are highly effective in protecting an object against firebrand attacks.

Chapter 6

Discussion

6.1. Introduction

In the last three chapters, the experimental results on the performance of screens against firebrand attacks and fire radiant heat flux were presented. This chapter aims to discuss the significance of the findings in terms of the effectiveness of screens in protecting from wildfire. In section 6.2, criteria for the effectiveness of screens in containing firebrand attacks and fire RHF are addressed. Following that, discussions on their effectiveness are presented in sections 6.3 and 6.4. Section 6.5 discusses the benefits to the wildfire protection communities and different stakeholders who are directly or indirectly engaged in activities against wildfires of using screens as fire barriers. A summary of the chapter is provided in section 6.6.

6.2. Effectiveness Criteria

Containment in current fire glossaries implies the condition that fire propagation is controlled and the fire is suppressible within a boundary by firefighting (National Wildfire Coordinating

Group 2006; National Fire Protection Association (NFPA) 2012). Based on this definition, the containment of firebrands and radiant heat flux can be expressed as a condition in which the levels of firebrand attack and fire radiation decrease to suppressible levels. It can be helpful to identify the suppressing threshold levels.

In the case of firebrand attacks, the information provided on the performance of screens is not sufficient to assess their potential and further studies are still required. This work only provided the ratio of intensity of firebrands across two sides of screens without defining the acceptable level of firebrand intensity on fuel beds. To define the acceptable ratio, both the intensity of approaching firebrand showers and the acceptable level of firebrand intensity on the fuel bed should first be identified. As previously stated in the literature review (section 2.3), the intensity of a firebrand attack is dependent on many parametres such as the local wind as well as density and type of vegetation. On the other hand, the possibility of firebrand-induced ignition is related to the type of fuel beds and their moisture content at the time of attack. The above parametres should be added to the effect of land slope and topography where firebrand attacks occur, showing that the containable condition can be unique for each wildfire incident. Therefore, providing an exact threshold at this stage is not feasible and further study is required.

In contrast with firebrand attacks, it is possible to set criteria for the performance of screens against RHF. The threshold level of radiant heat flux received by surrounding objects can be set to a harmless level. The harmless level is related to the value of RHF, distances between object and fire as well as the type of object. Objects are different in terms of resistance against fire radiant heat flux. The literature declares humans, houses and natural resources such as forests and bushes as the greatest losses in wildfire incidents. A threat to humans by fire radiation is severe skin burn which may lead to death when it exceeds a certain level. House components, such as metals, deform or lose integrity when they are under an extreme radiation condition. Some components such as wooden logs dehumidify under severe radiation exposure and ignite quickly either by long radiation exposure or by landed firebrands. The ignitability of vegetation is critical in fire spread. The fire radiation causes evaporation of vegetation moisture and their auto-ignition or ignition by embers or flames. Many studies provided the effect of different levels of radiant heat flux on humans, materials and vegetation. Therefore, the effectiveness of screens to contain fire radiant heat flux can be assessed for different types of objects as follows:

- **Human:** No first-degree skin burn
- **Houses:** No house ignition by 10 minutes of exposure
- **Vegetation:** No auto-ignition of forest litter

6.3. Metal screens versus Radiant Heat Flux (RHF)

This study identified that square woven wire screens are capable of reducing the direct light intensity by more than is suggested by screen solid area. The tunnel vision effect of screens limits the light intensity regardless of the size of the light source. It was concluded that screens are effective in blocking fire RHF and can perform better for larger fires such as wildfire fronts.

Table 6-1 Thermal radiation threshold for different objects.

Effect	Thermal radiation (kW/m^2)	Reference
Maximum tolerable value for firefighters completely covered and protected by special Nomex protective clothes	7.0	(Butler and Cohen 1998) (Zárate et al. 2008)
Minimum level required to cause pain after 60 seconds	2.1	(Zárate et al. 2008)
House ignition after 10 minutes exposure	20	(Cohen 1999)
Damage to process equipment and collapse of mechanical structures	37.5	(Zárate et al. 2008)
Spontaneous ignition of wood	40	(Boonmee and Quintiere 2002)
Spontaneous ignition of various types of forest litter for 1 min exposures	15	(Durda and Kring 2004)

In section 6.2, the criteria for screens to contain fire radiant heat flux was set based on the vulnerability of humans, houses and vegetation. Table 6.1 lists the thermal radiation thresholds for different objects. The formulas presented in chapter 3 provide an opportunity to compare the radiation received by the objects listed in table 6.1 in the absence and presence of a screen.

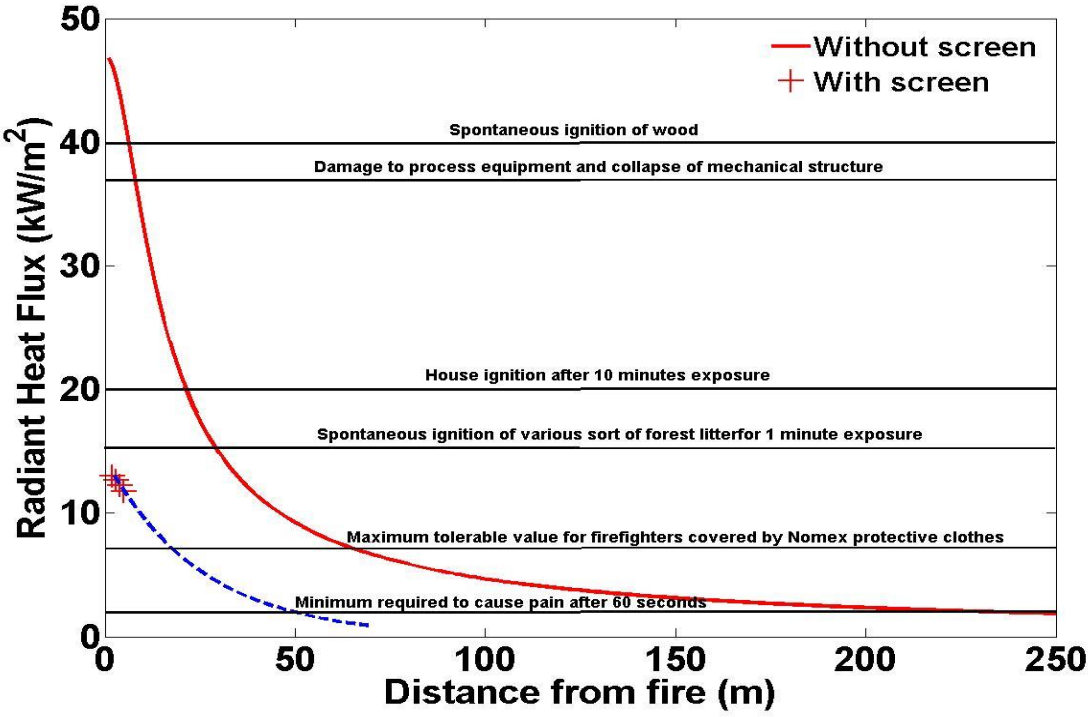

Figure 6.1 Numerical results for change of radiant heat flux received by an object at different distances from a fire with a height of 20 m, width of 20 m in the presence and absence of a screen with porosity of 41%.

Figure 6.1 displays the radiant heat flux emitted by a fire with 20 metre width and height and its variation with respect to distance from the fire. The figure also presents the estimation of fire radiant heat flux through a woven wire screen with 41% porosity versus distance. For the fire, an emissivity of 1 and temperature of 1200 K were assumed based on the previous radiation models in the literature (see section 2.2.1). This includes the sum of estimated direct and indirect radiant heat flux. For the stainless steel screen at 1 metre distance from the fire, the temperature was assumed to be 750°C (1023 K). The emissivity of the screen was assumed to be 0.6 based on an average of presented emissivities for stainless steel in Lienhard (2011). The view factor of an object to the fire without a screen was estimated assuming the fire and object are square planes through the following formula (Lienhard 2011)

$$VF = \frac{((\frac{w_1}{d}+\frac{w_2}{d})^2+4)^{0.5}-((\frac{w_1}{d}-\frac{w_2}{d})^2+4)^{0.5}}{\frac{2w_1}{d}} \qquad (6.1)$$

where w_1 and w_2 represent the width of object and fire respectively and d denotes the distance between object and fire. It should be noted that the empirical formulas presented in chapter three are only valid under certain conditions. The distance between object and screen should not lead to a tunnel-vision area greater than the size of the screen. Therefore, there is a limit for the distance of the object and the screen and the results are only valid for a short distance of 6 metres in the example. It is expected that RHF reduces by further increasing the distance between the object and the screen due to the reduction in view factor. For further distances, the formula overestimates the RHF as it assumes the size of the fire grows simultaneously with the size of the tunnel-vision area. In this case, the overestimated values are presented in Figure 6.1 only for comparison purpose.

Table 6.1 presents thermal radiation thresholds set in the previous section for humans, houses and vegetation. The thresholds are indicated as horizontal lines in figure 6.1. Based on the figure, a minimum safety distance of 225 metres should be maintained between people and the fire in the absence of a screen to avoid skin pain. The distance tremendously decreases to 51 metres as a screen with porosity of 41% is applied, which yields a 77.3% reduction in safety distance. Figure 6.1 indicates that the safety distance for firefighters covered by Nomex protective clothes is 67 metres in the absence of the screen, while it decreases to 20 metres by mounting the screen in front of the fire. Furthermore, the level of fire radiation can lead to auto-ignition of forest litters up to a distance of 30 metres in the case of without a screen; however, the screen can prevent their ignition at any distance. For houses, the level of radiant heat flux is sufficient to ignite houses up to 22 metres distance from the fire. Application of a screen considerably reduces the level of radiant heat flux and prevents any house ignition. As indicated in figure 6.1, in the absence of the screen, the fire can cause mechanical failures of the structure and auto-ignition of wood at 9 metres and 7 metres from the fire, respectively. The risk can be completely avoided by shielding them against the fire with the screen.

The above example indicates the great effectiveness of the screen to reduce required safety distances. For a house and the described fire, a safety distance is not required in the presence

of the screen as the level of radiation is less than the house ignition threshold even at zero distance. Firefighters and people are still required to maintain a distance to ensure their safety. However, it should be noted that the required safety distance is a function of the size of the fire as well as the type of the object. Therefore, the above discussion is only valid for a fire with size of 20×20 metres.

6.4. Metal screens effectiveness against firebrands

In this study, two mechanisms of firebrand passage through the screens were identified. Firebrands may shatter into small pieces or burn behind the screen to fit the screen opening size. Metal screens do not quench the firebrands. The experimental results showed that the mechanism of the passage depends on screen geometries. More importantly, it was found that a combination of buffer zone and screen significantly reduces the number of firebrands reaching the fuel bed, and as a result reduces the number of burning points on the fuel bed.

In a wildfire event, metal screens can reduce the potential of firebrands to initiate new spot fires. The firebrands hit the metal screen and shatter into smaller pieces or lose their size by continuing to burn behind the screen. The reduction in the size of firebrands greatly reduces their residence time and diminishes their capability to transfer heat to an object upon landing. However, the increase in the number of firebrands (fragmentation ratio of greater than one) causes their accumulation on the objects behind the screen, which may increase the heat transfer on the object and lead to ignition. This study found that a buffer zone can significantly prevent such accumulation. A large fraction of smaller secondary firebrands reach their burnout time for a larger buffer zone. Therefore, the possibility of firebrand-induced ignition considerably decreases.

The above discussion can be supported by an example. Assuming a house with a 20 m^2 front area is under a firebrand attack with an intensity of approximately 550 000 firebrands per minute. This intensity corresponds with the maximum intensity applied in this study (469 firebrands/m^2.s). In this case, two million and two hundred thousand firebrands reach the house within four minutes. Such massive numbers of firebrands can cause accumulation of burning firebrands and hence simultaneous fires at various parts of the house which can burn it down. If a screen with a 1 mm opening size is mounted 4.5 metres away from the house, as the results in chapter 5 suggest, only 22 000 smaller burning firebrands (equivalent of 1%)

reach the house in the same period. As the literature stated, the reduction in the size and number of firebrands greatly decreases the probability of ignition of the object. The example indicates that the combination of screen and buffer zone is effective in reducing the probability of house burning and making the firebrand attack fightable. It is expected that with the increase in length of the buffer zone, further decrease of the burning firebrands becomes achievable.

A combination of buffer zone and screen can reduce the length of the buffer zone recommended by current wildfire management guidelines. As stated in chapter 1, the prescribed buffer zone is currently being practised under various names such as “home ignition zone” or “asset protection zone”. The lengths of these zones are varied and depend on a thorough risk assessment of the structure and surrounding landscape. For example, in the United States, the National Fire Protection Association recommends a buffer zone between 30 and 60 metres from forests for any structure in wildfire-prone areas. As a combination of screen and buffer zone is able to reduce the size and number of firebrands, this can greatly help to shrink the buffer zone without diminishing the performance of buffer zones. A positive impact of the shrinking is a reduction in the costs associated with fuel treatment within the zone.

The results presented in this work are indicative and the actual results may vary under real wildfire conditions. This might be due to differences in initial temperature of objects (fuel beds in this case) during the experiment in laboratory and real wildfires, wind speed, shape and type of vegetation (e.g. cones and twigs, instead of mulch and leaf).

The above discussion addressed the benefits of using screens in real wildfires and highlighted the limits of this study. However, despite the limitations, the overall results are not expected to change due to the enormous changes between the results of the two cases with and without screens.

6.5. Challenges of design and implementation

The current study is limited in its ability to assess the viability of employing metal screens as fire barriers and therefore no recommendation on using metal screens as fire barriers can be made as an outcome. The applications for screens still require further extensive studies on various parameters that have not been addressed in this thesis and on the comprehensive design of metal screens as fire barriers for different wildfire conditions.

This study implies a link between the opening size of screens and the required width of the corresponding buffer zone to effectively mitigate firebrand attacks. Defining the relationship between screen opening size and the width of the buffer zone is necessary for the future design and application of screens. In addition, other parameters such as variations in wind speed and direction, exposure time, type of vegetation and size of screens may have considerable impacts on the results and these will require further investigation.

The results presented are under wind tunnel conditions for screens and firebrands where all firebrands are forced to pass through the screen. In the real world, some firebrands may pass over the screen or accumulate underneath the screen due to built-up of stagnation pressure behind the screens. In wind tunnel conditions, the wall of the wind tunnel may also have a considerable impact on the results which is not the case in a real wildfire. Also, in a real wildfire the distance between fire and screen continuously decreases but of course it was constant in this study. This leads to a wider range of firebrand statuses in terms of burning conditions under real world conditions. A full scale experiment is essential to address the above issues in the future.

Fire barriers require efficient and well-adapted transport and installation methods. The transporting of metal screens is a function of their weight and different approaches should be examined to find an appropriate technique for easy delivery and accessibility of screens under various wildfire conditions and topographies. The installation of screen barriers can also be affected by the weight of the screens and the drag force imposed by the wind on screens. Resistance wires or special poles can be used to fix screens in some topographies. In addition, the effect of thermal stress on metal screens and their resilience under real fire conditions is another important factor in the use of metal screens.

The above issues are critical factors for the application of screens as fire barriers. Any recommendation on fire barrier practices will be possible only when the above issues have been examined and/or resolved.

6.6. Impacts to wildfire protection communities

The potential of metal screens could deliver great benefits to the protection against wildfires and cause positive impacts on communities that are directly or indirectly engaged with the problem. However, the stakeholders in wildfire protection have different views on the wildfire issues, which may shape their perceptions of the advantages of using metal screens.

The following sections address the potential benefits for four major stakeholders: local residents of wildfire prone areas, fire fighters, insurance companies and government agencies.

6.6.1. Local residents

The most significant effect of wildfires is to the local communities who lose their houses or lives. For their safety, the wildfire related policies in some countries such as in the United States order for a mass evacuation or like in Australia offer people to stay and defend if they are prepared or evacuate early before fire arrival. However, the evacuation approach has been criticised since it is not always helpful and may cause risks such as entrapment by rapid moving fires (Krusel and Petris 1983; Handmer and Tibbits 2005; McCaffrey et al. 2015). In Australia, the stay or go policy is being practiced based on evidence that the chance of house survival increases if occupants stay and extinguish spot fires on or around the house during the passage of the fire front (Handmer and Tibbits 2005). The stay and defend policy is not always free of risk, especially for fierce fires such as those that occurred in Victoria, Australia in 2009. After that event, the viability of the stay and defend policy was under scrutiny (Whittaker et al. 2013) since 113 deaths out of the 173 toll were found in or around their houses (Whittaker et al 2013). Also, a review of fatalities in the period 1955–2008 in Australia shows that 38.4% of deaths were people who stayed to defend their houses (Haynes et al. 2010).

The difficulties of these fires for the people who stay and defend their houses are associated with severe attacks of firebrands and the excessive radiant heat flux of the approaching fire. The massive heat radiation restrains residents to actively protect their properties since they should shelter in a safe place until the fire front passes the area. Use of metal screens as barrier with an appropriate buffer zone can contain fire radiant heat flux within metres of the house and provide a risk-free zone for the residents. The reduced number of spot fires gives them sufficient time to quench the spot fires one-by-one before they can develop into fully-sustained fires. The residents' preparation is limited to mist systems that keep the surfaces of houses and surroundings wet. As radiant heat flux is reduced by screen barriers, constant wetting of house surfaces and surroundings with water hoses or sprinklers becomes more practical since the wetness stays longer on the surfaces and makes them more resilient against any possible ignitions. Also, exposure to excessive heat impairs the residents' mental and physical abilities and causes trauma (McLennan et al. 2014). The condition will be improved using screen barriers and enables residents physically and mentally to fight fires.

6.6.2. Firefighters

Fire crews and volunteers are the vital elements of the suppression activities against devastating wildfires. As stated in chapter 1, in ferocious wildfires, the suppression activities by firefighters may become overwhelming due to the rapid propagation of fires in bushlands. The efficiency of firefighting reduces since the wildland fire fighters should put their efforts into saving houses rather than attacking the fires (Bailey 2007). The firefighting operations may take weeks, which makes firefighters susceptible to various health problems (Guidotti and Clough 1992; Shusterman et al. 1993) and sometimes lead to their deaths.

The benefits of containing firebrands and radiant heat flux by metal screens boost the effectiveness of firefighting operations and enhance the safety of firefighters, particularly for fires with a high spread rate and intensity. The firefighters can erect the screens as barriers along their fire line well before the fire front arrival. As the radiant heat flux is reduced by screens, the firefighters' safety distance considerably reduces and enables them to operate in the vicinity of the fire's edge. Also, firefighters can use back-burning technique on the fire side of the screen before the fire front arrival. However, the back-burning may naturally take place by accumulation of firebrands on the fire side of the screen and may impair the advance of an approaching fire. A screen reduces the number of spot fires in and beyond the buffer zone, which makes it easier for firefighters to contain those occasional spot fires. Screen barriers can help to reduce the workload of firefighters by enabling residents to defend their houses. As the rate of fire spread reduces, the risk of firefighters' entrapment becomes low, since it provides sufficient time for firefighter assessment. Moreover, firefighters can erect screen barriers with an appropriate buffer zone from the evacuation roads to provide safe evacuation routes for people. The safety of roads also supports a better mobilisation of firefighters and their equipment across the affected areas.

6.6.3. Insurance companies

Wildfires incur losses of billions of dollars to the insurance companies. The losses are paid in the form of compensation to the people due to damage to insured properties, injury and death. A report shows that the economic losses derived from wildfire incidents across the world was around $US52 billion for the period 1984–2013 (Doerr and Santin 2013). The cost in the two continents of Oceania and America was nearly $US2 billion and $US25 billion in this period, respectively. As the statistics suggest, the rising cost of damages is expected to continue to

soar in the future (Doerr and Santin 2013). It is not surprising to find that insurance companies implement harsher measures such as refusing to issue new policies or putting caps on their payouts (Mcqueen 2008).

Undoubtedly, the insurance companies would have a great financial stake in the proposed technique as it effectively contains the conflagration and is able to minimise losses to a certain extent. With a successful implementation of the technique, fewer houses would be affected by wildfires and more lives would be saved. In this condition, the insurance companies can make more profit from the collected premiums. Since the risk of wildfires will be downgraded, the premium also can be reduced, which may increase the number of customers. Further discussions on the cost benefits of using screens require a comprehensive financial analysis, which was not within the scope of this study.

6.6.4. Local and national governments

The state and national governments present initiatives to mandate specific measures that address the safety of the people who live in wildfire prone areas. Some examples are the National Fire Plan (NFP) in the United States or the Bushfire Management and National Environment law in Australia (Australian Goverment 2010). The plans include assistance to local communities with programmes to implement risk assessments and planning, activities to reduce the amounts of hazardous fuel, thereby decreasing the risk of catastrophic wildfires, and pre-fire risk mitigation strategies (Bihari and Ryan 2012; Schoennagel et al. 2009). Besides the government laws, standards bodies such as (Standards Australia 2009) or the (National Fire Protection Association 2008) in the United States provide certain codes for construction in wildfire prone areas to make structures resistant against wildfires. The governments not only fund the wildfire aftermath losses, but also pay the wildland firefighting operations during wildfires as well as pre-fire prevention projects.

The proposed technique would greatly assist governments to reduce their expenses. The metal screen barriers improve firefighting, protection of residents and their assets as well as reducing the devastating scale of natural resources and ecosystems. The proposed firefighting plan is capable of reducing the excessive power of fires and therefore may decrease required manpower. By containing the wildfire using the barriers at the early stages of fires, more natural resource such as bushlands, forest, grasslands etc. can be saved and thus reduce the cost of recovery projects. In addition, the cost of social services provided by the governments

such as consultancies to the affected people would also be expected to reduce as barriers safeguard people against the wildfires' impacts.

6.7. Summary

A discussion on the effectiveness of metal screens to contain fire RHF and firebrand attacks was presented in this chapter. The effectiveness criteria of screens based on their performance against both fire RHF and firebrand attacks were discussed. In the case of RHF, a typical calculation for the performance of a screen with porosity of 41% against RHF was presented. By comparing the RHF received to an object in the presence and absence of the screen, it was found that metal screens can effectively reduce the level of fire RHF and the safety distance between an object and a fire. Following that, the effectiveness of screens to contain firebrand attacks was discussed. The discussion indicated that screens are effective in containing firebrands in the presence of a buffer zone between the screens and object. Also in this chapter, some notable benefits of using screen barriers in wildfire protection for local residents of wildfire prone areas, fire fighters, insurance companies and governments were outlined.

Chapter 7

Conclusions and further work

7.1. Summary and Conclusions

Current protection techniques are insufficient to save people and assets in wildfire incidents. Wildfires are known by their severe radiant heat flux and firebrand attacks that cause their rapid propagation. The success of the protection techniques relies on their performance against the two propagation mechanisms. Previous reports underlined the possible effectiveness of metal screens in containing firebrands and the fire radiant heat flux. However, further progress on using metal screens highly depends on their potential to contain these mechanisms, which had not been addressed properly. The aim of this research was to explore the potential of screens and attempt to answer an important question:

- Do metal screens have the potential to contain fire radiant heat flux and firebrand attacks?

Available screens on the market suggest the possibility of various arrangements and layouts of screens. The screens with various geometries and configurations can be erected with different buffer zones with respect to an object intended for protection. This study fulfilled its objectives in two separate parts. The effects of geometry variables including screen opening

size and wire diameter, screen manufacturing type, screen opening shape and screen orientation with respect to firebrand flow on the performance of the screen against leaf firebrands were examined. Also, for mulch firebrands, the performance of a combination of buffer zone and screens with various opening sizes against firebrand attacks was investigated.

A methodology with a light source was developed to investigate the effect of a square woven wire screen to contain direct light intensity. Four woven wire screens with porosities in the range 41–66% were applied in this study. The tunnel vision effect of the screen was observed and measured. For all the cases, the level of passing light intensity was less than the one that screen porosity suggests. The direct radiant heat flux decreased as the porosity reduced and empirical formulas were presented to estimate RHF for various sizes of fires. Further discussion was provided to link the experimental results to the possible practical implementation of metal screens. For this, the radiant heat flux for an assumed fire was calculated in the cases without and with a screen using the presented empirical formulas. A comparison between the radiation received by humans, houses and vegetation and their radiation thresholds in the cases with and without was provided. The conclusion for this part of the study is that:

"*Woven wire screens are effective in significantly reducing the level of RHF and consequently safety distances between objects and fire*."

In the second part of this study, an Ember Shower Simulator (ESS) was designed and fabricated which enabled experiments to be carried out, applying low-porosity screens at relatively-high wind speeds. The characteristics of the ESS were investigated through several preliminary experiments. The simulator's flow uniformity in the test section was affected mostly due to mounting the flap at the vicinity of the test section entrance. The ESS had acceptable non-uniformity in comparison with other available wind tunnels used in fire research. The wind speed could be set to up to 21 m/s when there was no screen mounted in the system. The mass and projected areas of firebrands generated by the ESS had similarities with those measured for real wildfires.

The effect of geometry on the performance of screens was examined using ESS based on the fragmentation ratio, which was defined as the number of leaving glowing firebrands divided by the number of arriving glowing firebrands. The geometric parameters – such as screen opening size and wire diameters, screen manufacturing type and firebrand flow orientation with respect to screen – were the effective parameters in changing the fragmentation ratios.

Further in this study, the effects of the combination of buffer zone and woven wire screens with different opening sizes on their potential to contain firebrands were investigated. The experiments were performed using the ESS and an L-shaped stand at the exit of the ESS to capture the mulch firebrands and direct them to the fuel beds. The firebrands were monitored as they arrived on the screen, during their passage through the buffer zone and at their falling on the fuel beds. The number of firebrands on the fuel bed remarkably reduced with the decrease of opening size since the observations revealed that many firebrands quench in the buffer zone. As a consequence, the number of burning points on the fuel bed was reduced when the screen with a smaller opening size was applied.

A discussion on extending the results for real wildfire incidents was provided. It was discussed that the metal screen may cause the increase of firebrands at the leaving side of the screen due to the shattering mechanism and therefore may lead to firebrand accumulation on objects behind the screen. However, this study found that the shattered or reduced size firebrands quench within a buffer zone between screens and objects. Since firebrands fly further in the buffer zone, the smaller, alight firebrands that reach the object are less able to induce ignition. It was concluded that the metal screens can effectively mitigate the risk of firebrands with a short buffer zone (4.48 m). It appears that metal screens may eliminate the risk of firebrands if a longer buffer zone is applied. The main conclusion for this part of study can be expressed as:

"*The metal screens have the potential to effectively mitigate the risk of firebrand attacks with a buffer zone of approximately 4.5 m and might be able to eliminate the risk if a longer buffer zone between screen and the protected object is provided."*

This study confirmed that the metal screens perform well in mitigating the effect of both propagation mechanisms. The screen can eliminate the risk of fire RHF but may need an appropriate buffer zone (safety distance) for the objects with lower radiation thresholds. There is a possibility for the risk of firebrands to be eliminated by a screen if a screen is erected with a longer buffer zone (longer than applied in this study) separating the protected object. In both cases, buffer zones have a noticeable role to help the screen in eliminating the effects of the propagation mechanisms.

7.2. Main achievements

The main achievements of this study can be listed as:

- Design and manufacture an Ember Shower Simulator with the capability to work with a high wind speed and low porosity screens. The introduction of machine will provide great opportunity in the future to investigate the application of screen in wildfire and assist people who work on wildfire standard for testing new approaches or product for better implication of screen to protect properties.
- Presentation of an experimental correlation for screen porosity and DRHF. The formulas are its first kind to facilitate the estimation of radiation through screen. The implication of formula is not only for wildfire and can be used for other application such as designing shading screens for houses or textile industry.
- Discovery of the shattering mechanism of firebrands. The mechanism is documented in this work for the first time and showed great effect of shattering on increasing intensity of firebrands behind the screen. This will greatly impact the standard revision in respect with screen for house openings in the future and protective methods using screens. It also might improve current methodologies in firebrand studies to understand the phenomena.
- Identification of the impact of a combination of buffer zone and screen. This work for the first time confirmed the effectiveness of screen and buffer zone that would be really supportive for better application of current ignition zones around the properties and make them more effective especially in terms of firebrand attack.

7.3. Further work

The current research study assessed the potential of metal screens against firebrand attacks and fire radiant heat flux and unveiled the performance of metal screens to contain the propagation mechanisms. In chapter 6, the limited scope of the study was discussed. Further studies are required to address those limitation and other necessary aspects in employing screens at real wildfire conditions. The following lists some further work that is required:

- Further study can consider the improvement of ESS in terms of controlling device that provides experiment easier working condition with the apparatus. This features can be such as fan controllers, controlling device for flap height changes etc.
- The great effect of the buffer zone on the performance of screens and its relation with screen opening size was shown. It is possible a minimum buffer zone for each screen exists

to eliminate the risk associated with firebrand attacks. A thorough study to determine the minimum buffer zone is required.

- Prior to this study, most research was conducted at wind speeds less than 10 m/s. In this study, a new mechanism for firebrand passage has been identified. However, the maximum wind speed of 14.5 m/s in this study still does not represent the worst-case scenario. Further study is required to address the effect of high wind speed.
- This study only assessed the potential of screens in containing firebrand attacks and fire radiant heat flux. However, a precise design in the application of screens is required. The design should address issues such as the resistance of the structure to wind force, mounting and dismounting methods and the required weight of the screen for different applications.
- A thorough cost analysis of using metal screen barriers in comparison with the current costs of wildfire protection can be the subject of a future investigation.

References

Àgueda, A., Pastor, E., Perez, Y. & Planas, E., 2010. Experimental study of the emissivity of flames resulting from the combustion of forest fuels. *International Journal of Thermal Sciences*, 49(3), pp.543–554. doi:10.1016/j.ijthermalsci.2009.09.006

Albini, F.A., 1979. Spot fire distance from burning trees--a predictive model. *USDA Forest Service Research Note*.

Albini, F.A., 1981. Spot fire distance from isolated sources--extensions of a predictive model. *USDA Forest Service Research Note*, INT-309.

Alexander, M., 2001. *Fire behavior as a factor in Forest and Rural fire suppression'*,New Zealand Research Institute.

Almeida, M., Viegas, D.X., Miranda, A.I. & Reva, V., 2009. Combustibility of potential embers. In *18th World IMACS/MODSIM Congress*. pp. 4388–4394.

Almeida, M., Viegas, D.X. & Miranda, a. I., 2013. Combustion of eucalyptus bark firebrands in varying flow incidence and velocity conditions. *International Journal of Wildland Fire*, 22(7), pp.980-991.doi:10.1071/WF12210

Anthenien, R.A., Tse, S.D. & Carlos Fernandez-Pello, A., 2006. On the trajectories of embers initially elevated or lofted by small scale ground fire plumes in high winds. *Fire Safety Journal*, 41(5), pp.349–363. doi:10.1016/j.firesaf.2006.01.005

Australian Goverment, 2010. *Bushfire Management and National Environment Law*, Department of Sustainability, Environment, Water, Population and Communities.

Australian Institute of Criminology, 2009. *Cost of bushfires*, Canberra,Australia.Bulletin no. 60.

Babrauskas, V., 2003. *Ignition Handbook: Principles and Applications to Fire Safety Engineering, Fire Investigation, Risk Management and Forensic Science* illustrate., Fire Science Publishers.

Bailey, D.W., 2007. The wildland / urban interface crisis , Is there a solution ? In *Wildfires*. Sevilla, Spain.

Barrow, G.J., 1944. A survey of houses affected in the Beaumaris fire, January 14, 1944. *Journal of the Council for Scientific and Industrial Research*, 18, pp.27–43.

Baum, H.R. & McCaffrey, B.J., 1989. Fire induced flow field–theory and experiment. *Proceedings of the Second International Symposium*, pp.129–148.

Bihari, M. & Ryan, R., 2012. Influence of social capital on community preparedness for wildfires. *Landscape and Urban Planning*, 106(3), pp.253–261. doi:10.1016/j.landurbplan.2012.03.011

Boonmee, N. & Quintiere, J.G., 2002. Glowing and flaming autoignition of wood. *Proceedings of the Combustion Institute*, 29(1), pp.289–296. doi:10.1016/S1540-7489(02)80039-6

Böttcher, J. & Wedemeyer, E., 2006. The flow downstream of screens and its influence on the flow in the stagnation region of cylindrical bodies. *Journal of Fluid Mechanics*, 204(-1), p.501.doi: 10.1017/S0022112089001850

Boulet, P., Parent, G., Acem, Z., Kaiss, A., Billaud, Y., Porterie, B., Pizzo, Y. & Picard, C., 2011. Experimental investigation of radiation emitted by optically thin to optically thick wildland flames. *Journal of Combustion*, 2011, pp.1–8.doi:10.1155/2011/137437

Bradstock, R., Gill, A.M. & Williams, J.R. eds., 2012. *Flammable Australia : Fire regimes, Biodiversity and Ecosystems in a changing world*, CSIRO Publishing.

Butler, B. & Cohen, J., 1998. Firefighter safety zones: A theoretical model based on radiative heating. *International Journal of Wildland Fire*, 8(2), p.73. doi:10.1071/WF9980073

Butler, B.W., Bartlette, R.A., Bradshaw, L.S., Cohen, J.D., Andrews, P.L., Putnam, T. & Mangan, R.J., 1998. *Fire behaviour associated with th 1994 South Canyon Fire on Storm King Mountain , Colorado*, RMRS-RP-9. Ogden, UT: US Department of Agriculture, Forest Service, Rocky Mountain Research Station.

California Residential Code, 2014. *California Code of Regulations Title 24, Part 2.5*, Sacramento, CA.

Cebeci, T., 1974. *Analysis of turbulent boundary layers*, Academic Press.

Chandler, C., Cheney, P., Thomas, P., Trabaud, L. & Williams, D., 1983. *Fire in forestry. Volume 1. Forest fire behavior and effects. Volume 2. Forest fire management and organization*, John Wiley & Sons.

Chen, K., 2004. Quantifying bushfire penetration into urban areas in Australia. *Geophysical Research Letters*, 31(12), p.L12212. doi:10.1029/2004GL020244

Cohen, J.D., 2004. Relating flame radiation to home ignition using modeling and experimental crown fires. *Canadian Journal of Forest Research*, 34(8), pp.1616–1626.doi:10.1139/x04-049

Cohen, J.D., 2010. The wildland-urban interface fire problem. *Fremontia*, 38(2), pp.16–22.

Cohen, J.D., 2000. *What is the Wildland Fire Threat to Homes ?*, School of Forestry , Northern Arizona University.

Cruz, M.G., Sullivan, A.L., Gould, J.C., Sims, N.C., Bannister, A.J., Hollis, J.J. & Hurlet, R.J., 2012. Anatomy of a catastrophic wildfire: The Black Saturday Kilmore East fire in Victoria, Australia. *Forest Ecology and Management*, 284, pp.269–285. doi:10.1016/j.foreco.2012.02.035

Cruz, M.G., Butler, B.W., Viegas, D.X. & Palheiro, P., 2011. Characterization of flame radiosity in shrubland fires. *Combustion and Flame*, 158(10), pp.1970–1976. doi:10.1016/j.combustflame.2011.03.002

CSIRO, 2007. *Natural hazards in Australia: Identifying Risk Analysis Requirements* Miriam H.Middelmann, ed., Canberra: Geosience Australia,.

Davis, K.P. & Byram, G.M., 1959. Combustion of forest fuels. In *Forest Fire: Control and Use*. McGraw-Hill, pp. 61–89.

Doerr, S. & Santin, C., 2013. *Wildfire: A Burning Issue for Insurers?*, Lloyd's.

Drysdale, D., 1999. *An introduction to fire dynamic* Second Ed., John Wiley & Sons. West Sussex, England.

Durda, D.D. & Kring, D. a., 2004. Ignition threshold for impact-generated fires. *Journal of Geophysical Research E: Planets*, 109(8), pp.1–14.doi:10.1029/2004JE002279

Ellis, P., 2015. The likelihood of ignition of dry-eucalypt forest litter by firebrands. *International Journal of Wildland Fire*.doi: 10.1071/WF14048

Ellis, P.F.M., 2013. Firebrand characteristics of the stringy bark of messmate (Eucalyptus obliqua) investigated using non-tethered samples. *International journal of wildland fire*, (2013), pp.642–651.doi:10.1071/WF12141

Ellis, P.F.M., 2011. Fuelbed ignition potential and bark morphology explain the notoriety of the eucalypt messmate "stringybark" for intense spotting. *International Journal of Wildland Fire*, 20(7), pp.897–907.doi:10.1071/WF10052

Ellis, P.F.M., 2000. *The aerodynamic and combustion characteristics of eucalypt bark : a firebrand study*. Australian National University.

Foote, E., Liu, J. & Manzello, S., 2011. Characterizing firebrand exposure during wildland urban interface fires. In *Proceedings of Fire and Materials* pp.1–12.

Frankman, D., Webb, B.W., Butler, B.W., Jimenez, D., Forthofer, J.M., Sopko, P., Shannon, K.S., Hiers, J.K. & Ottmar, R.D., 2013. Measurements of convective and radiative heating in wildland fires. *International Journal of Wildland Fire*, 22(2), p.157.doi:10.1071/WF11097

Fried, J.S., Torn, M.S. & Mills, E., 2004. The impact of climate change on wildfire severity: A regional forecast for northern California. *Climatic Change*, 64(1-2), pp.169–191.doi: 10.1023/B:CLIM.0000024667.89579.ed

Ganslandt, R. & Hofmann, H., 1992. *Handbook of Lighting Design*, Vieweg publishing company. Germany

Ganteaume, A., Guijarro, M., Jappiot, M., Hernando, C., Lampin-Malliet, C., Perez-Gorostiago, P. & Vega, J.A., 2011. Laboratory characterization of firebrands involved in spot fires. *Annals of Forest Science*, 68(3), pp.531–541.doi:10.1007/s13595-011-0056-4

Ganteaume, A., Lampin-Maillet, C., Guijarrro, M., Hernando, C., Jappiot, M., Fonturbell, T., Perez-Gorostiago, P. & Vega, J.A., 2009. Spot fires: fuel bed flammability and capability of firebrands to ignite fuel beds. *International Journal of Wildland Fire*, 18(8), pp.951-969.doi:10.1071/WF07111

Grantham, C., 1984. Electrical safety in hazardous environments. *International Journal of Electrical Power & Energy Systems*, 7(4), pp.194–200.doi:10.1016/0142-0615(85)90020-1

Guidotti, T. & Clough, V., 1992. Occupational health concerns of firefighting. *Annual Reviews Health*, (3).doi: 10.1146/annurev.pu.13.050192.001055

Hammer, R.B., Stewart, S.I. & Radeloff, V.C., 2009. Demographic Trends, the Wildland-Urban Interface, and Wildfire Management. *Society & Natural Resources*, 22(8), pp.777–782.doi: 10.1080/08941920802714042

Handmer, J. & Tibbits, A., 2005. Is staying at home the safest option during bushfires? Historical evidence for an Australian approach. *Environmental Hazards*, 6(2 SPEC. ISS.), pp.81–91. doi:10.1016/j.hazards.2005.10.006

Hurley, M.. et al., 2016. *SFPE Handbook of fire protection engineering*, Springer.

Harris, H., 2011. *Analysis and parameterization of the flight of ember generation experiments*. Clemson university.

Haynes, K., Handmer, J., McAneney, J., Tibbits, A. & Coates, L., 2010. Australian bushfire fatalities 1900–2008: exploring trends in relation to the “Prepare, stay and defend or leave early” policy. *Environmental Science & Policy*, 13(3), pp.185–194. doi:10.1016/j.envsci.2010.03.002

El Houssami, M., Mueller, C., Flikov, A., Thomas, J., Skowronski, N., Gallagher, M.R., Clark, K., Kremens, R. & Simeoni, A., 2015. Experimental Procedures Characterising Firebrand Generation in Wildland Fires. *Fire Technology*.doi: 10.1007/s10694-015-0492-z

Ian Weir, 2015. We can build homes to survive bushfires, so why don’t we? *The conversation*. Available at: http://theconversation.com/we-can-build-homes-to-survive-bushfires-so-why-dont-we-35899.

International Code Council (ICC), 2012. *International Wildland-Urban Interface Code (IWUIC)*,

Kalabokidis, K.D., 2000. Effects of wildfire suppression chemicals on people and the environment - a review. *Global Nest: the Int. J.*, 2(2), pp.129–137.

Knight, I., 2001. The design and construction of a vertical wind tunnel for the study of untethered firebrands in flight. *Fire Technology*, pp.87–100.doi:10.1023/A:1011605719943

Knight, I.K. & Sullivan, A.L., 2004. A semi-transparent model of bushfire flames to predict radiant heat flux. *International Journal of Wildland Fire*, 13, pp.201–207.doi:10.1071/WF03047

Kortas, S., Mindykowski, P., Consalvi, J.L., Mhiri, H. & Porterie, B., 2009. Experimental validation of a numerical model for the transport of firebrands. *Fire Safety Journal*, 44(8), pp.1095–1102. doi:10.1016/j.firesaf.2009.08.001

Krusel, N. & Petris., S., 1983. Staying alive: lessons learnt from a study of civilian deaths in the Ash Wednesday bushfires. *Fire Management Quarterly*, pp.3–19.

Leonard, J.E., Blanchi, R. & Bowditch, P.A., 2004. *Bushfire impact from a house ' s perspective*, Earth Wind and Fire–Bushfire Conference, Adelaide.

Lienhard, J.H., 2011. *A heat transfer textbook*, Courier Dover Publications, Cambridge Massachusett.

Lomas, C.G., 2011. *Fundamentals of hot wire anemometry* Cambridge University Press, ed.,

Long, A. & Randall, C.K., 2004. Wildfire risk assessment guide for homeowners in the southern united states,School of Forest Resources and Conservation, University of Florida.

Manzello, S.L, Shields, J.R., Hayashi, Y. & Nii, D., 2008. Investigating the vulnerabilities of structures to Ignition from a firebrand attack. *Fire Safety Science*, 9, pp.143–154. doi:10.3801/IAFSS.FSS.9-143

Manzello, S.L, Shields, J.R., Yang, J.C., Hayashi, Y. & Nii, D., 2007. On the use of a firebrand generator to investigate the ignition of structures in wildland–urban interface (WUI) fires. In *Eleventh International Fire Science and Engineering Conference (INTERFLAM)*. pp. 3–5.

Manzello, S.L., Park, S.H., Shields, J.R., Hayashi, Y. & Suzuki, S., 2010. *Comparison Testing Protocol for Firebrand Penetration through Building Vents : Summary of BRI / NIST Full Scale and NIST Reduced Scale Results NIST Technical Note 1659.*

Manzello, S.L., Park, S.H., Suzuki, S., Shields, J.R. & Hayashi, Y., 2011. Experimental investigation of structure vulnerabilities to firebrand showers. *Fire Safety Journal*, 46(8), pp.568–578. doi:10.1016/j.firesaf.2011.09.003

Manzello, S.L., Maranghides, A., Shields, J.R., Mell, W.R., Hayashi, Y. & Nii, D., 2009. Mass and size distribution of firebrands generated from burning Korean pine (Pinus koraiensis) trees. *Fire and Materials*, 33(1), pp.21–31.doi:10.1002/fam.977

Manzello, S.L., Cleary, T.G., Maranghides, A., Mell, W.E, Yang, J.C., Hayashi, Y., Nii, D. & Kurita, T., 2008. On the development and characterization of a firebrand generator. *Fire Safety Journal*, 43(4), pp.258–268. doi:10.1016/j.firesaf.2007.10.001

Manzello, S.L., Cleary, T., Shields, J.K. & Yang, J.C., 2006. On the ignition of fuel beds by firebrands. *Fire and Materials*, 30(1), pp.77–87.doi:10.1002/fam.901

Manzello, S.L. & Foote, E.I.D., 2012. Characterizing Firebrand Exposure from

Wildland–Urban Interface (WUI) Fires: Results from the 2007 Angora Fire. *Fire Technology*, 50(1), pp.105–124.doi: 10.1007/s10694-012-0295-4

Manzello, S.L., Maranghides, A. & Mell, W.E., 2007. Firebrand generation from burning vegetation. *International Journal of Wildland Fire*, 16(4), pp.458-462.doi:10.1071/WF06079

Manzello, S.L., Park, S.-H. & Cleary, T.G., 2009. Investigation on the ability of glowing firebrands deposited within crevices to ignite common building materials. *Fire Safety Journal*, 44(6), pp.894–900. doi:10.1016/j.firesaf.2009.05.001

Manzello, S.L. & Suzuki, S., 2013. Experimentally Simulating Wind Driven Firebrand Showers in Wildland-urban Interface (WUI) Fires: Overview of the NIST Firebrand Generator (NIST Dragon) Technology. *Procedia Engineering*, 62, pp.91–102. doi:10.1016/j.proeng.2013.08.047

Manzello, S.L. & Suzuki, S., 2012. The new and improved NIST Dragon's LAIR (Lofting and Ignition Research) facility. *Fire and Materials*, 36(8), pp.623–635.doi:10.1002/fam.1123

Manzello, S.L., Suzuki, S. & Hayashi, Y., 2012. Enabling the study of structure vulnerabilities to ignition from wind driven firebrand showers: A summary of experimental results. *Fire Safety Journal*, 54, pp.181–196. doi:10.1016/j.firesaf.2012.06.012

Maranghides, A. & Mell, W., 2011. A Case Study of a Community Affected by the Witch and Guejito Wildland Fires. *Fire Technology*, 47(2), pp.379–420.doi:10.1007/s10694-010-0164-y

McCaffrey, S., Rhodes, A. & Stidham, M., 2015. Wildfire evacuation and its alternatives: perspectives from four United States' communities. *International Journal of Wildland Fire*, 24, pp.170–178.doi: 10.1071/WF13050

McLennan, J., Strickland, R., Omedei, M. & Suss, J., 2014. Stress and wildland firefighter safety-related decisions and actions. In *Human Factors Challenges in Emergency Management: Enhancing Individual and Team Performance in Fire and Emergency Services,19*.

Mcqueen, M., 2008. Where wildfires burn, insurer get cold feet. *The wall street journal*. Available at: http://www.wsj.com/articles/SB121867195558038891.

Mileti, D., 1999. *Disasters by Design: A Reassessment of Natural Hazards in the United States*, Joseph Henry Press.

Mitchell, J. & Patashnik, O., 2006. Firebrand protection as the key design element for structure survival during catastrophic wildland fires. *The Tenth International Symposium of Fire and Materials*, pp.29–31.

Mitchell, J.W., 2006. Wind-enabled ember dousing. *Fire Safety Journal*, 41(6), pp.444–458. doi:10.1016/j.firesaf.2006.04.002

Möller, M., Cohen, S., Prikner, M., Israeli, Y. & Tanny, J., 2010. Transmission of short-wave radiation by agricultural screens. *Biosystems Engineering*, 107(4), pp.317–327. doi:10.1016/j.biosystemseng.2010.09.005

National Fire Protection Association, 2008. *NFPA 1144–Standard for protection of life and property from wildfire*, Batterymarch Park, MA.

National Fire Protection Association (NFPA), 2012. *NFPA Glossary of Terms*.

National Wildfire Coordinating Group, 2006. *Glossory of wildland fire terminology*.

Ocean Optics, 2008. *USB4000 fiber optic spectrometer installation and operation manual*.

Parent, G., Acem, Z., Lenchene, S. & Boulet, P., 2010. Measurement of infrared radiation emitted by the flame of a vegetation fire. *International Journal of Thermal Sciences*, 49(3), pp.555–562.doi:10.1016/j.ijthermalsci.2009.08.006

Pekic, Z., 2007. High rate spray technique – a new way for effective aerial wildfire suppression. In *4th International Wildland Fire Conference*. Sevilla, Spain.

Poon, S.L. & England, J.P., 2002. *Literature review of Bushfire Construction materials and proposed test protocols for Performance Assessment*, *WFRA Project* 20551.

Ramsay, C., Rudolph, L.S. & Rudolph, L., 2003. *Landscape and building design for bushfire areas*, CSIRO Publishing.

Rissel, S. & Ridenour, K., 2013. Ember production during the Bastrop complex fire. *Fire Management today*, 7.

Robertson, K., Fogarty, L. & Webb, S., 1997. *Firebombing effectiveness - where to from here ?*, Fire Technology Transfer Note 11

San-Miguel-Ayanz, J., Schulte, E., Schmuck, G., Camia, A., Strobl, P., Liberta, G., Giovando, C., Boca, R., Sedano, F., Kempeneers, P., McInerney, D., Withmore, C., Oliviera, D., Rodrigues, M., Durrant, T., Corti, P., Oehler, F., Vilar, L. & Amatull, G., 2012. *Comprehensive monitoring of wildfires in Europe: the European forest fire information system (EFFIS)*,

San-Miguel-Ayanz, J., Moreno, J.M. & Camia, A., 2013. Analysis of large fires in European Mediterranean landscapes: Lessons learned and perspectives. *Forest Ecology and Management*, 294, pp.11–22. doi:10.1016/j.foreco.2012.10.050

Schoennagel, T., Nelson, C.R., Theobald. D.M., Carwath, G.C. & Chapman, T.B., 2009. Implementation of National Fire Plan treatments near the wildland-urban interface in the western United States. In *Proceedings of the National Academy of Sciences of the United States of America*. pp. 10706–10711.

Serway, R. & Jewett, J.W., 2010. *Physics for Scientistis and Engineers with Modern Physics* 9th ed., Boston, USA: Cengage learning.

Sharifian, A. & Buttsworth, D., 2008. Direct radiation from wildfires through square woven screens. In *ASME Summer Heat Transfer*. Jacksonville, Florida USA. doi:10.1115/HT2008-56270

Sharifian, A. & Buttsworth, D., 2010. Double-layered metal mesh screens to contain or exclude thermal radiation from bush fires. *Journal of Fire Protection Engineering*, 20(4), pp.291–311. doi:10.1177/1042391510367366

Sharifian, A. & Buttsworth, D.R., 2007. Computational Simulation of the Wind-force on Metal Meshes. In *16th Australasian Fluid Mechanics Conference*. Gold Coast, Australia, pp. 2–6.

Sharifian, Ahmad, & & Buttsworth, D., 2005. Minimum safe standoff distance for protection from bushfire radiation by commercial metal meshes. In *8th Australasian Heat and Mass Transfer*. Perth,Western Australia. doi: 10.1615/ICHMT.2005.AustHeatMassTransfConf.250

Shusterman, D., Kaplan, J.Z. & Canabarro, C., 1993. Immediate health effects of an urban wildfire. *Western journal of medicine*, 158(2), pp.133–138.

Silvani, X. & Morandini, F., 2009. Fire spread experiments in the field: Temperature and heat fluxes measurements. *Fire Safety Journal*, 44(2), pp.279–285. doi:10.1016/j.firesaf.2008.06.004

Standards Australia, 2009. *"Construction of Buildings in Bush Fire Prone Areas (AS 3959)*, Sydney, Australia.

Stephen L. Quarles, Valachovic, Y., Nakamura, G.M., Nader, G.A & Delasaux, M.J., 2010. Home survival in wildfire-prone areas: building materials and design considerations. *University of California*.

Stephen L. Quarles, 2012. Vulnerabilities of Buildings to Wildfire Exposures. *extension*. Available at: http://www.extension.org/pages/63495/vulnerabilities-of-buildings-to-wildfire-exposures#.VPeXW_mUeQB.

Stephens, S.L., Adams, M., Kearns, F.R., Leicester, B., Leonard, J. & Moritz, M., 2009. Urban–wildland fires: how California and other regions of the US can learn from Australia. *Environmental Research Letters*, 4(1), p.014010.

Sullivan, A.L., Knight, I.K., Hurley, R.J. & Webber, C., 2013. A contractionless, low-turbulence wind tunnel for the study of free-burning fires. *Experimental Thermal and Fluid Science*, 44, pp.264–274. doi:10.1016/j.expthermflusci.2012.06.018

Sullivan, A.L., Ellis, P.F. & Knight, I.K., 2003. A review of radiant heat flux models used in bushfire applications. *International Journal of Wildland Fire*, 12(1), pp.101-110. doi:10.1071/WF02052

Suzuki, S., Manzello, S.L., Lage, M. & Laing, G., 2012. Firebrand generation data obtained from a full-scale structure burn. *International Journal of Wildland Fire*, 21(8), pp.961-968.doi:10.1071/WF11133

Suzuki, S., Brown, A., Manzello, S.L., Suzuki, J. & Hayashi, Y., 2014. Firebrands

generated from a full-scale structure burning under well-controlled laboratory conditions. *Fire Safety Journal*, 63, pp.43–51.doi:10.1016/j.firesaf.2013.11.008

Suzuki, S., Manzello, S.L., Kagiya, K., Suzuki, J. & Hayashi, Y., 2014. Ignition of mulch beds exposed to continuous wind-driven firebrand showers. *Fire Technology*, pp.1–18.doi:10.1007/s10694-014-0425-2

Suzuki, S. & Manzello, S., 2011. On the development and characterization of a reduced scale continuous feed firebrand generator. *Fire Safety Science*, 10, pp.1437–1448.doi: 10.3801/IAFSS.FSS.10-1437

Suzuki, S., Manzello, S.L. & Hayashi, Y., 2013. The size and mass distribution of firebrands collected from ignited building components exposed to wind. *Proceedings of the Combustion Institute*, 34(2), pp.2479–2485.doi:10.1016/j.proci.2012.06.061

Tarifa, C.S., Notario, P.P., Del Mareno, F.G. & Villa, A.R., 1967. Transport and combustion of firebrands. *U.S. Department of agriculture, forest service*, II.

Tolhurst, K. & Howlett, K., 2003. House ignition likelihood index—An hazard assessment method for land managers in the wildland-urban interface. *10th AFAC Conference and 4th International Wildland Fire Conference', Sydney, Australia*.

Tse, S.D. & Fernandez-Pello, A.C., 1998. On the flight paths of metal particles and embers generated by power lines in high winds—a potential source of wildland fires. *Fire Safety Journal*, 30(4), pp.333–356. doi:10.1016/S0379-7112(97)00050-7

Tsokos, K.A., 2010. *Physics for the IB diploma* 2nd ed., Cambridge , UK: Cambridge University Press.

Valendik, E.N. & Kosov, I. V., 2008. Effect of thermal radiation of forest fire on the environment. *Contemporary Problems of Ecology*, 1(4), pp.399–403.doi:10.1134/S1995425508040012

Victoria Building Commission, 2010. *A guide to retrofit your home for better protection from a bushfire*,

Viegas, D., 2009. *Recent forest fire related accidents in Europe*, *European Commission Joint Research Centre Institute for Environment and Sustainability, Luxembourg.*

Wahlquist, A., 2006. An unstoppable force. *the Australian*.

Wang, H., 2006. Ember Attack: Its role in the destruction of houses during ACT bushfire in 2003. *Australasian Bushfire Conference*.

Weber, R.., 1989. Anlytical models for fire spread due to radiation. *Combustion and Flame*, 78, pp.398–408. doi:10.1016/0010-2180(89)90027-8

Weise, D.R., 1994. A tilting wind tunnel for fire behavior studies. Res. Note PSW-

RN-417. Albany, CA: Pacific Southwest Research Station, Forest Service, U.S. Department of Agriculture

Weise, D.R. & Biging, G.S., 1996. Effects of wind velocity and slope on flame properties. *Canadian Journal of Forest Research*, 26, pp.1849–1858.doi:10.1139/x26-210

Wells, R.W., 1968. *Fire at Peshtigo*, Prentice Hall.

Whittaker, J., Haynes, K., Handmer, J. & McLennan, J., 2013. Community safety during the 2009 Australian "Black Saturday" bushfires: An analysis of household preparedness and response. *International Journal of Wildland Fire*, 22(6), pp.841–849.doi:10.1071/WF12010

Woycheese, J.P. & P. J. Pagni., 1999. Combustion models for wooden brands. In *3rd Int. Conf. on Fire Research and Engineering, Society of Fire Protection Engineers*. Washington, USA, pp. 53-70

Woycheese, J.P., Pagni, P.J. & Liepmann, D., 1999. Brand propagation from large-scale fires. *Journal of Fire Protection Engineering*, 10(2), pp.32–44. doi:10.1177/104239159901000203

Xanthopoulos, G., 2007. Forest fire related deaths in Greece: confirming what we already know. In *4th International Wildland Fire Conference*. Sevilla, Spain.

Yin, P., Liu, N., Chen, H., Lozano, J.S & Shan, Y., 2012. New correlation between ignition time and moisture content for pine needles attacked by firebrands. *Fire Technology*, 50(1), pp.79–91.doi:10.1007/s10694-012-0272-y

Zárate, L., Arnaldos, J. & Casal, J., 2008. Establishing safety distances for wildland fires. *Fire Safety Journal*, 43(8), pp.565–575. doi:10.1016/j.firesaf.2008.01.001

Zhou, K., Suzuki, S. & Manzello, S.L., 2014. Experimental study of firebrand transport. *Fire Technology*, pp.1–15.doi:10.1007/s10694-014-0411-8